Design of a Folding Antenna-Integrated Micro UAV

by

My H. Vu

B.S. Mechanical Engineering
Massachusetts Institute of Technology, 2011

Submitted to the Department of Mechanical Engineering
in partial fulfillment of the requirements for the degree of

Master of Science in Mechanical Engineering

at the

MASSACHUSETTS INSTITUTE OF TECHNOLOGY

September 2013

Signature of Author: _____
Department of Mechanical Engineering
August 9, 2013

Certified by: _____
David Wallace
Professor of Mechanical Engineering
Thesis Supervisor

Accepted by: _____
David E. Hardt
Professor of Mechanical Engineering
Chairman, Committee on Graduate Students

Design of a Folding Antenna-Integrated Micro UAV

by

My H. Vu

Submitted to the Department of Mechanical Engineering
on August 9, 2013 in partial fulfillment of the
requirements for the degree of Master of Science in
Mechanical Engineering

ABSTRACT

Micro-UAV devices can be used for a variety of purposes. This project is concerned with the design of such a device that will be used for high altitude antenna calibration. Such a UAV requires that an omni-directional antenna be integrated into the frame of the device to reduce signal interference. The device is to fold into a flare cartridge and withstand high deployment forces out of an aircraft. Design requirements include a rectangular working volume of 1.89" X 2.44" X 7.04", a minimum additional payload of 70 g, hang time requirements, and antenna operating frequencies. A standard design process was used to develop a functional prototype. Several different concepts were developed, analyzed, and tested until a discone parachute device was chosen. An umbrella-like mechanism that utilized aerodynamic forces for deployment was developed for the ground plane.

A functional demonstration prototype was built and tested to ensure the device's survivability and deployment functionality. The results of the test were successful and proved that the design is viable and can be further developed and optimized to improve performance.

Thesis Supervisor: David Wallace
Title: Professor of Mechanical Engineering

Acknowledgements

I would like to thank my advisor David Wallace for offering me guidance and support throughout the research process. David provided valuable feedback and suggestions after every milestone of the process.

I would also like to thank Lincoln Labs and their members for their support and advice through the project. Lincoln Labs presented the research problem and helped to define the scope of the project. They provided feedback on concepts and prototypes along the way as well.

Next, I would like to thank my colleague, Lauren Hernley, for her contributions to initial stages of the design process. Lauren was my research partner on the project for the first year and helped in the concept development and selection phases as well as the feasibility calculations for the parachute and balloon flight modes. She also offered advice and consultation in the later portions of the project.

I would also like to thank John O'Sullivan and Daniel Huertas, two MIT undergraduates, who assisted as UROPs for the project. They both assisted in providing background research and concept suggestions. John participated in the flight mode prototypes over the summer as well.

Finally, I would like to thank Troy Niekamp, another MIT graduate student, for his help with the testing stages of the final prototype. Troy volunteered a day out of his time to help set up and run the air cannon test and drop test. He also provided valuable advice and input.

Table of Contents

ABSTRACT 3

Acknowledgements 5

List of Figures 9

List of Tables 12

1 Introduction 13

1.1 Objective and Scope of Problem 14
1.2 Related Research at MIT 17
1.3 Antenna Background 18
1.3.1 Antennas Profiles of Interest 18
1.3.2 Radiation Pattern 20
1.4 Principals of Flight 21
1.5 Atmospheric Conditions 23
1.6 Deployment Conditions 24

2 Concept Development and Selection 25

2.1 Group Brainstorming 25
2.2 Concept Down-Selection 28
2.3 Final Selected Concepts 31

3 Flight Concept Exploration 34

3.1 Feasibility Analysis 34
3.1.1 Parachute 34
3.1.2 Balloon 36
3.1.3 Glider 41
3.2 Prototyping & Testing 43
3.2.1 Parachute: Effects of Ground Plane Geometry 43
3.2.2 Glider: Addressing Stability Concerns 46
3.3 Feasibility Conclusions 48

4 Folding Concept Exploration 50

4.1 Pop-Out Design 50
4.2 Umbrella Design 52
4.3 Choosing a Mechanism 55

5 Integration and Fabrication 57

5.1 Detailed Design 57
5.1.1 Final Folding Mechanism 57
5.1.2 Modeling the Design 59
5.1.3 Antenna Integration 62
5.2 Device Fabrication 64
5.3 Deployment Package 68
5.3.1 Ejection Conditions 68
5.3.2 Design and Fabrication of the Deployment System 69
5.3.3 Optimizing Space Usage 72

6 Testing the Device **75**

6.1 Impulse Survivability 75
6.2 Deployment Validation 78

7 Conclusion **81**

7.1 Summary of Work 81
7.2 Future Work 84
7.2.1 Design Improvements 84
7.2.2 Progression to a Fully Functional Device 85

Bibliography **87**

Appendix A: Parachute Feasibility MATLAB **89**

Appendix B: Balloon Feasibility MATLAB **92**

Appendix C: Glider Feasibility Calculations & MATLAB **96**

Appendix D: Carbon Fiber FEA Report **100**

Appendix E: Aluminum FEA Report **123**

List of Figures

Figure 1: High altitude antenna calibration device [4]..... 14
Figure 2: MJU-10/B cartridge of outer dimension 2.0" x 2.5" x 8.0"..... 15
Figure 3: Available system envelope [7]. 15
Figure 4: Schematic of flare cartridge system [7]. 16
Figure 5: Antenna integrated parachute UAV final prototype—close up (left) and opened state during drop test (right). 17
Figure 6: Dipoles and their radiation patterns (green): straight dipole, bowtie, and discone [4]. 18
Figure 7: Three-dimensional discone monopole and it radiation pattern (green) [2]. 19
Figure 8: Two-dimensional log periodic directional antenna and its radiation pattern (green) [4]..... 20
Figure 9: Omni-directional techniques for V-pol and H-pol [4]..... 21
Figure 10: Folding concepts from top, left to right: (1) folding, (2) hinging, (3) twisting, (4) telescoping, (5) deformable, and (6) inflatable. 27
Figure 11: Flying concepts from top, left to right: (1) rotating airfoil, (2) parachutes, (3) stationary airfoil, and (4) lighter-than-air. 28
Figure 12: Ten fully integrated concept sketches..... 30
Figure 13: Concept #1 - Discone parachute with folding ground plane..... 31
Figure 14: Concept #2 – Balloon with printed or embedded antenna..... 32
Figure 15: Concept #3 – Foldable dipole hang glider..... 33
Figure 16: Position and velocity of chute. 36
Figure 17: Helium properties at sea level and 30,000 ft. 37
Figure 18: Volume at different altitudes for a balloon that would remain mutually buoyant at 10,000 ft..... 38

Figure 19: Solution space for required payload and gas mass needed to remain aloft. 40
Figure 20: Glider dimensions used in feasibility analysis. 41
Figure 21: Glider altitude v. Time with cutoff time of 30 min and cutoff altitude of 10,000 ft marked. 42
Figure 22: Ground plane prototypes from left to right going down: mesh circle, fabric circle, mesh square, fabric square, and "spider" 44
Figure 23: Left: Scaled-down parachute prototype with fabric square ground plane. Right: Weight added to prototype. 45
Figure 24: Hang glider prototype in three boom configurations: front, middle, back. Bottom images show corresponding Velcro connection points. 47
Figure 25: Unfolded sketch model and joints. 50
Figure 26: Folded sketch model. 51
Figure 27: Sketch model unfolding. 51
Figure 28: 3D Printed connectors. 52
Figure 29: Left shows a labeled diagram of one spoke of umbrella folding mechanism; right shows an expanded view of the final spoke, highlighted in red. (Diagram not drawn to scale) 53
Figure 30: Acrylic prototype open (left) and closed (right). 54
Figure 31: CAD showing open and closed device 58
Figure 32: FEA of carbon fiber spoke under initial loading conditions. 60
Figure 33: FEA of Aluminum spoke under initial loading conditions. 61
Figure 34: Sectional view of UAV central strut with antenna integration 63
Figure 35: Waterjet aluminum linkages (L2, L5, L3, L4) and 3D printed bottom and top center discs. 64
Figure 36: Assembled folding mechanism with close up of pin joints 64
Figure 37: Ground plane fabric with pocket for linkage. 65

Figure 38: Ground plane with antenna hardware installed minus soldered cone wires. 66
Figure 39: Closed and open device. 66
Figure 40: Top and bottom view of 3D-printed springer device. 67
Figure 41: Springs placed in the center of the folding mechanism. Left shows partially closed and right shows fully opened position. 67
Figure 42: Top plot shows the sabot's altitude and the bottom shows the velocity ratio both versus time. 69
Figure 43: Open sabot made of Al-5054 sheet metal. 70
Figure 44: Close-up of servo and opening mechanism with notches in tab and in opposite wall of second angle also shown. 71
Figure 45: Diagram of mechanism showing pin in locked position (left) and open position (right). Sidewall shown as green, bottom plate as blue, and pin highlighted in red. 71
Figure 46: Side view of UAV package with one face cut away. Components: sabot walls (green), payloads (magenta), parachute space (red), springer (yellow), UAV device (white and black in top left), and deployment electronics (bottom below payload). 72
Figure 47: 3D printed payload and springer mechanism. 73
Figure 48: Steps to properly packing the parachute inside the sabot. 74
Figure 49: Fully assembled deployment package. 74
Figure 50: Testing setup with air cannon and two cameras. 75
Figure 51: Test block and actual sabot with drag ribbon. 76
Figure 52: Trajectory of UAV (red) and sabot (blue) after being shot from air cannon at 35 PSI. 77
Figure 53: Trajectories of sabot (blue) and UAV (red) during drop test. 79

List of Tables

Table 1: Design requirements. 17

Table 2: Atmospheric conditions up to 30,000 ft. 23

Table 3: Decision matrix of folding v. flight concepts for five antenna types. 29

Table 4: Testing matrix with varying ground plane configurations and summary of results. 46

Table 5: Comparison of performance between carbon fiber and Al-2024. 62

1 Introduction

Unmanned aerial vehicles (UAVs) carrying antenna payloads can be used for various purposes. As it exists, the UAVs can create disturbances in the signal produced by the antenna. This research focuses on the development of a high altitude antenna calibration device where the antenna is integrated into the structure of the UAV. By doing so, extraneous structure is removed and a clean signal can be sent back to the on ground device undergoing calibration.

The thesis is organized into the following chapters:

Chapter 1 presents the objective and scope of the research problem, describing design requirements and operating conditions of the device. Background on prior research, VHF antennas, and flight principles are also discussed.

Chapter 2 presents the methods used in concept development and selection of possible design solutions. Three promising solutions are chosen for further development.

Chapter 3 presents the results from the exploration of the flight methods employed by the three promising concepts. Feasibility calculations and quick sketch model prototyping narrow down the scope to one promising solution.

Chapter 4 presents the results from the exploration of the folding concepts. This includes the design and feasibility analysis of different folding mechanisms.

Chapter 5 presents detailed design and fabrication of the final mechanism and deployment system. This includes the CAD and physical prototypes for the mechanism as well as the sabot deployment system.

Chapter 6 presents the tests and results for survivability and mechanism deployment.

Chapter 7 is the conclusion of the thesis. A summary of the work is presented along with analysis of possible design improvements and future work.

1.1 Objective and Scope of Problem

The micro-UAV is intended to be an expendable device that will be deployed from a flare canister at a low altitude of around 30,000 ft and not recovered. Multiple devices are intended to be deployed from an airline carrier and used to establish a high altitude persistent OPS for antenna calibration.

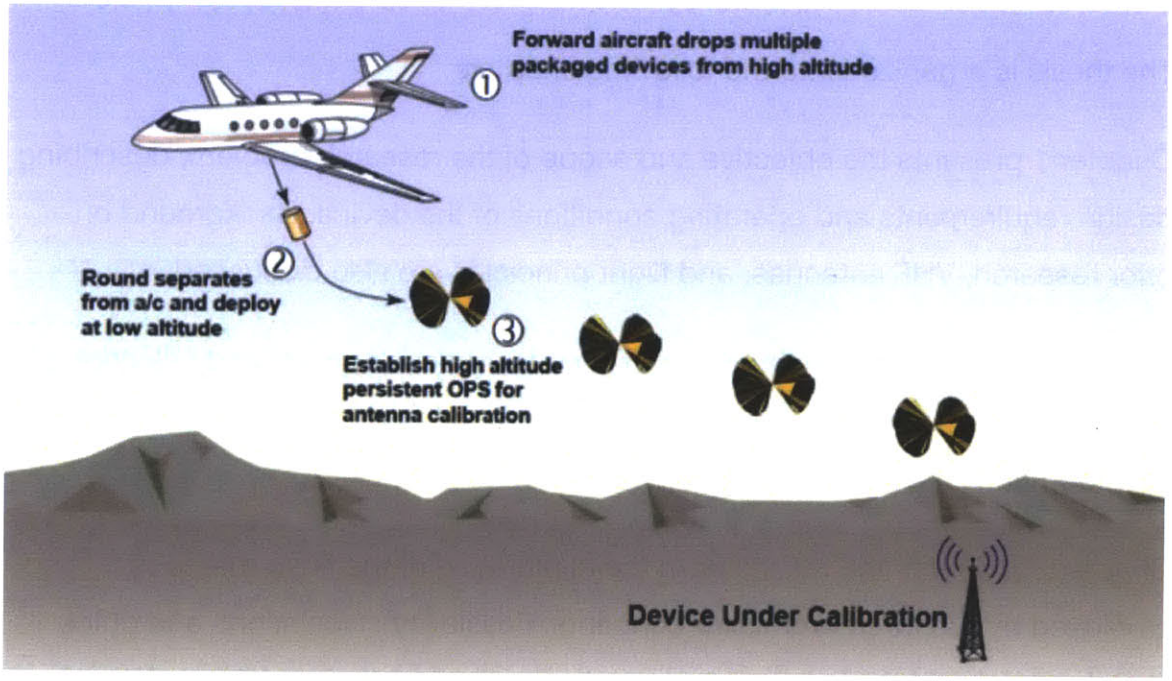

Figure 1: High altitude antenna calibration device [4].

The UAV must fold down for storage in an MJU-10/B flare cartridge and on deployment, will unfold to its full structure.

Figure 2: MJU-10/B cartridge of outer dimension 2.0" x 2.5" x 8.0".

The cartridge sets the maximum system envelope for the UAV package at 48 mm x 62 mm x 180 mm with a 3.175 mm corner radius.

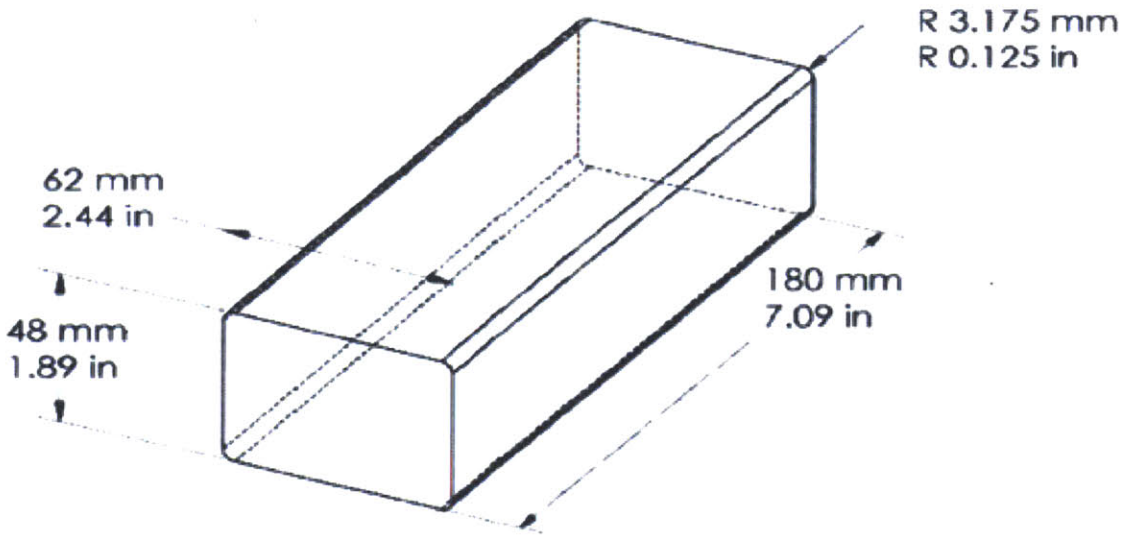

Figure 3: Available system envelope [7].

Figure 4 shows the schematic of the flare cartridge system. The system envelope is encased by the shell of the flare canister and sealed with a cap, crimped at the edges to keep it locked to the shell. The ejection method from the flare canister is an explosive charge from the pyrotechnic cartridge that pushes the UAV package with the piston. The force with required to open the cap is 125 lbf and the acceleration experienced during ejection is 300 G, resulting in an exit speed of about 55 mph.

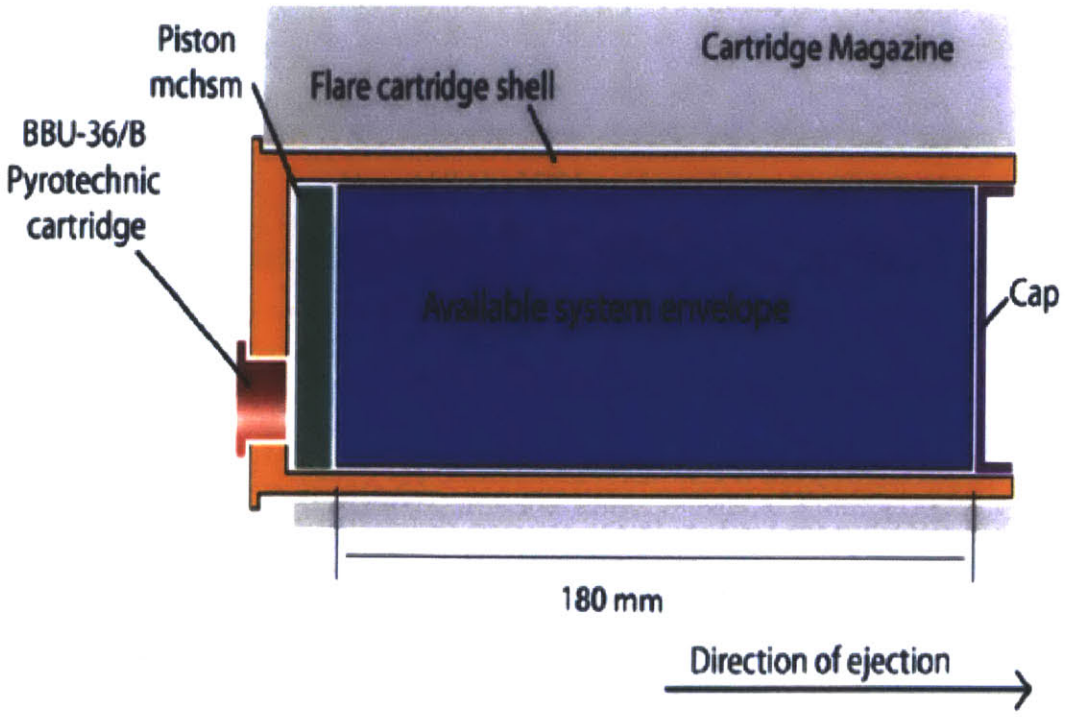

Figure 4: Schematic of flare cartridge system [7].

The flare will be deployed under the following conditions:

- Altitude: 5,000/30,00 ft AGL (min/max)
- Speed: 250 KIAS (max)
- Duration: 1 to 3 hrs
- Weight: 4 lb (max)
- Temperature: -35 cold soak (max)

Only forms of unpowered flight will be considered in the design of the UAV to minimize the weight, size, and cost of the device. This also allows the payload it carries solely to be used to power the antenna structure rather than contributing to lift or thrust. The device's size and shape will be dictated by the geometry of the antenna necessary to operate in the desired frequencies. The following table summarizes the requirements that the UAV must satisfy.

Table 1: Design requirements.

	Baseline	Stretch
Hang Time	30+ mins (from 30,000-10,000 ft AGL)	30+ mins (from 30,000-20,000 ft AGL)
Antenna	120-300 MHz V-Pol or H-Pol Omni-directional	50-1,200 MHz V-Pol and/or H-pol, Omni-directional
Payload	2.25" x 1.5" x 1.0", 70 g	2.25" x 1.5" x 2.0", 150 g
Control	Pitch stable ± 15°	Pitch stable ± 15°, controlled drift direction

The resulting design integrates a discone antenna into the structure of a parachute UAV. The cone of the antenna is formed by wires leading up to the parachute while the disc is formed by a umbrella-like mechanism that allows it to fold down into the flare cartridge.

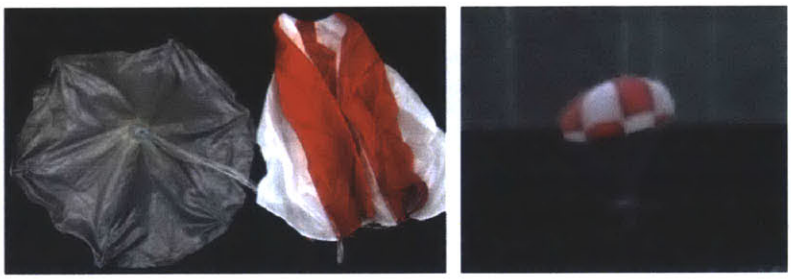

Figure 5: Antenna integrated parachute UAV final prototype—close up (left) and opened state during drop test (right).

1.2 Related Research at MIT

A similar project was presented MIT's Fall 2010 Flight System Engineering class. The goal of the project was to design a high-altitude persistence micro-UAV. The devices were similarly deployed from flare cartridges but used powered flight to maintain different levels of altitude. Each device was equipped with a payload that consisted of sensors and batteries and was used for weather data

acquisition at fixed altitudes. With the initial design established, MIT graduate student Tony Tao did further research into the design of the device in his Master's thesis [7].

1.3 Antenna Background

The ultimate goal of this project is design a UAV that can have an antenna directly integrated into its structure. The type of antenna as well as desired operating frequency will dictate the geometry and size of the required device.

1.3.1 Antennas Profiles of Interest

Five antenna profiles were chosen for the project: dipole, bowtie, discone, bicone, and log periodic. They are listed in order from simple to complex. Greater bandwidth is achievable with a more complex design. These antenna profiles were chosen as a base due to their simplicity and omni-directional capabilities. Their geometries could also be easily adapted into a UAV.

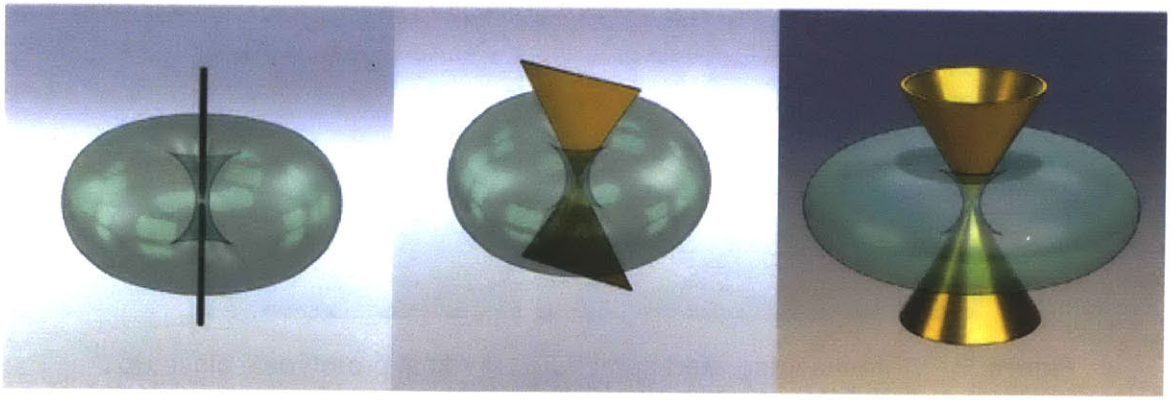

Figure 6: Dipoles and their radiation patterns (green): straight dipole, bowtie, and discone [4].

The straight dipole antenna is the simplest antenna that could be adopted. It can be created using a wire or a strip. Increasing its width effectively increases its bandwidth as well. The bowtie antenna is essentially a dipole antenna that has been fanned out for better performance. Both of these are two-dimensional dipole antennas. One of the most commonly used antennas is the half-

wavelength dipole, which will be considered in this study [1]. By rotating a bowtie antenna about its z-axis, a three-dimensional bicone antenna profile can be achieved for broadband capabilities. The operating wavelength for these antennas is governed by Equation 1:

$$\lambda_{dipole} = \frac{c}{2\nu} \qquad \text{Eq. 1}$$

Figure 7: Three-dimensional discone monopole and it radiation pattern (green) [2].

Another antenna design of interest is the discone, which is formed by placing a monopole cone above a conductive ground plane. This causes energy from the actual source to radiate in all directions. Waves radiating from the source will undergo a reflection below the ground plane (Balanis, 1982). Ideally, the plane is infinitely large so that a quarter-wavelength monopole antenna would be equivalent to its half-wavelength dipole counterpart. Although this is not the case, the use of a large enough ground plane will result in a radiation pattern that sufficiently simulates this. Typically, the length of the cone sides, $\lambda_{discone}$, is one-quarter wavelength of the minimum operating frequency and positioned at

an angle between 25 and 40 degrees. The disc is 0.7 times one-quarter of the minimum frequency's operating wavelength.

$$\lambda_{cone} = \frac{c}{4v} \quad \text{Eq. 2}$$

$$\lambda_{disc} = 0.7 \cdot \lambda_{cone} \quad \text{Eq. 3}$$

In the case of the bowtie, discone, and bicone configurations, the antennas do not need to be formed with continuous surfaces. Rather, materials such as a mesh surface or many wire tines can be used to create the outline of the shape.

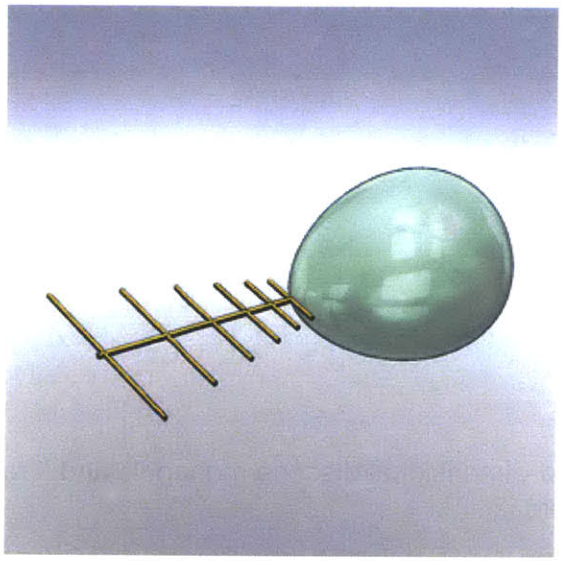

Figure 8: Two-dimensional log periodic directional antenna and its radiation pattern (green) [4].

Finally, log periodic antenna was also considered. It is a type of antenna configuration that closely parallels the concept of frequency independence, meaning the antenna can accommodate the entire frequency band of a given system.

1.3.2 Radiation Pattern

One parameter of interest is the radiation pattern of the antenna. The desired antenna would produce an omnidirectional radiation pattern. This type of pattern

is essentially non-directional in a given plane and directional any orthogonal plane. A directional pattern is one in which the radiating or receiving electromagnetic waves are more effective in some directions than others (Balanis, 1982). The antennas can then be placed in different configurations to accomplish omni-directionality in either V-pol or H-pol. The possible configurations are shown in Figure 9.

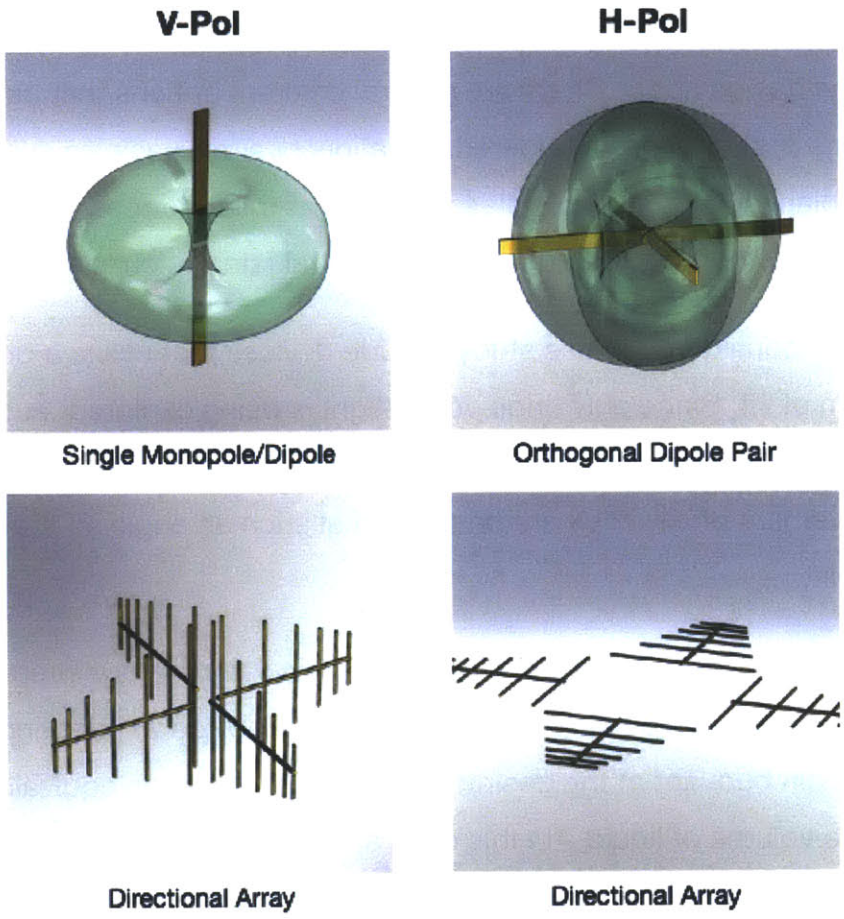

Figure 9: Omni-directional techniques for V-pol and H-pol [4].

1.4 Principals of Flight

This study is concerned primarily with unpowered flight. The typical aerodynamic forces of lift and drag will be considered. They are calculated as follows[6]:

$$F_L = A\frac{1}{2}\rho_{air}(h) \cdot v^2 C_L \quad \text{Eq. 4}$$

$$F_D = A\frac{1}{2}\rho_{air}(h) \cdot v^2 C_D \quad \text{Eq. 5}$$

These forces are dependent on the dynamic pressure, $\frac{1}{2}\rho_{air}v^2$, which is a function of altitude, the force coefficients, and the area of the device (wing planform for wings and frontal area for bodies).

Exploring the design space, there are several different options that can be pursued. One option to be considered is stationary airfoil vehicles such as fixed wing gilder planes, hang gliders, kites, and other similar devices. These are characterized by their lift to drag (L/D) ratio to evaluate performance.

Rotary airfoils considered in this study include devices that utilize a propeller for its main form of lift. Since only unpowered flight is being explored, auto-gyros are of particular interest. These devices have rotor blades that spin through the upward movement of air. They are positioned at such an angle so that flow of air produces a lift.

Lighter than air devices are also considered. Particularly, we are interested in larger sized weather balloons. The fidelity of such a device will depend on its ability to remain buoyant at the desired altitudes. Buoyancy is equivalent to the weight of the volume of liquid—in this case air—that has been displaced and is also changing as a function of height.

$$F_b = \rho_{air}(h) \cdot V_{air} \quad \text{Eq. 6}$$

The lighter than air system will remain neutrally buoyant or aloft if the following condition is satisfied.

$$F_b - m_{tot}g \geq 0 \quad \text{Eq. 7}$$

Parachute devices will also be considered. These are drag devices and the amount of drag they are capable of producing is dependent drag coefficient of the chute's geometry.

1.5 Atmospheric Conditions

During the 20,000 ft descent, the device will be undergoing changing atmospheric conditions that will affect the performance of the device. The following table summarizes the changing atmospheric conditions at the altitudes of interest.

Table 2: Atmospheric conditions up to 30,000 ft [8].

Altitude (ft)	Temperature (°C)	Acceleration of Gravity ($kg*m/s^2$)	Absolute Pressure (N/m^2)	Air Density (kg/m^2)	Dynamic Viscosity ($N*s/m^2$)
0	15.00	9.806	101325	1.225	488003.737
5000	5.09	9.802	84309	1.055	488003.637
10,000	-4.80	9.797	69692	0.905	488003.534
15,000	-14.69	9.793	57206	0.771	488003.43
20,000	-24.59	9.788	46602	0.653	488003.324
25,000	-34.47	9.783	37652	0.549	488003.217
30,000	-44.35	9.779	30151	0.459	488003.107

At higher altitudes, the drag forces on the device are much lower due to a significant reduction in air density. The temperature, however, is also much lower, and these factors must all be considered when making design decisions.

1.6 Deployment Conditions

Upon deployment, the UAV will be shot out of flare canisters at an explosive acceleration of 300 G. Assuming the impulse lasts for 0.1 seconds, the device will accelerate to a relative speed of about 29.4 m/s (65.8 mph). Combined with the speed of the jet at 250 KIAS, this equates to a total speed of 128.6 m/s (287.7 m/s) before slowing down to terminal velocity. Additionally, 125 lbf is required to break through the lid of the flare canister [7].

To help survive these deployment conditions, a sabot was also be designed to encapsulate the antenna UAV. The sabot will be responsible for taking much of the initial impulsive forces and to decelerate the package to a reasonable terminal velocity before ejecting the antenna.

2 Concept Development and Selection

In order to develop a suitable solution for the project, several rounds of brainstorming and concept generation were employed. The problem space was broken down into three categories: antenna type, flight concept, and folding mechanism. Possible solutions were independently developed for the each of the latter two areas of concern, while taking into account the geometry and functionality of the five antenna types.

Once a substantial number of ideas were generated, they were organized into similar categories and the promising ideas for the two categories were integrated into ten full solutions. The top three promising solutions were selected for further prototyping.

2.1 Group Brainstorming

To quickly generate many ideas, group brainstorming sessions were held with experts in the areas of fluids, flight, and mechanical design. Participants were divided into sections focusing on idea generation for flight methods or folding mechanism, depending which subject better suited their area of expertise.

For each session, participants were shown five shapes related to the five antenna types and given the challenge to come up with as many ideas as possible for one of two prompts:

> (1) How would you make this shape stay fly/stay aloft for an extended period of time, unpowered?
>
> (2) How would fit this shape into a small cartridge of 2.5" x 2" x 8"?

The participants were not informed that the end goal was to incorporate this into an antenna integrated UAV so as to not introduce bias and limit their range of ideas.

Each shape was introduced to them one at a time and they had three minutes to independently develop and roughly sketch out their ideas. At the end of fifteen minutes, everyone briefly presented his or her ideas. The ideas were categorized by shape and briefly discussed.

The next phase of the exercise broke the group up into small teams of 2 to 3 people. Each team was asked to pick one or two designs and spend 10 minutes refining their ideas. Once again, each team discussed the refined ideas to all members of the session.

From these sessions, common themes emerged for each antenna type. There were several duplicates and variations for certain concepts. To better analyze the large amount of results, common ideas were grouped into categories to define the problem space. Figures 10 and 11 summarize the concept categories for flight methods and folding concepts.

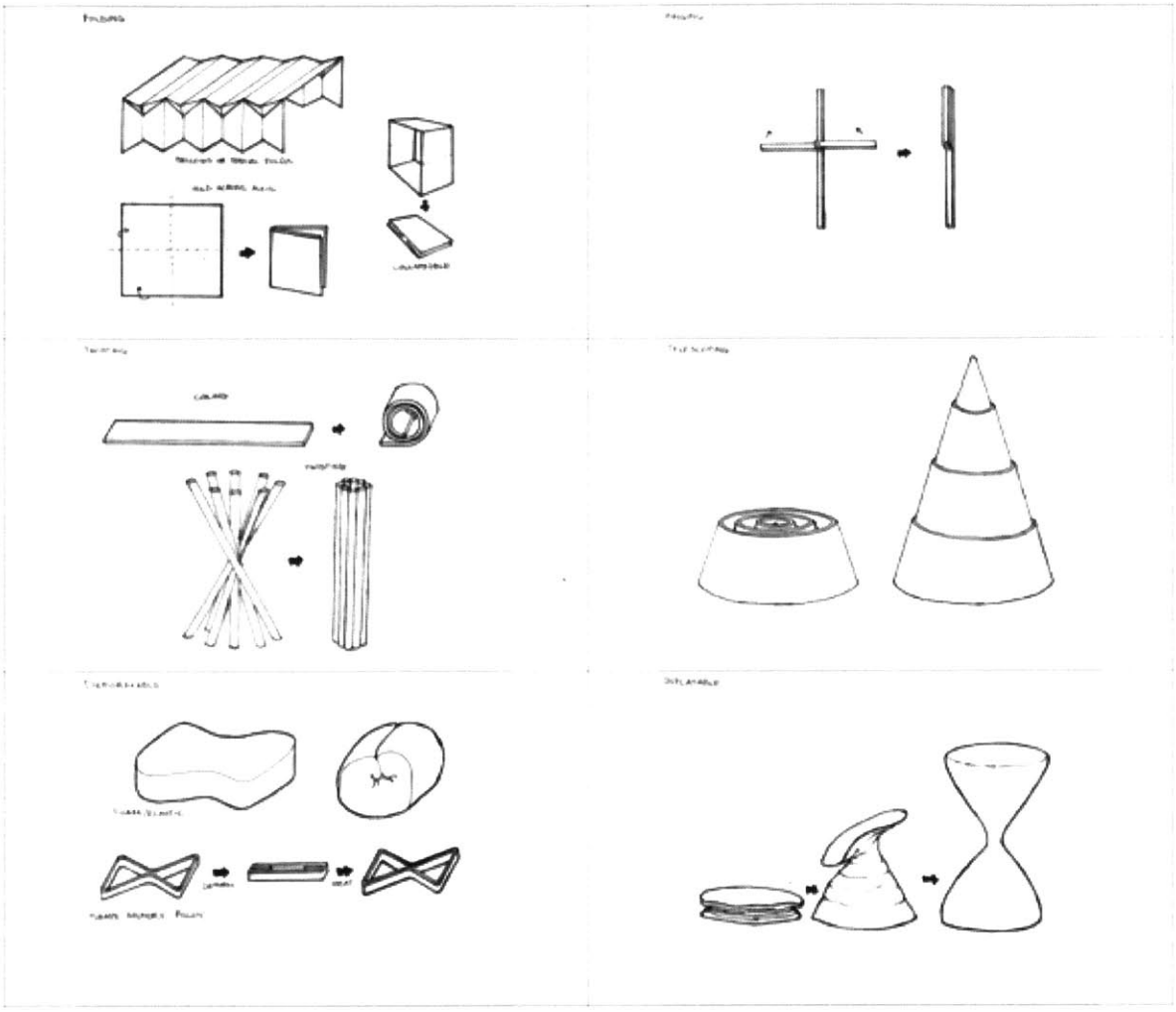

Figure 10: Folding concepts from top, left to right: (1) folding, (2) hinging, (3) twisting, (4) telescoping, (5) deformable, and (6) inflatable.

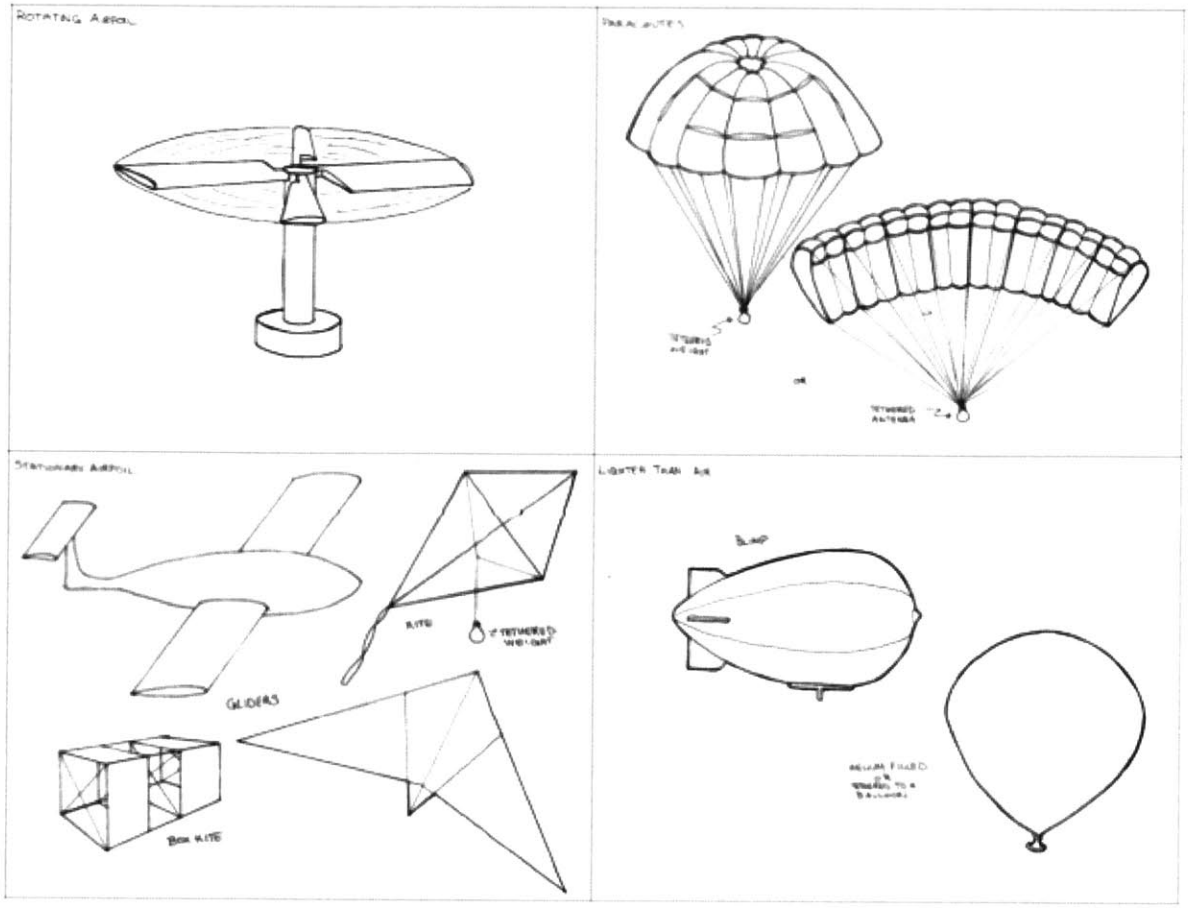

Figure 11: Flying concepts from top, left to right: (1) rotating airfoil, (2) parachutes, (3) stationary airfoil, and (4) lighter-than-air.

2.2 Concept Down-Selection

Once the concepts were categorized, a decision matrix was used to evaluate the ideas. Table 2 shows the matrix with folding categories on the horizontal and flying antenna concepts on the vertical. The antenna concepts on the vertical are further grouped into the flying concepts presented in the previous section. The x's mark all the different combinations of ideas that were generated. The top most interesting concepts are highlighted in yellow.

Table 3: Decision matrix of folding v. flight concepts for five antenna types.

	Folding	Hinging	Twisting	Telescoping	Deformable	Inflatable
Dipole Glider	x	x	x	x	x	x
Log Periodic Glider	x		x	x	x	x
Glider with Bowtie in Wing	x	x	x		x	x
Log Periodic or Dipole Kite	x		x	x	x	
Dipole Pyramid Kite	x		x	x	x	
Bicone Box Kite	x		x	x	x	
Bow-tie Box Kite	x		x		x	
Vertical Log Periodic Turbine		x		x	x	
Dipole or Bowtie Rotor	x	x		x	x	
Dipole Maple Seed Helicopter			x		x	
Discone with Ground Plane Rotor	x	x	x	x	x	x
Bicone with Rotors				x		
Discone with Ground Plane and Metal Twine Cone			x	x	x	
Any Antenna Tethered to Chute	x	x	x	x	x	
2D Antenna Integrated in Chute					x	
Antenna Tethered Balloon	x	x	x	x	x	
Antenna-Shaped Balloon						x
Balloon Inside Discone or Bicone	x		x	x		

The ten promising ideas were further developed and concept sketches of these solutions were created. The sketches presented full high-level solutions for how all three areas—flight, folding, and antenna geometry—could all be integrated. The concept sketches are shown below:

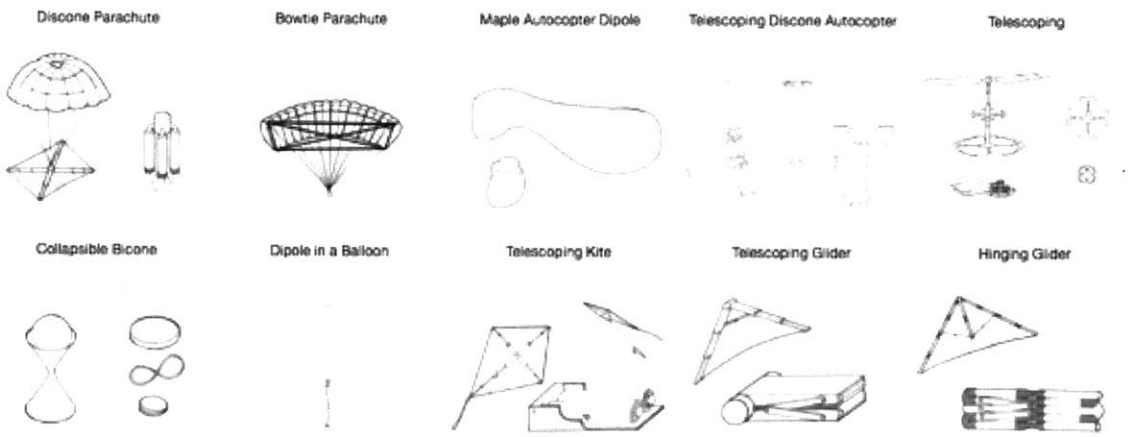

Figure 12: Ten fully integrated concept sketches.

The three autocopter concepts (Fig. 7, row 1, #3-5) would have been too complex in design to pursue and determined to have poor endurance performance. The collapsible balloon was determined to be an unnecessary over-complication while the kite was determined to be a less stable configuration of the glider concepts. The most promising concepts were a discone parachute device (Row 1, #1), a balloon (Row 2, #2), and a folding/collapsible glider (Row 2, #3/4).

2.3 Final Selected Concepts

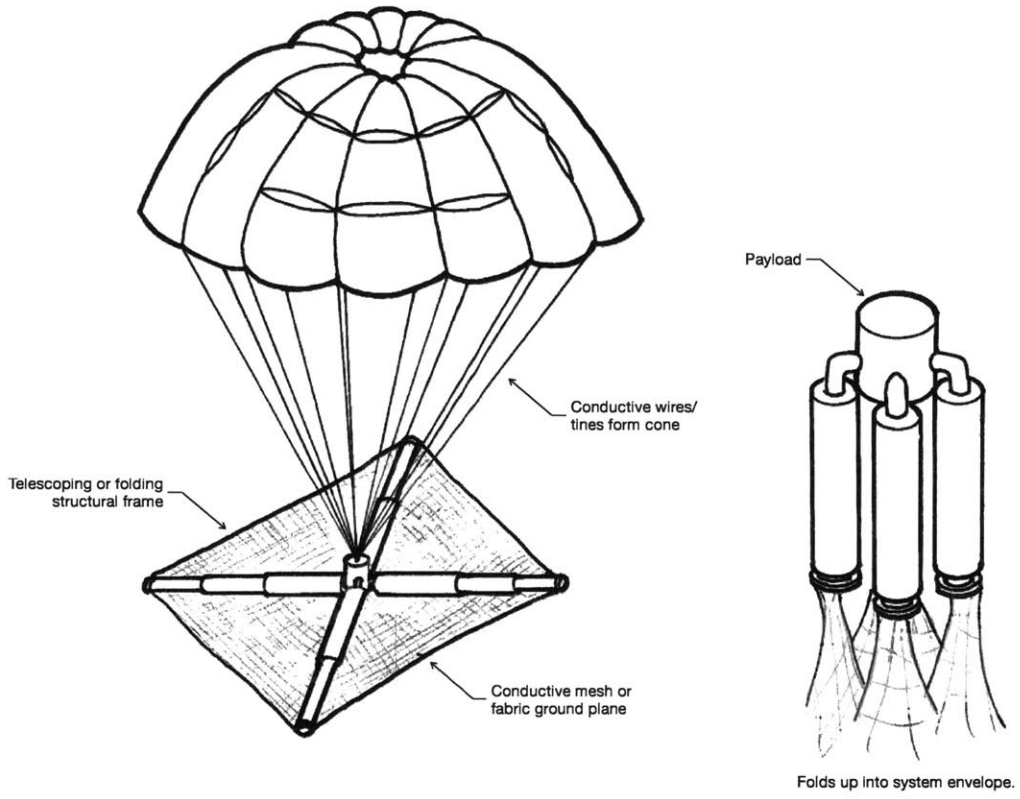

Figure 13: Concept #1 - Discone parachute with folding ground plane.

The parachute design chosen would form a discone antenna. The tines of the chute would form the cone of the antenna by running current through them. A conductive mesh or fabric such as aluminize Mylar would be used to form the ground plane. To maintain the structure of the plane, a collapsible lightweight frame that could fit into the system envelope would be used. Challenges associated with this design include endurance time, stability challenges, ground plane deployment/unfolding mechanism, structural strength of ground plane, and the effects of the ground plane on parachute performance.

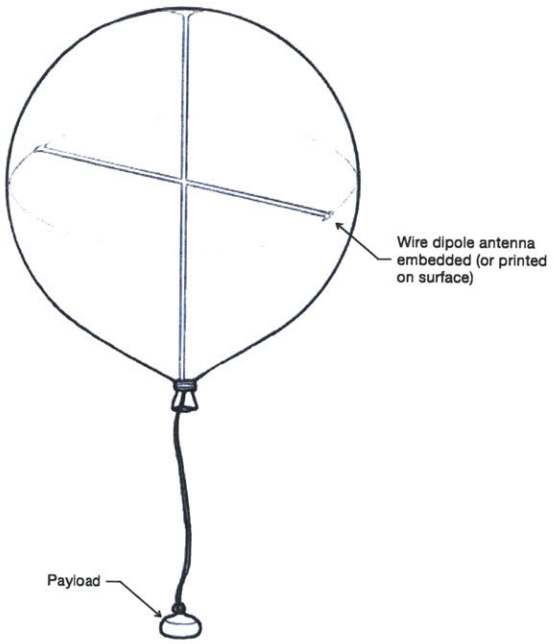

Figure 14: Concept #2 – Balloon with printed or embedded antenna.

The balloon concept was chosen for its simplicity. It would simply be a large balloon that would be inflated after deployment from the flare canister via a lighter-than-air (LTA) compressed gas canister. The antenna would simply be printed on the surface of the balloon or embedded inside with metallic tines. The payload would be tethered to the bottom of the balloon to provide some stability as it descended. Challenges associated with this design direction included survivability and the effects of system envelope volume restriction on the amount of gas available to fill the balloon.

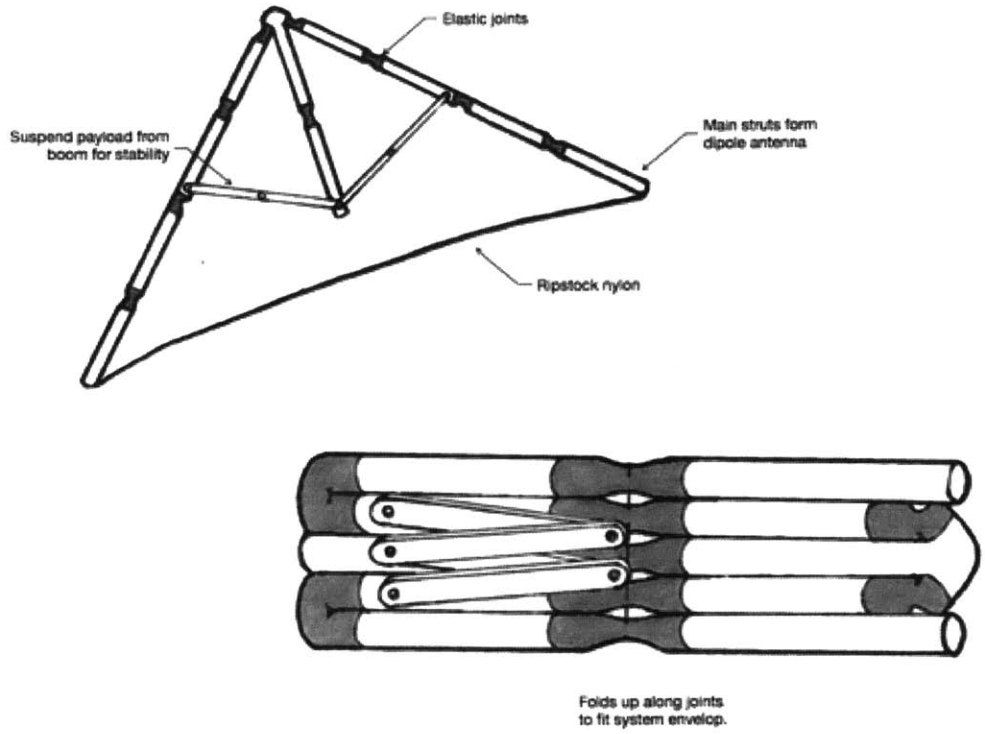

Figure 15: Concept #3 – Foldable dipole hang glider.

The final design considered is that of a collapsible hang glider. The frame of the hang glider would be constructed from a sturdy and lightweight material that could fold up into the system envelope. The frame would need to fold up using elastic or spring-loaded joints. The main struts of the hang glider would form the two dipoles of the antenna. A light but strong fabric such as rip-stop nylon would be used to create the wings. The payload would then hang below the glider to provide balance and stability. Challenges associated with this design included endurance time, durability and strength of frame, flight stability without active control, and ability to fold into desired system envelope.

3 Flight Concept Exploration

In order to choose one concept to pursue, the three potential designs were evaluated for feasibility. This was done through size and flight calculations, research into the different flight methods, and quick sketch model prototyping and testing.

3.1 Feasibility Analysis

The baseline design requirements for the project are used to determine the feasibility of each design. The device must have an endurance of thirty minutes from a descent of 30,000 ft to 10,000 ft with a payload of 70 g. The lower end of the antenna operating frequency dictates the minimum size of the fully opened device. The baseline requirements specify a minimum operating frequency of 120 MHz which can be used to determine required antenna dimensions.

3.1.1 Parachute

The parachute design calls for a discone antenna. To satisfy operating conditions of at least 120 MHz, Eq. 2 and 3 can be used to determine the proper dimensions. Such a parachute calls for a ground plane with a diameter of 0.437 m and a cone side length of 0.625 m. The suggested cone angle is between 25 and 40 degrees, which correspond to a chute diameter between 0.528-0.803 m. For this analysis, a circular chute (Fruity Chutes Elliptical 30" (0.762 m) parachute with a drag coefficient of 1.55 is used.

The total mass assumes the required payload of 70 g (m_{req}), the mass of the parachute (m_p), and the mass of the ground plane (m_g).

$$m_{tot} = m_{req} + m_p + m_g \qquad \text{Eq. 8}$$

Nylon density of 0.061 kg/m^2 is used to calculate the mass of the parachute. A half sphere is used to approximate the surface area of the chute. The mass of the chute is estimated to be 0.056 kg.

$$m_p = 2\rho_{nylon}\pi r^2 \qquad \text{Eq. 9}$$

The structural frame of the ground plane is assumed to be eight spokes of carbon fiber about .25" square cross section. The density of carbon fiber is 1600 kg/m^3. The rest consists of a nylon conductive fabric plane. The ground plane is estimated to be 0.113 kg.

$$m_g = 8\rho_{CF}(0.25^2 r) + \rho_{nylon}\pi r^2 \qquad \text{Eq. 10}$$

To determine the parachute's position and endurance time, the following equation is integrated assuming an initial vertical velocity of 0 and a starting altitude of 30,000 ft.

$$\frac{dv}{dt} = \frac{A\frac{1}{2}\rho_{air}(h)\cdot v^2 C_D}{m_{tot}} - g = 0 \qquad \text{Eq. 11}$$

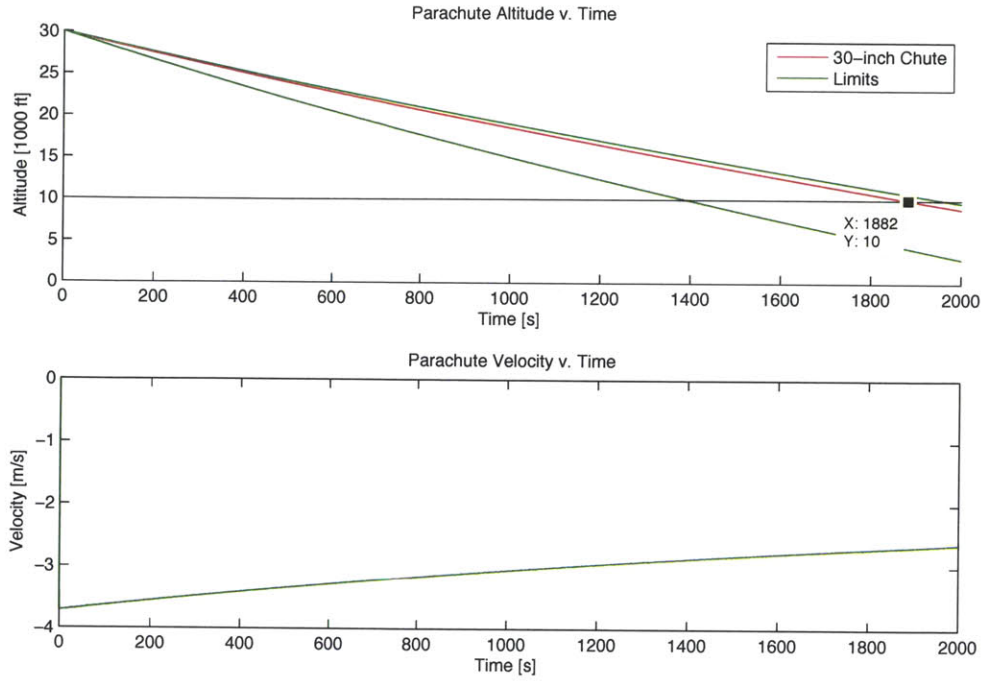

Figure 16: Position and velocity of chute.

For the given assumptions, a parachute device would exceed the required minimum hang time of 30 minutes. In regards to the size constraints, the packing volume of such a chute is orders of magnitude below the given maximum volume of 0.021 m^3. The ability to fit within the sabot is solely dependent on what kind of folding mechanism can be developed.

Based on this primary analysis, a parachute device would be viable. Different parameters could also be varied to even further increase the endurance time. An additional concern that would need to be tested in future steps is the effect of the ground plane on the performance of the chute. Would the ground plane interfere with proper chute deployment and does the geometry of the plane matter?

3.1.2 Balloon

The design calls a dipole antenna stretch across the diameter of the balloon. According to Equation 1, the minimum antenna length, and therefore

corresponding the balloon diameter, must be 1.25 m. This requires a balloon volume of 1.634 m^3. The analysis assumes that balloon will stay neutrally buoyant the deployment altitude of around 30,000 ft. Helium would be used to fill the balloon. The following plot shows the density of helium with varying altitude.

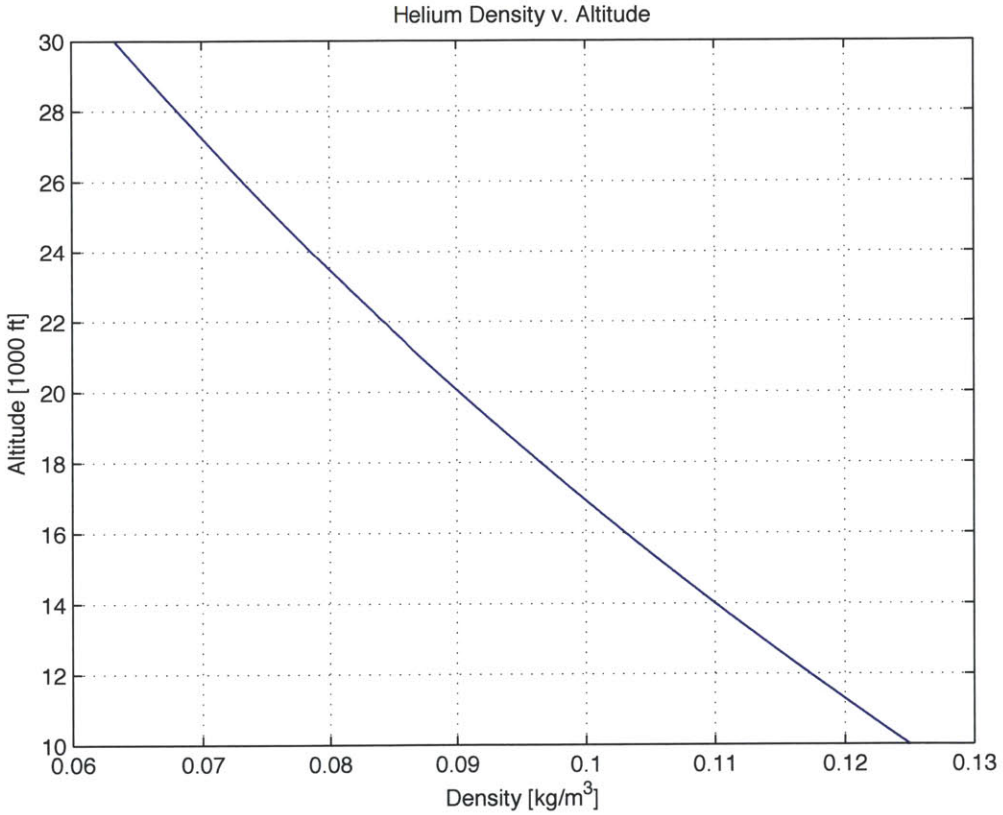

Figure 17: Helium properties at sea level and 30,000 ft.

To remain mutually buoyant, Equation 7 must be satisfied. Due to the changing density, the balloon volume will also be affected depending on where the balloon is. The balloon is smallest at its lowest point of 10,000 ft where the density of He is about .125 kg/m^3. To achieve this volume, 0.204 g of He is needed. The following plot shows the balloon's volume at various altitudes:

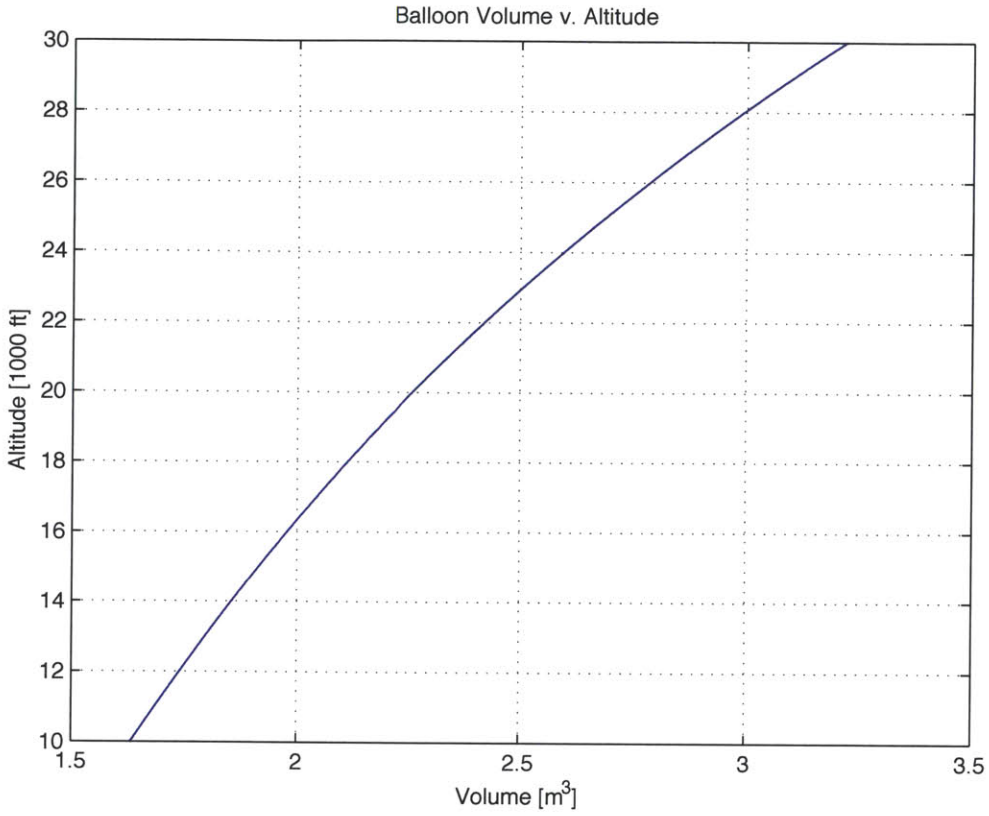

Figure 18: Volume at different altitudes for a balloon that would remain mutually buoyant at 10,000 ft.

At 30,000 ft, the balloon has an initial release volume of 3.221 m^3. There are several types of weather balloons available: pilot, ceiling, and sounding balloons. Sounding balloons are larger and used at higher altitudes, appropriate for this application. The first concern is whether or not an appropriate balloon exists which will not burst. To determine this, the burst data for sounding balloons can be used. The Hoskin Scientific Company [3] has several balloons that can be used—any of their balloons model TA 350 or higher would perform adequately.

Next, we can determine the payload range necessary to achieve successfully flight. The baseline requirements specify a payload mass 70 g (m_{req}). Additionally, we must account for the mass of the metal tines (m_w) that will be used for the antenna and the weight of balloon's latex (m_l).

$$m_{balloon} = m_{req} + m_w + m_l \quad \text{Eq. 12}$$

To determine the length of wire needed for the antenna, four circumference lengths of the balloon cross-section are used. Using 18 gauge copper wire with a density of 0.00728 kg/m^3, the mass of copper is determined to be 0.114 kg.

$$m_w = 4\rho_{Cu}\pi r^2 \quad \text{Eq. 13}$$

A conservative range for the balloon latex mass should be at least 0.35 kg and no more than 3 kg. According to the Hoskin burst data, an upper limit of 1.0 kg was sufficient for our analysis, having a burst diameter much larger than what we needed. This corresponds to a balloon mass range of 1.164-1.814 kg. To determine the solution space, Equations 6, 7, 9, and 10 are combined to yield:

$$\left(\frac{\rho_{air}}{\rho_{He}} - 1\right) m_{He} - m_{balloon} \geq 0 \quad \text{Eq. 14}$$

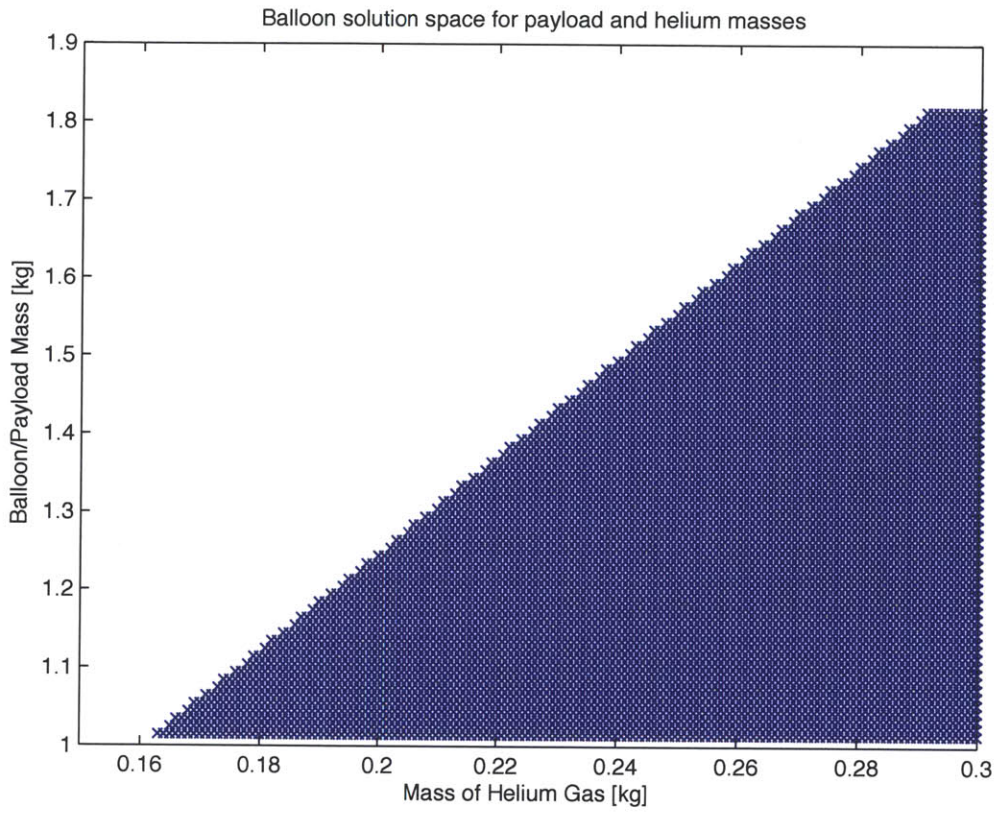

Figure 19: Solution space for required payload and gas mass needed to remain aloft.

Using helium's vapor density of 0.138 kg/m^3, only 0.0029 kg of helium can be stored within the sabot. According to Equation 11, the maximum supportable payload for successful flight must be less than 0.0186 kg. This is much lower than the required payload. Additionally, balloons are difficult to control and neutral buoyancy is near impossible without active control. In this analysis, it is assumed that the balloon stays neutrally buoyant at deployment, but in reality, any change it experiences will cause it to undergo volume changes. With these factors in mind, the balloon design was eliminated and a physical prototype was not pursued.

3.1.3 Glider

A hang glider was also of particular interest. The boom of the glider would serve as a dipole antenna and help to maintain stability. As mentioned in the previous section, the boom would need to be 1.25 m. Suspending such a boom from the glider lowers the center of gravity and increases its rotational stiffness, similar to a pilot and control frame [2].

The analysis assumes a glider based upon the Prism 4-D Ultra-light Stunt Kite of the following dimensions:

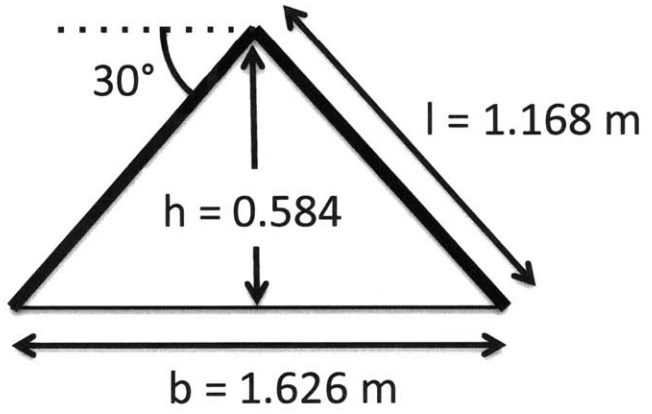

Figure 20: Glider dimensions used in feasibility analysis.

The frame of the glider can be approximated to be a triangle with rods of a circular cross section of 0.125". The total mass is estimated to be 0.902 kg.

$$m_{tot} = m_{req} + \rho_{CF}(2l + b)(\pi 0.125^2) + 0.5\rho_{nylon} bh \qquad \text{Eq. 15}$$

Maximum endurance of a glider occurs at minimum power. The lift coefficient at minimum power is given by the following equation, where C_{D0} is assumed to be somewhere between 0.012-0.015 [5] and K is dependent on the glider geometry (refer to Appendix C for full derivation) [6]:

$$C_L = \sqrt{\frac{3C_{D0}}{K}} \qquad \text{Eq. 16}$$

$$C_D = C_{DO} + KC_L^2 + C_D^{boom} \qquad \text{Eq. 17}$$

To determine the position of the glider, the following equation was integrated [6]:

$$\frac{dy}{dt} = -\frac{C_D^{\min P}}{C_L^{\min P}} \sqrt{\frac{2m_{tot}g}{\rho_{air}(h)AC_L^{\min P}}} = 0 \qquad \text{Eq. 18}$$

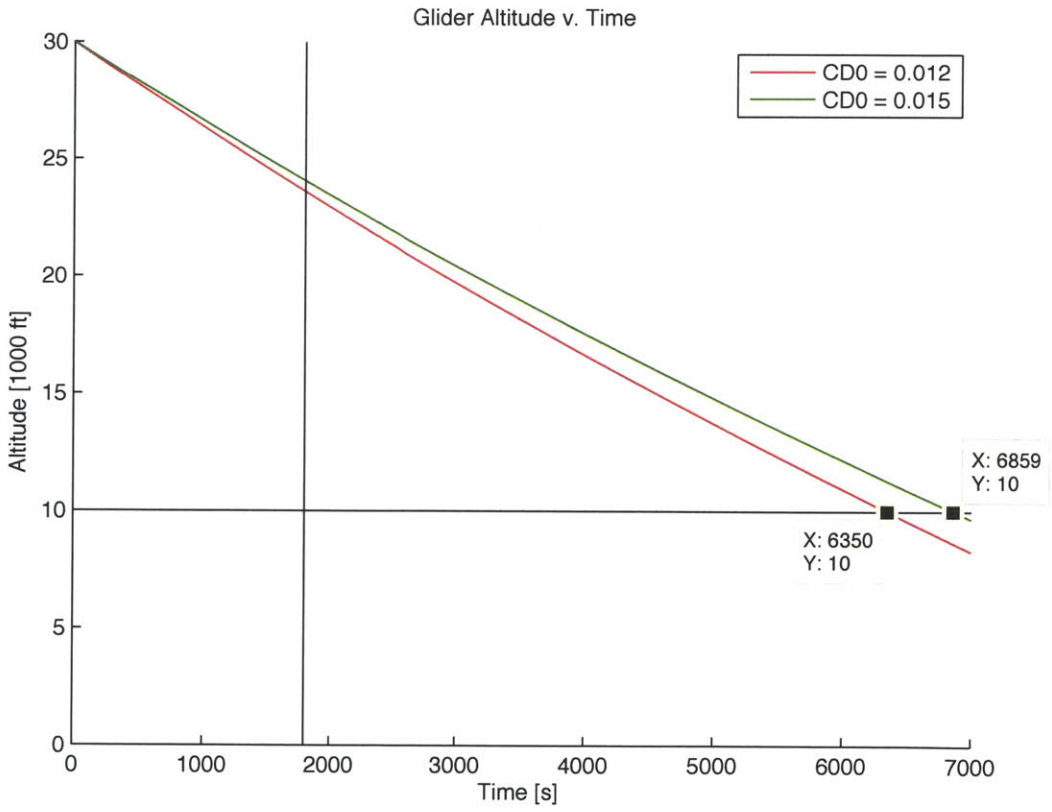

Figure 21: Glider altitude v. Time with cutoff time of 30 min and cutoff altitude of 10,000 ft marked.

A glider would exceed the required time conditions and even meet stretch requirements. Additionally, hang gliders posses many other desirable qualities. Its dynamic stability properties are very similar to that of a conventional airplane

except the lateral directional stability margins are significantly larger [2]. However, gliders also have a spiral stability mode that would be detrimental to the performance of the device [2].

For successful flight, frame must be structurally sound to achieve necessary lift and avoid stability issues. A viable glider would require a complex framework that would be difficult to fold or collapse down into the volume constraints of the system envelope. The weight of a complex structure would also decrease the estimated endurance time, making the glider a less attractive design option.

3.2 Prototyping & Testing

After additional research on the different flight methods and performing initial feasibility calculations, general conclusions could be drawn but there still remained a few areas of doubt. To gain more clarity on the two remaining concepts of interest, simple sketch models were created to test critical areas of concern.

3.2.1 Parachute: Effects of Ground Plane Geometry

One area of concern that still existed after performing the feasibility calculations was the effect of the ground plane on the parachute's deployment and performance. Quick prototypes were constructed for five ground plane variations and a simple drop test was performed.

The ground plane of the prototypes were created using balsa wood, spring steel, polyester mesh, and/or conductive fabric. The five designs were: mesh square, fabric square, mesh circle, and fabric circle, and wire tines (or "spider"). In particular, we wanted to see the effect of geometry on the performance. Additionally, it was also desirable to see if the existence of a large plane would impede the flow of air needed to fill the chute. Mesh and fabric ground planes were used to test this as one let more air through than the other. The "spider"

design was even more minimalistic, eliminating the plane area completely and creating the plane with a circular array of metal tines.

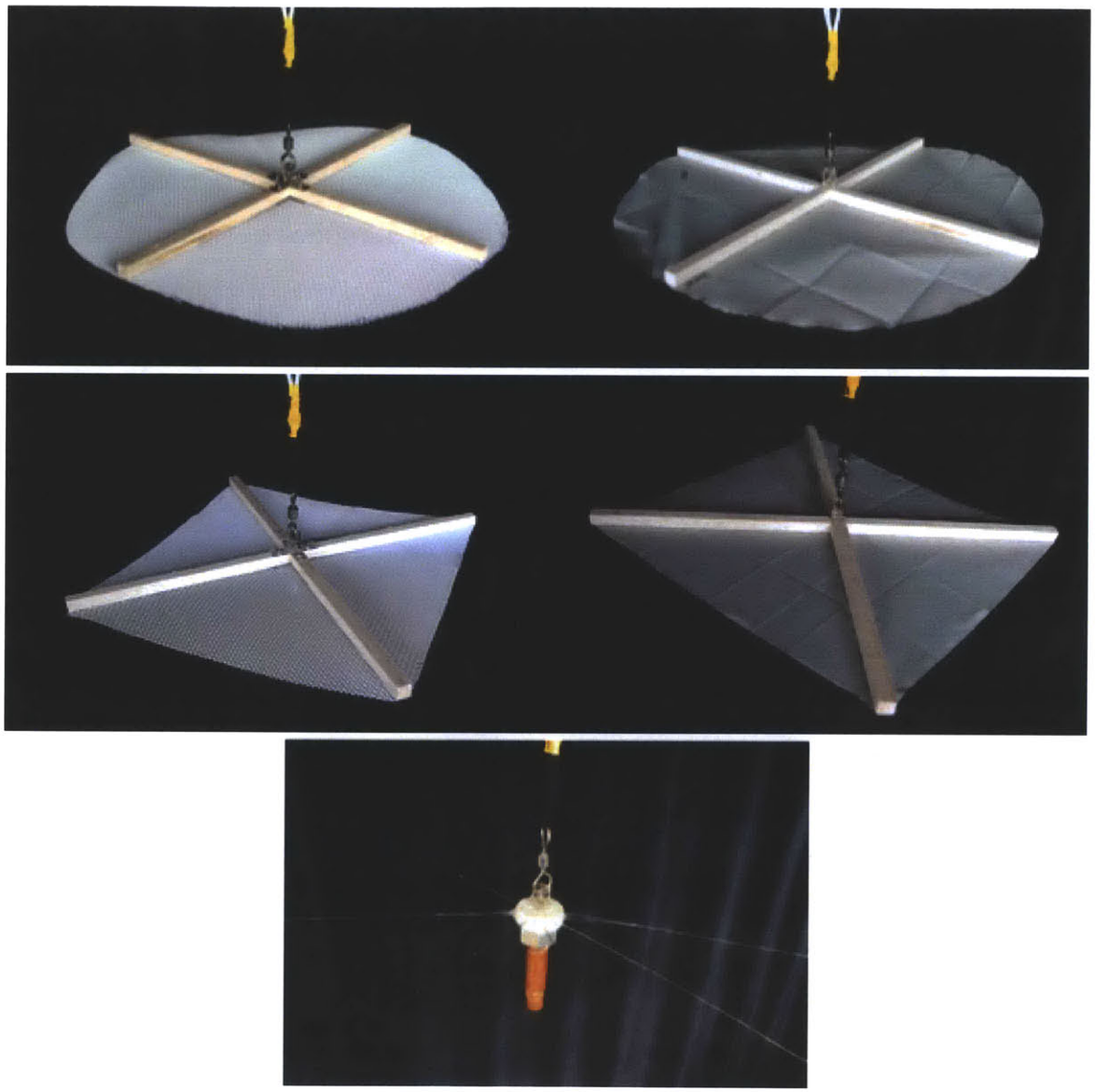

Figure 22: Ground plane prototypes from left to right going down: mesh circle, fabric circle, mesh square, fabric square, and "spider"

Each device was then attached to the center of the planes to bring the total mass to 115±1 g. Laser cut acrylic hooks were used to tether the planes to the parachute. The parachutes were 18"-diameter circular chutes.

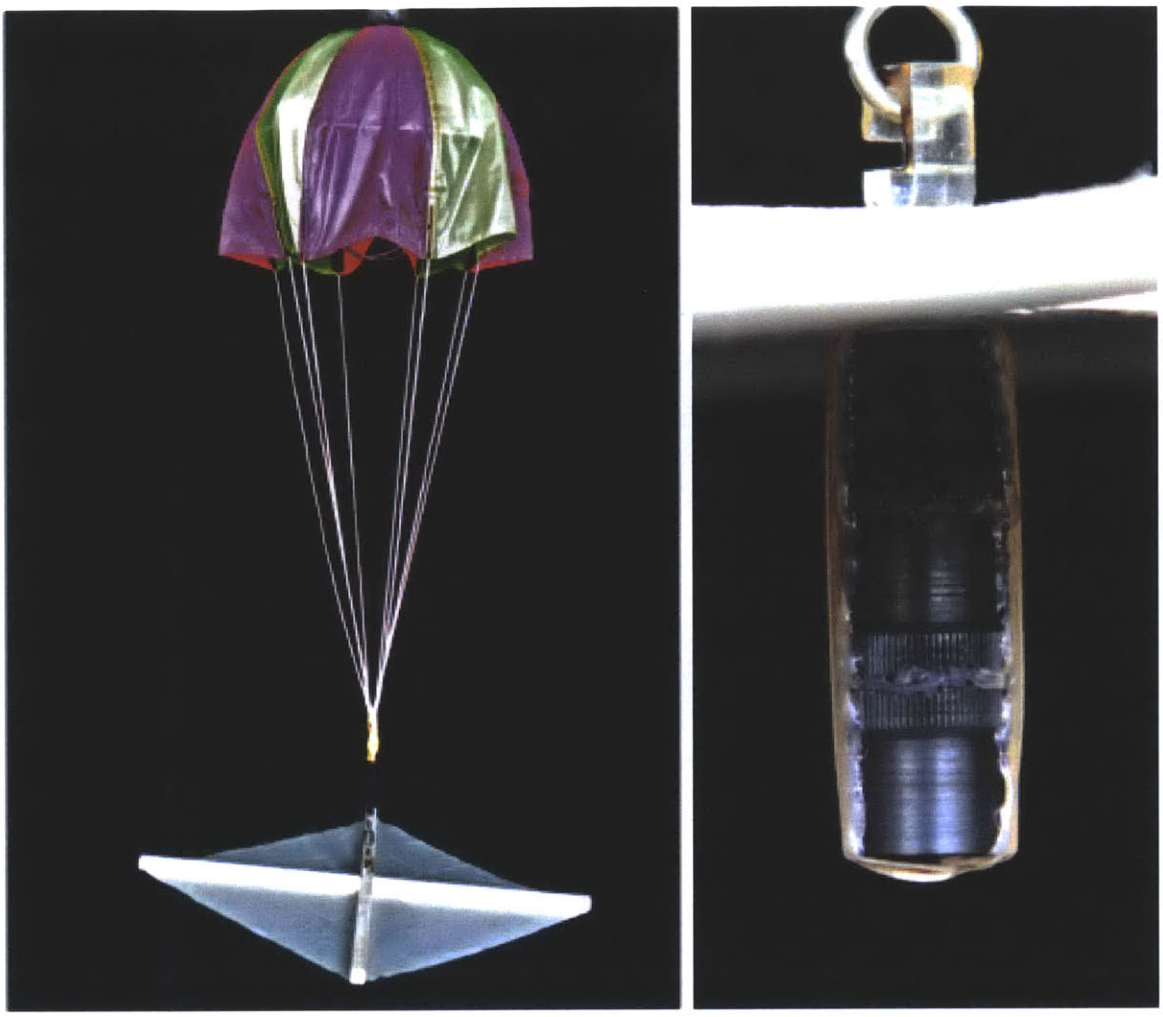

Figure 23: Left: Scaled-down parachute prototype with fabric square ground plane. Right: Weight added to prototype.

The devices were then dropped off from a three story building of about 30 feet and a video camera was used to capture the descent from two angles—one shot perpendicular to the descent and another from the ground. The fall rates and general performance of each device was noted. The next table presents a matrix the varied design parameters and their respective performances during the test.

Table 4: Testing matrix with varying ground plane configurations and summary of results.

	Mesh Circle	Fabric Circle	Mesh Square	Fabric Square	Wire Spider
Area	254.47 in^2 (D = 18 in)	254.47 in^2 (D = 18 in)	162 in^2 (13" x 13")	162 in^2 (13" x 13")	Negligible
Fall Time	4 s	4.2 s	4 s	4.8 s	N/A (Crashed)
Pros	Rigid mesh preserved shape	Drag from fabric increased fall time	Mesh very durable	Drag from fabric increased fall time	Lightweight Min. material Survived crash
Cons	Little additional drag contribution	Took a lot of damage	Little additional drag contribution	Slack from fabric did not retain shape	No additional drag contribution

Testing suggests the addition of a ground plane adds to the drag of the device through the air, improving flight endurance performance. This suggests that the plane should be created with solid fabric rather than just a wire framework or perforated material.

Though it is difficult to make a conclusive statement about the geometry of the plane, the shape does not seem to have a significant effect. Different factors were considered to determine which geometry to pursue. Though the square plane maintained its shape better, a typical discone antenna employs a circular ground plane. Additionally, the radial symmetry would facilitate the design of a foldable mechanism that could expand to 18" (diameter or diagonal length) but foldable to something that could fit in the small volume of the flare canister.

3.2.2 Glider: Addressing Stability Concerns

The glider concept could theoretically achieve reasonable flight endurance. However, a few concerns still remained:

(1) What kind of effect would the required 1 m boom would have on the performance of the device?

(2) Where should the boom be positioned to maintain the best stability and would active control be required?

To create the sketch model, an existing stunt kite (Prism 4-D Ultralight Stunt Kite) was modified to include the additional antenna structure. A one-meter rod of balsa wood was wrapped in aluminized Mylar and affixed to the kite using Velcro so that the boom could be moved relative to the center of mass. A payload of 70 g was put at the end of boom where the center of mass was determined to be located. The lowered position of the boom would theoretically increase the control sensitivity [2]. Three strings were used to help stabilize the position of the boom.

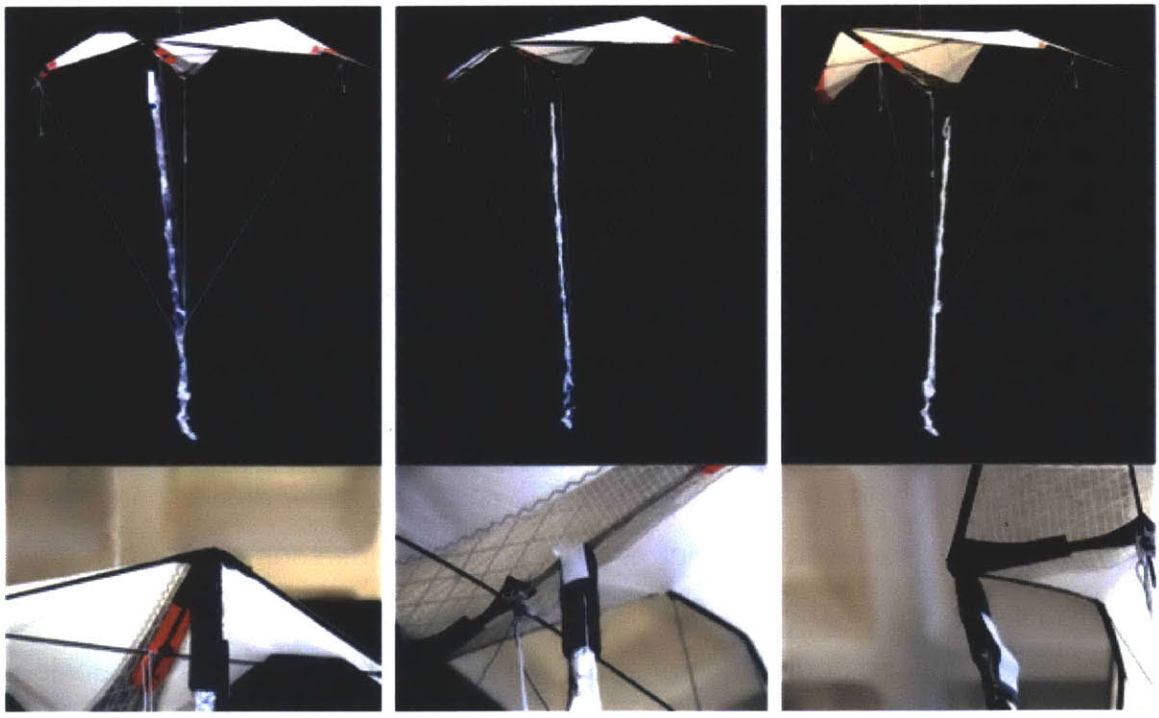

Figure 24: Hang glider prototype in three boom configurations: front, middle, back. Bottom images show corresponding Velcro connection points.

The glider model was then ready for testing. The intended procedure was to bring the glider to a four-story drop zone, adjust the position of the boom, and evaluate the performances of each configuration. However, when testing commenced, it was very difficult to get the glider to achieve stable flight. Regardless of the position of the boom, the prototype wanted to flip. This made testing with the model impossible and reconfirmed existing doubts about its feasibility.

After further evaluation, it was concluded that even if stable flight could be maintained without active control, the glider possessed too many parts to maintain structure that it would be very difficult to develop a mechanism that fold and auto deploy the glider but also fit within the limited size constraints.

3.3 Feasibility Conclusions

After narrowing down the initial ten concepts to three, a first-order feasibility analysis and sketch models were used to pick the most promising concept to pursue a detailed design for. Feasibility calculations showed that a lighter than air UAV device could not satisfy the design constraints. Changing altitude and atmospheric conditions had too significant of an effect on balloon performance making it difficult to design a reliable device. Additionally, the size constraint could not be met with a balloon since the volume of compressed gas needed exceeded available canister space.

Calculations suggested that both a parachute and hang glider design could potentially work. However, pursuing a glider would be quite complicated. Stability issues remained a significant concern due to its bistable nature. The lack of symmetry and abundance of structural parts would also make the design of folding mechanism that could fit in the volume constraints very complicated and close to impossible--such a device frame would have to be inflatable. Pursuing such a design would pose too many risks.

The parachute concept had the most potential given the time frame and scope of the project. Calculations suggested that required parameters could be met and testing help to address potential concerns were not a big issue. It was a simple and elegant solution that could be easily implemented and thoroughly explored. The fewer areas of concern and parameters to worry about made it so that optimization of the design could be easily achieved.

4 Folding Concept Exploration

The next step in the design process was to prototype different mechanisms to fold up the ground plane. To achieve a baseline operating frequency of 120 MHz, the plane would have to be at least 17.2" in diameter while fitting in a 1.89" x 2.44" x 7.09" space. The mechanism would also have to be robust enough to withstand impulsive forces—once during the initial cartridge ejection and again when the parachute opens—as well as retain its structure during the descent. It would also have to be lightweight enough to help reduce weight and thus increase endurance time. Two designs were developed and quickly tested—a pop-out tent inspired one and an umbrella inspired one.

4.1 Pop-Out Design

The first design uses spring-loaded hinges to unfold two sets of armatures out from a central spine.

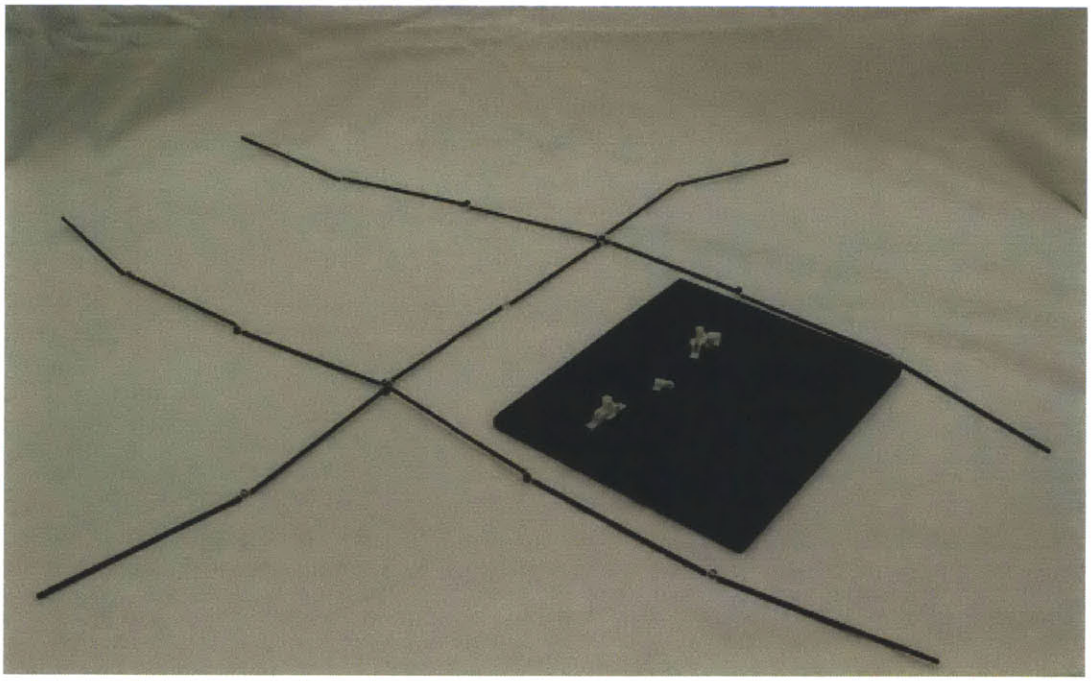

Figure 25: Unfolded sketch model and joints.

The framework is composed of circular carbon fiber tubes that fold up against one another to be stored inside the cartridge. Torsional springs were glued in between 6-inch tubes of carbon fiber to test the folding and sizing of the structure.

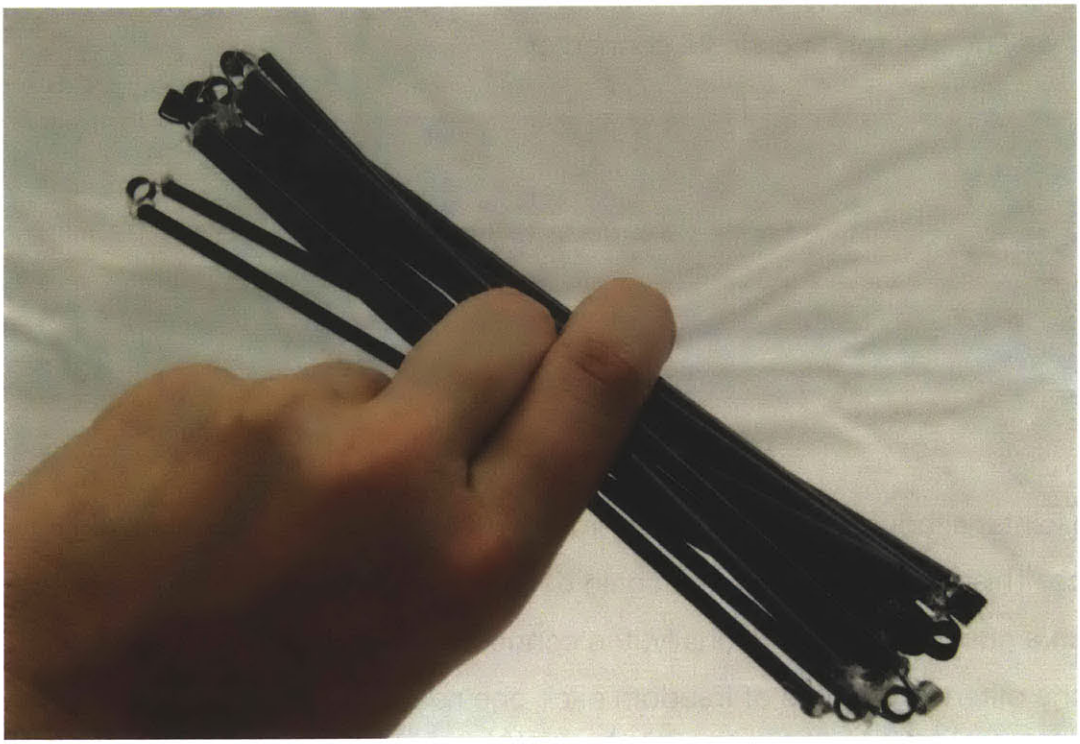

Figure 26: Folded sketch model.

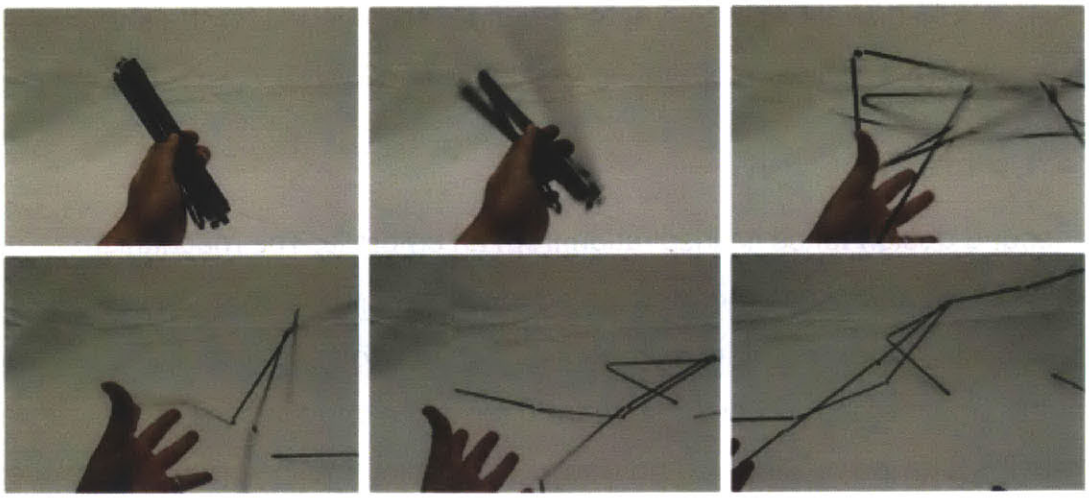

Figure 27: Sketch model unfolding.

The structure would automatically open as desired, but it would droop due to the weight of the tubes. In order to constrain each armature from sagging down below horizontal, joints were designed for each specific location. Each pair of joints would create hard stops to prevent over-rotation. Three types of connectors were designed to form the necessary joints: three way connector, four way connector, and single connector.

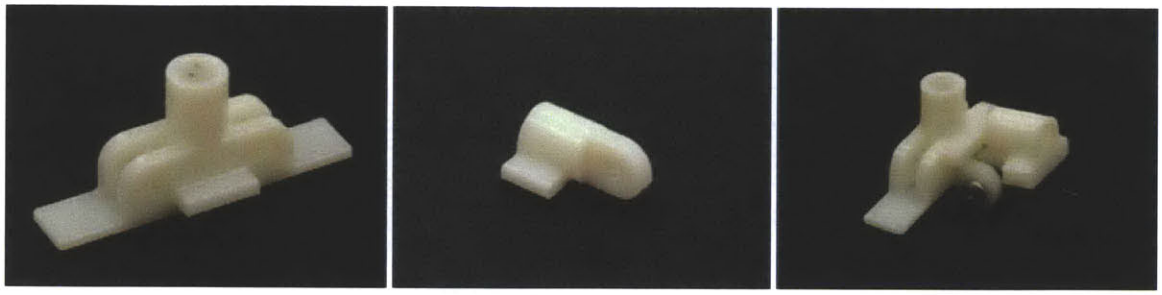

Figure 28: 3D Printed connectors.

The joints, although preventing over-rotation, did not lock the mechanism into place. This meant that the arms could deflect away from their desired positions given a gust of wind. Additionally, the connectors were bulky to accommodate for the different degrees of freedom each one needed to support. The design, however, did accomplish its goal of folding a large ground plane down into the available working volume supplied by the cartridge. If optimized, it could even be used to fold down a 41.2" diameter ground plane needed for the stretch requirements of a minimum operating frequency of 50 MHz.

4.2 Umbrella Design

The second design takes its inspiration from an umbrella. The mechanism consists of eight spokes around about a central strut. The spokes utilize a four bar mechanism with two of its members pinned to two central strut and left free to rotate. One member is constrained from moving along the central strut while the other is allowed to slide up and down. This sliding motion opens and closes the mechanism.

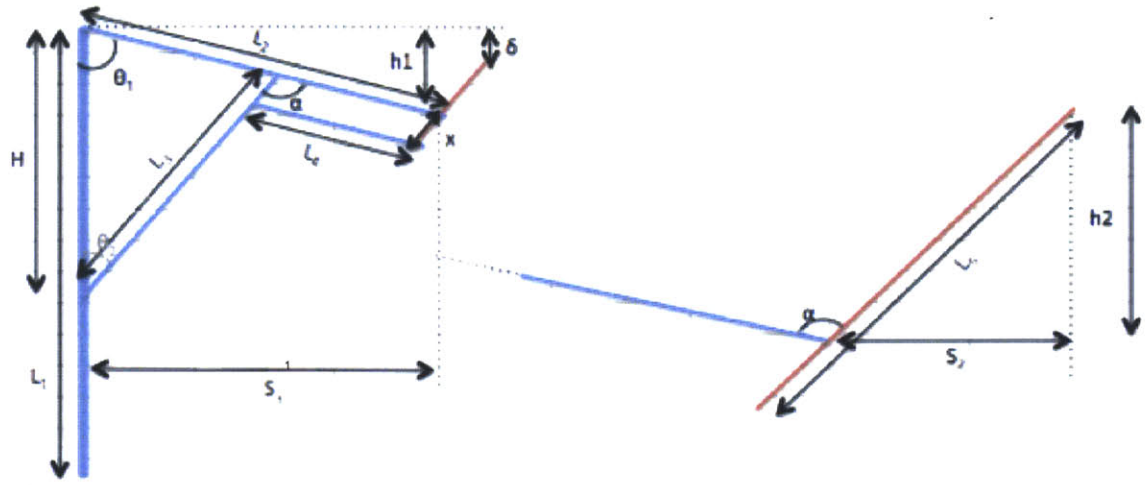

Figure 29: Left shows a labeled diagram of one spoke of umbrella folding mechanism; right shows an expanded view of the final spoke, highlighted in red. (Diagram not drawn to scale)

Figure 29 shows a diagram of what one spoke would look like and labels different parameters that can be optimized. Each member and its length is labeled with *L*#. Input parameters were chosen to be:

(1) Distance between L_2 and L_3 when opened (H)

(2) Span of the mechanism when opened ($S_1 + S_2$)

(3) Length of the mechanism when closed (L_1)

(4) Angle between L_1 and L_2 (θ_1)

(5) Angle between L_5 and L_2 (θ_1)

The additional parameters were calculated using the following equations:

$$L_2 = \frac{S_1}{\sin \theta_1} \qquad \text{Eq. 19}$$

$$x = L_1 - L_2 \qquad \text{Eq. 20}$$

$$\theta_2 = 2 * \tan^{-1}\left(\frac{\cos\theta_1 - H}{\mathrm{L} * \sin\theta_1}\right) + \theta_1 \quad \text{Eq. 21}$$

$$L_4 = L_2 - \left(\frac{H}{\cos\theta_1 + \frac{\sin\theta_1}{\tan\theta_2}}\right) + x \quad \text{Eq. 22}$$

$$L_3 = \frac{\sin\theta_1}{\sin\theta_2}(L_2 - L_4) \quad \text{Eq. 23}$$

$$L_5 = 2 * \tan^{-1}\left(\frac{S_2}{\cos(90 - \theta_1)}\right) + x \quad \text{Eq. 24}$$

A sketch model was then created once a set of workable dimensions was established. All the pieces were laser cut out of 1/8" acrylic, with each strut measuring 1/4" wide. The members were held together with half pressed rivets to serve as pin joints.

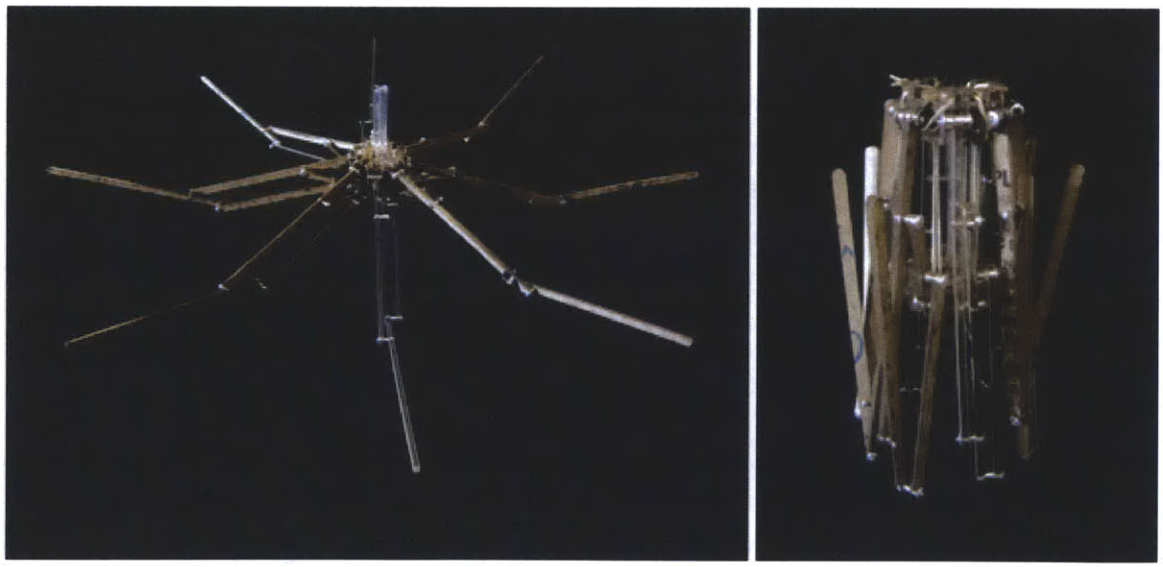

Figure 30: Acrylic prototype open (left) and closed (right).

The sketch model served as a proof of concept in the mechanism's ability to fold down an appropriate size. The structure met the minimum 17.could also not be expanded much past 18". This is because any additional four bar linkages to

extend the length would increase the size of the closed mechanisms, exceeding the space constraints given. The design revealed interference points between linkages and pin joints. These could be addressed, however, by adding spacers between the linkages so that they could fold past one another. The prototype also showed a potential area of bi-stability that could potential pose an issue to the structure's integrity.

The model showed that this design provided a more rigid structure for the ground plane and thus had better potential to withstand high deployment forces. Additionally, the friction in the design suggested that it could maintain an open state without the need of a locking device. To open such a mechanism, the one of the central discs that the linkages were attached to could be tethered to strings of the parachute. The aerodynamic forces generated from the parachute deployment could then pull the slider up and open the mechanism.

4.3 Choosing a Mechanism

The two mechanisms both were able to successfully fold a large ground plane down to the available volume. Both designs were then evaluated for compactness when folded, simplicity and part count, structural integrity, and ability to resolve existing concerns.

Although the first design could potentially fold up a larger ground plane with little difficulty, the mechanism's structural integrity was at question. It could not maintain its shape very well and drooped under its own weight. A locking device or stiff elastic joints could potentially solve the problem. However, having locking capability added complexity and parts to the design, which is undesirable as it increases weight and makes manufacturing difficult. This is especially a problem since the current joints were quite big to begin and it would be optimal to be able to slim them down in the next iteration. Additionally, there was not much support for each of the armatures so it was questionable how well it would hold up under the dynamic forces on its descent.

The second design, though it could not support as large of a ground plane, did meet the base requirements. If desired, a more complex mechanism could possibly be incorporated to add additional linkages and extend the length at some later point. The interference between linkages and joints as well as the bi-stability were both two issues that could be easily mitigated by changing the dimensions and/or adding the ground plane. Additionally, the unfolding would be simple, coupling the aerodynamic forces of deployment. With its advantages greatly outweighing any concerns, the second design was chosen for further development and optimization.

5 Integration and Fabrication

With the flight and folding concepts chosen, the next step was optimization and integration into a functional system. Detailed design,with the aid of CAD and CAE, consisted of parameter optimization, material selection, and antenna integration. Additionally, the sabot and deployment method was designed as well.

After a design was finalized, an alpha prototype was built. The prototype employed all features of the design that were deemed reasonable for demonstration of a functional device.

5.1 Detailed Design

Dimensions needed to be optimized to fold the mechanism down as compactly as possible. Space for the payload, parachute, and any deployment hardware had to be accounted for as well. Different materials were chosen and tested through finite element analysis to ensure that the device could withstand high forces while not being too heavy. The details of how to turn the device into an antenna were also developed and were reflected in the prototype.

5.1.1 Final Folding Mechanism

The chosen mechanism still had some issues that needed to be addressed. The same input parameters and equations from Section 4.2 were used to determine the linkage dimensions. Additionally, the optimized parameters would also have to satisfy the following constraints:

(1) The folded height of the device not exceed 5.7" to allow space for the minimum payload volume of 2.25" x 1.5" x 1.0" and antenna integration hardware.

(2) The span of the open device should be at least 17.2" to meet minimum operating frequency.

(3) The diameter of the folded device should be less than 1.8".

(4) Link 3 and Link 5 must not interfere when closing.

(5) The number of spokes chosen should be small enough so that there is enough assembly room for screwing together the pin joints.

(6) There should adequate spacing between linkages so that they can clear each other and hinges, allowing them to fold up against each other.

(7) The end tip of Link 5 should be within 1" of the top of central disc, preferably lower, to allow proper ground plane attachment.

A worksheet was created to develop several sets of workable dimensions.

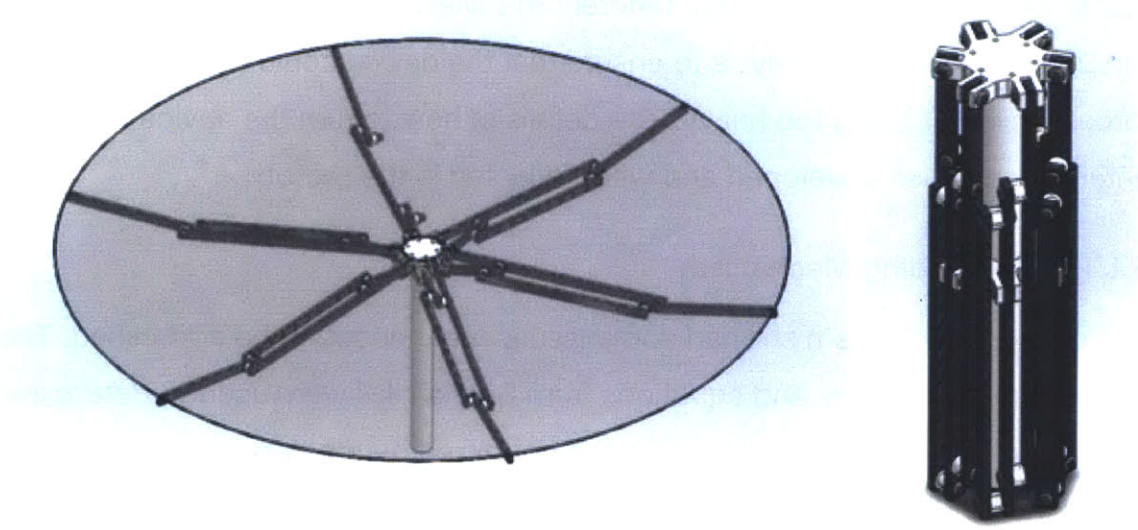

Figure 31: CAD showing open and closed device.

These sets were modeled in CAD, keeping in mind the actually materials that would be used, to ensure that the device would fold properly and would meet

size constraints in both open and closed positions. Many iterations were tested before a final set of dimensions was chosen.

The central tube and two center discs were ABS so that they were an insulator for the antenna electronics. The two discs were designed to be hexagonal with tabs for the linkages. The tabs of the top and bottom discs would be on opposite sides of the hexagon so that Link 2 and Link 3 could fold past one another. Pin joints would be used to hold the linkages to the center discs and to each other and a nylon spacer would be employed where needed to ensure proper spacing between linkages. The ground plane would be created with a circular conductive rip-stop nylon fabric and would provide a tension force to offset the bistable nature of the mechanism. In other words, it would prevent the plane from inverting. The center discs have 8 holes through which the strings of the parachute would be threaded. The strings were connected to the bottom disc to allow the deployment force of the parachute to slide the disc up and open the device. Finally, the linkages were flat struts of rectangular cross section, originally chosen to be carbon fiber for lightness and strength. However, in the next section, an analysis of material selection is done to determine whether this would even be necessary.

5.1.2 Modeling the Design

After the design was properly modeled in CAD with appropriate material properties, a finite element analysis was performed to ensure that the device could survive the deployment forces. Since the initial deployment speed is the fastest speed the open UAV should experience, the deployment forces should also be the strongest. A 30" diameter parachute was chosen.

The FEA was performed on one spoke of the mechanism using radial symmetry and used 1/6 of calculated deployment forces. Details on the exact setup and input can be found in Appendix D (carbon fiber) and Appendix E (Al-2024).

The device would open around 30,000 ft after the sabot reaches terminal velocity. This was calculated using the frontal face of the sabot measuring 1.89" x 2.44" with drag coefficient of 1.0 and a drag ribbon of 2.44" by 1.5 m with drag coefficient of 0.8". The terminal velocity of the sabot would determine the dynamic pressure felt by the faces of the linkages and the drag forces produced by the ground plane and the parachute. The combined weight of the sabot, parachute, payload, and deployment electronics was estimated to be 0.36 kg. The additional weight from the frame of the device would be dependent on the material of the linkages. The first material tested was carbon fiber, chosen for its low density but high ultimate tensile strength (UTS). The resultant stresses from the FEA are presented in Figure 32.

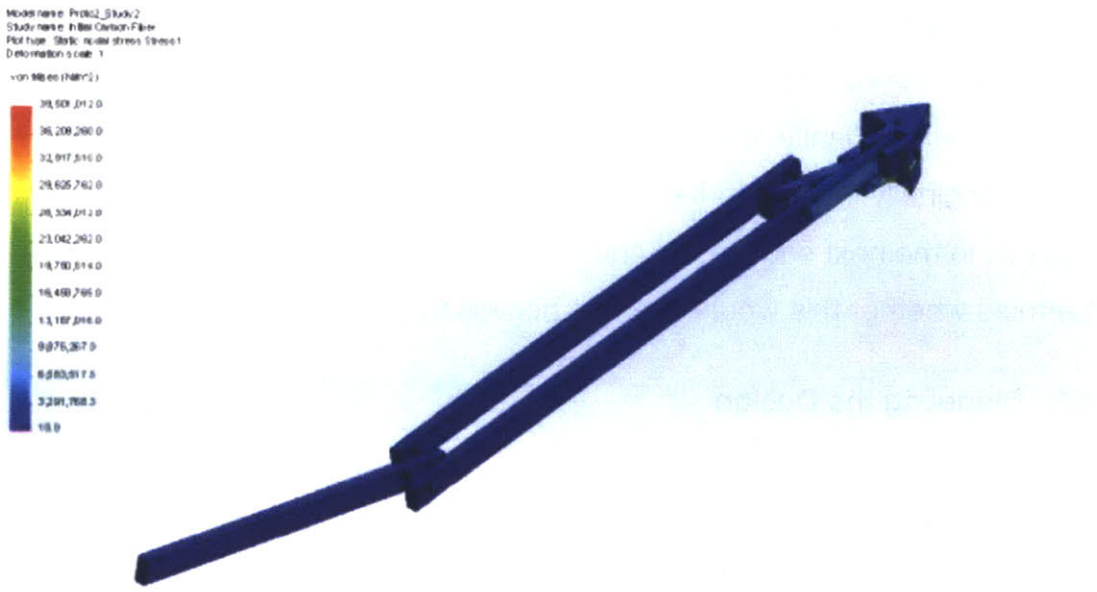

Figure 32: FEA of carbon fiber spoke under initial loading conditions.

The results from the analysis showed no potential hazard points. The maximum stress encountered by the mechanism is well below that of carbon fiber's

ultimate tensile strength resulting in a safety factor of at least 300. This prompted a reevaluation of the material choice.

Aluminum 2024 was chosen for analysis. It had a high yield strength and UTS, was still very light, and much more machinable than carbon fiber. The resultant stresses from the FEA are presented below:

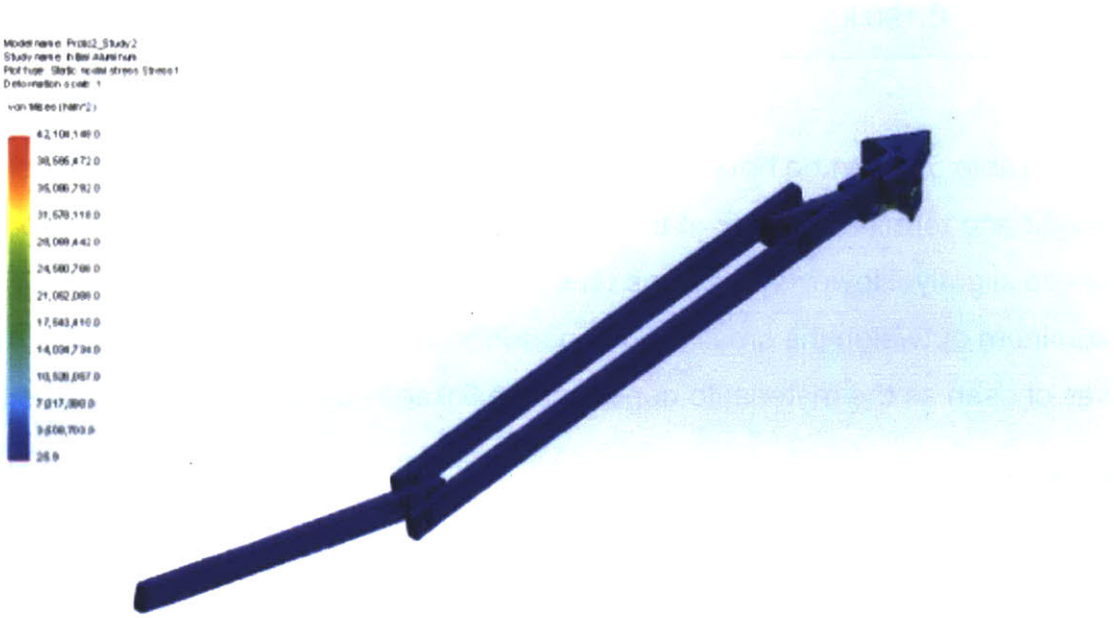

Figure 33: FEA of Aluminum spoke under initial loading conditions.

The results of the analysis show that aluminum could also withstand the deployment forces. The following table summarizes the results of the comparison.

Table 5: Comparison of performance between carbon fiber and Al-2024.

Material	Combined Mass	Deployment Velocity	Resultant Stress	Safety Factor	Machinability
Carbon Fiber	0.145 kg	52.1 m/s	39.5 MPa	380	Poor
Al-2024	0.190 kg	53.9 m/s	42.1 MPa	27	Very Good

From Table 5, it can be noted that the increased weight of Al-2024 increases the weight and terminal velocity of the sabot, decreasing the performance of the device slightly. However, the large time saved and convenience of working with aluminum outweigh the small drop in performance. With this in mind, Al-2024 was chosen as the material to construct the linkages out of for the prototype.

5.1.3 Antenna Integration

The next step of the design was to integrate the antenna hardware. The design called for a conductive ground plane to serve as the disc and six to eight wires to form the cone. As mentioned previously in the background, the ideal cone angle is 25 to 40 degrees from vertical. Using Equations 2 and 3 for minimum operating frequency, the diameter of disc and length of the cone were determined to be at least 17.2" and 24.6" respectively. Using geometry, the opening of the cone can range from a diameter of 20.8" to 31.6".

A 30"-diameter chute with eight lines was chosen. The lines would be made of nylon and strung through the central sliding discs of the mechanism to open the device and take most of the forces. The wire of the cone would be sewn to these nylon lines, clear of any sliding areas so that the electrical connections would not have to endure any force. The angle of the cone can be adjusted by changing the length of the wires and the nylon line.

To create the antenna, a 50-ohm coaxial cable would be used and passed through the ABS tube to the outside of the device. The top central disc of the mechanism has two holes—a center tapped hole for a retaining screw and hole to the side for the outer conductor to pass through. The outer conductor is soldered to a copper washer that sits in a groove on the surface of the central disc. The ground plane fabric is laid on top of the washer, followed by a small plastic disc to be used as an insulator between the disc and the cone. This disc thickness and size can be changed to vary the performance of the antenna. On top of the insulator, another copper disc is placed and a screw holds the components together. The top copper washer is soldered to the wires of the cones and the screw is soldered to the center conductor of the coaxial cable. The signal can then be passed to the cone and disc through the coaxial cable.

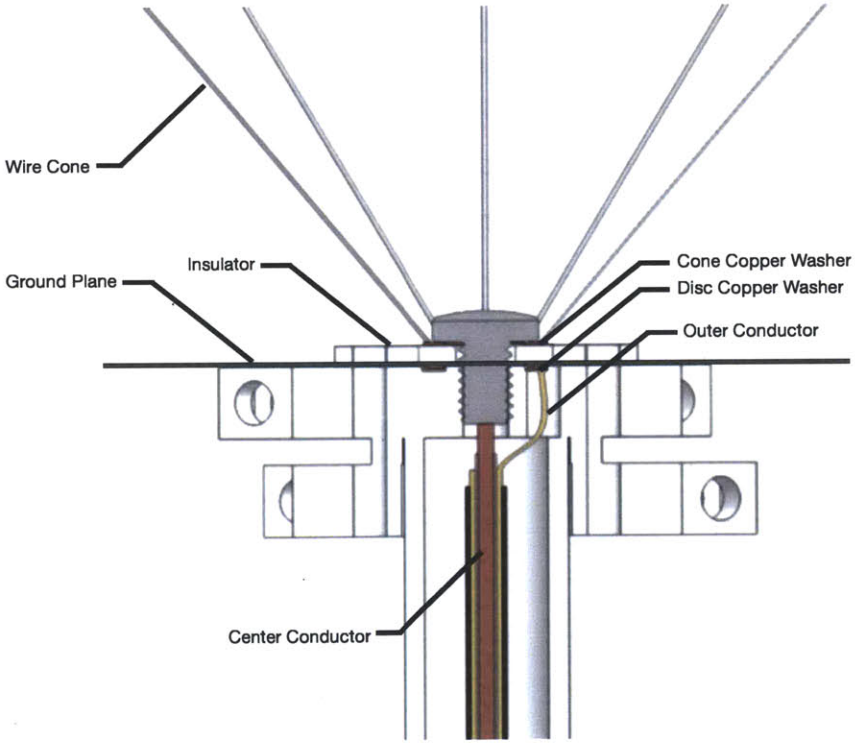

Figure 34: Sectional view of UAV central strut with antenna integration.

5.2 Device Fabrication

Once the details of the design were finalized, the fabrication of a demonstration prototype began. The center discs were 3D printed ABS and the linkages were cut from a 0.100" thick aluminum sheet using a waterjet. Six sets of four types of linkages were cut.

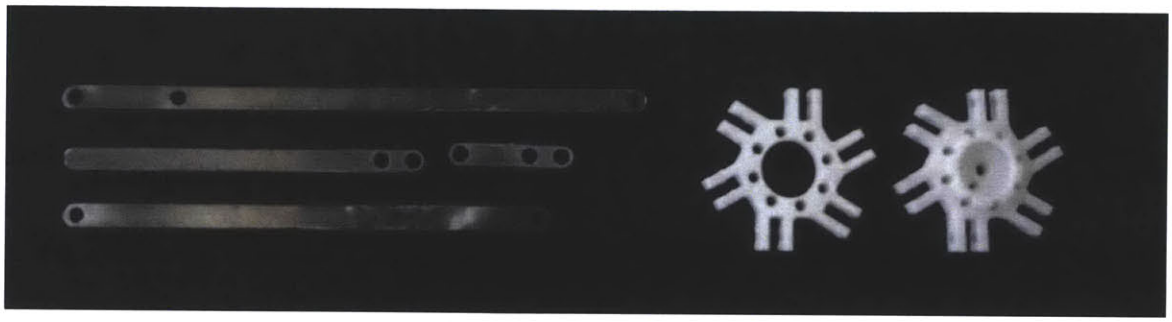

Figure 35: Waterjet aluminum linkages (L2, L5, L3, L4) and 3D printed bottom and top center discs.

Pin joints were used to connect the linkages to the center discs and each other. The joints consisted of an internally threaded steel standoff capped by machine screws. A little bit of Loctite was used to hold the joints in place once the mechanism was assembled. An ABS tube was then cut to length and epoxied to the top center disc.

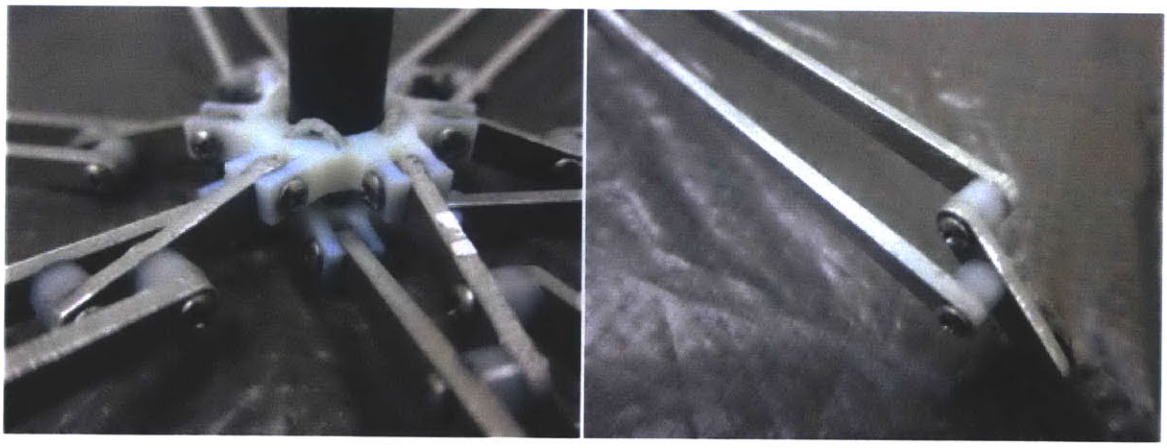

Figure 36: Assembled folding mechanism with close up of pin joints.

Next, the ground plane was created by hemming a 17.5"-diameter circular piece of conductive nylon. Six pockets were sewn so that the end of the folding mechanism could sit inside the pocket. A small hole was drilled in these linkages and the fabric plane was stitched to the linkage to secure it in place. The plane successfully held the structure in the desired positioned and helped to maintain its structure. A bit of flop and inversion was still observed if force was applied, but it did not greatly affect the desire size of the plane.

Figure 37: Ground plane fabric with pocket for linkage.

Once the ground plane was made, the antenna hardware could be installed as described in the previous section. The ground plane fabric had holes cut in for the center conductor as well the nylon strings that would pass through. The insulator was made with a laser cut piece of acrylic and sat on top of the fabric to prevent fraying from the holes. The wires of the cone can be super-flex wires or conductive thread, but they were not soldered to the top copper washer for this demonstration alpha prototype.

Figure 38: Ground plane with antenna hardware installed minus soldered cone wires.

With everything assembled, the mechanism was tested. The opening ability and closed and open states were examined.

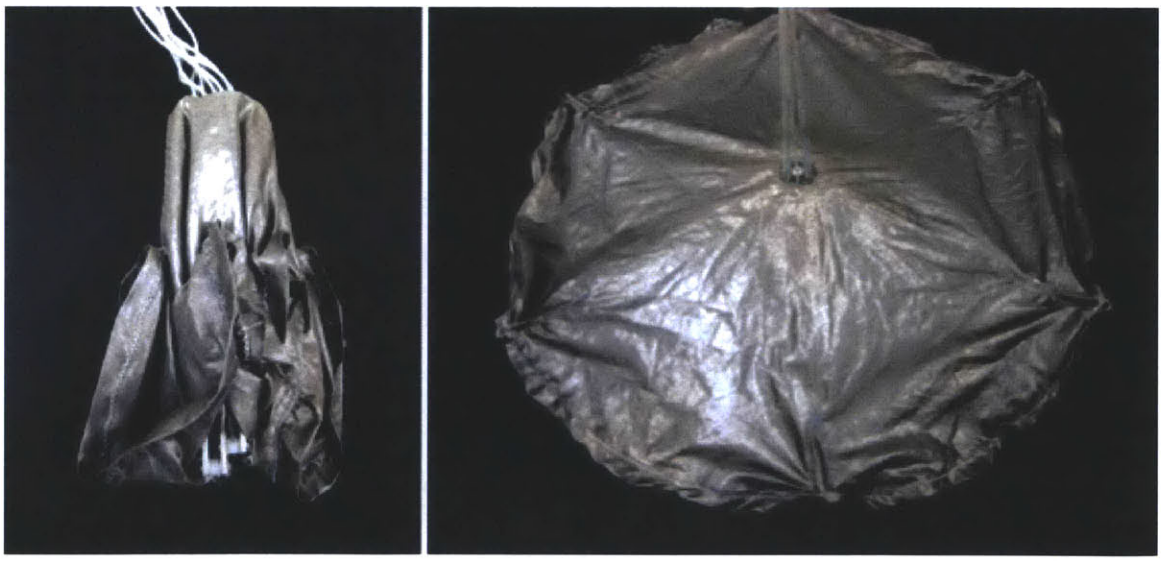

Figure 39: Closed and open device.

The prototype exhibited some difficulty opening due to a potential singularity when everything folded flat. However, if the spokes were pushed out just a little, the singularity was avoided and the mechanism could easily be open by pulling

on the nylon parachute strings. To remedy this issue, a spring-loaded mechanism was designed to push the spokes out upon deployment. The mechanism is hexagonal and would sit in the center of the closed device.

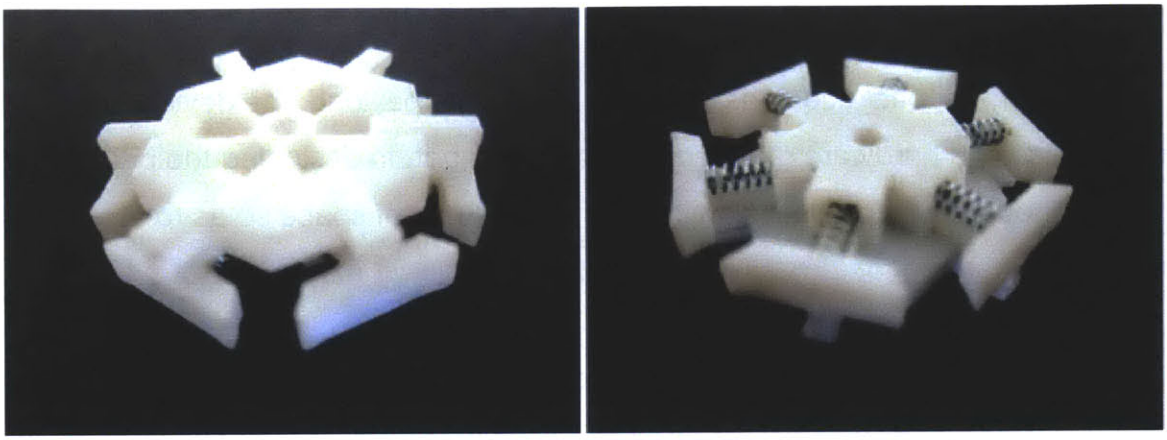

Figure 40: Top and bottom view of 3D-printed springer device.

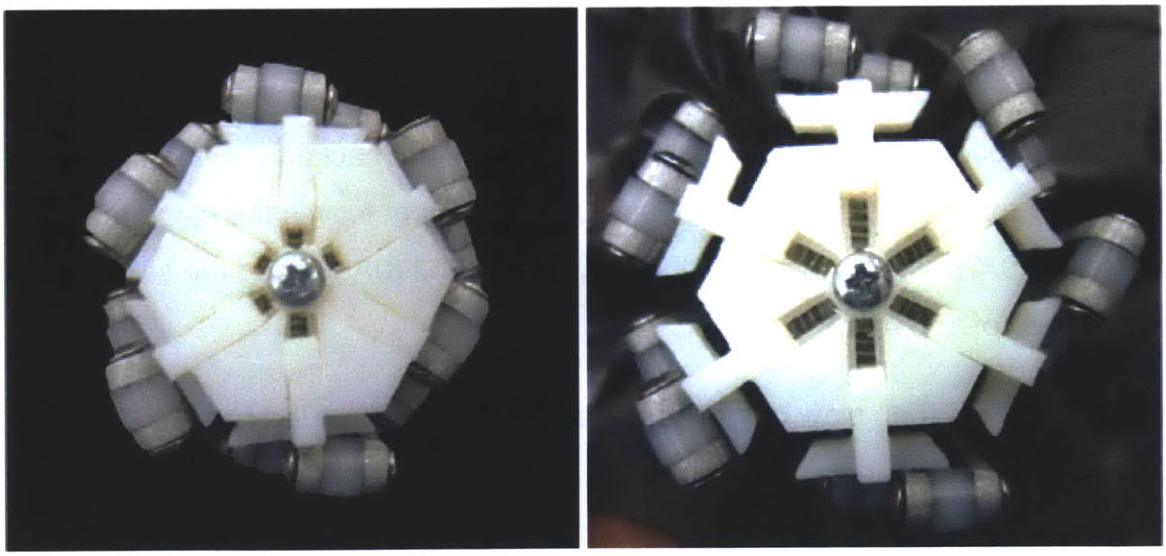

Figure 41: Springs placed in the center of the folding mechanism. Left shows partially closed and right shows fully opened position.

A little lubrication was also applied to the joints. With all these fixes in place, the mechanism easily opened with a little shake simulating its drop out of the sabot.

Altogether, the completed prototype weighed about .184 kg, which is about 0.2 kg lighter than the FEA estimated weight due to the removal of some excess

hardware that came with the parachute. The decrease in weight is reassuring as it validates the initially feasibility analysis was on the conservative side. A lower weight results in lower terminal velocity speeds and drag forces.

5.3 Deployment Package

The deployment package consists of the sabot, the payload, the device, and the electronics and hardware required to open the sabot. In designing the package, a lot of thought was put into how to optimize the use of space so as to fit everything needed for successful deployment.

5.3.1 Ejection Conditions

The sabot was designed so that it could take most of the compressive forces from the initial ejection as well as slow the package down to a reasonable speed before deploying the antenna. During ejection, the sabot must burst through the end cap of the flare cartridge, which requires 125 lbf.

During ejection, an explosion is used to accelerate the package up to 300 G. Assuming this impulse lasts for about 0.01 s, the sabot leaves the plane at a speed of 29.4 m/s. The plane itself is traveling at 250 KIAS giving the sabot a total speed of 158 m/s.

The sabot must then slow down. Terminal velocity is calculated to be 45.3 m/s assuming a total weight of around .5 kg. A ratio of the sabot's actual velocity to its terminal velocity can be used to evaluate when the UAV should be deployed. The following plot shows the sabot's descent over time from 30,000 ft.

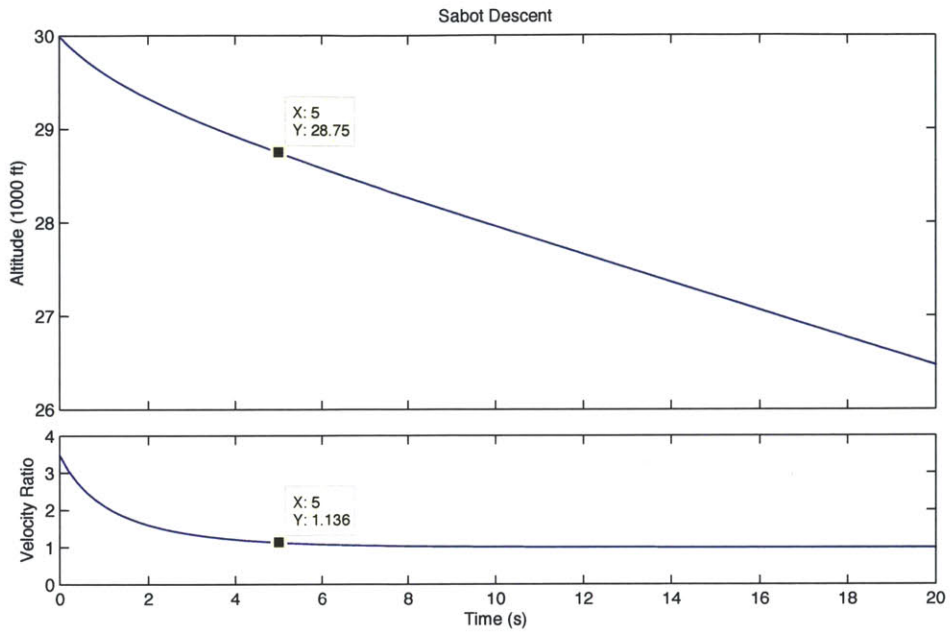

Figure 42: Top plot shows the sabot's altitude and the bottom shows the velocity ratio both versus time.

At five seconds, it can be noted that the drop in altitude is constant but the change in velocity ratio has become marginal. The velocity ratio has flattened out to around one. At this point, it would be most appropriate to deploy the UAV since waiting any longer would only lose more altitude without significant gains in speed reduction.

5.3.2 Design and Fabrication of the Deployment System

The sabot was made from 0.050" thick Al-5054 T3 so that it could achieve the required maximum bend radius of 0.075" required to maximize the usage of the working volume.

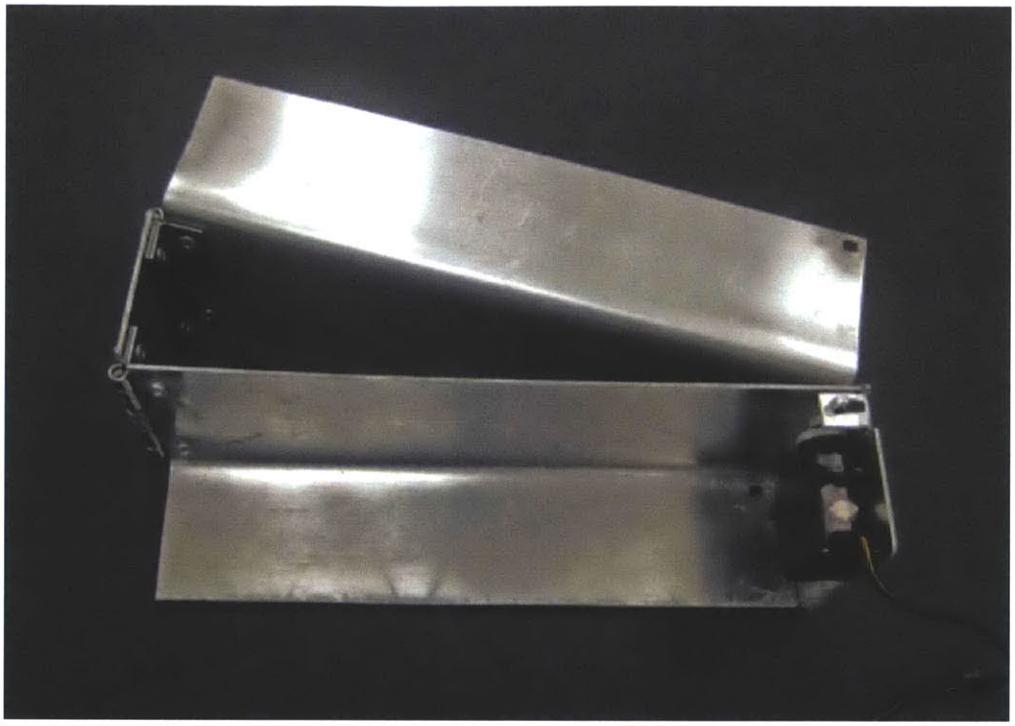

Figure 43: Open sabot made of Al-5054 sheet metal.

Two aluminum sheets, each bent at 90°, make up the four long sides of the sabot. These angle pieces were joined to a top aluminum plate by spring-loaded hinges. A drag ribbon can be attached to this top plate. Finally a bottom plate was epoxied to one of the angles. The top plate sits over the edges of the wall so that during ejection, forces are transferred along the sides of the sabot rather than to the device itself.

The bottom plate has a tab with a notch in it that matches up to a notch in the opposite wall of the other aluminum angle. A servo was epoxied to the inside face of the top plate. An aluminum linkage was attached to the plastic head of the servo.

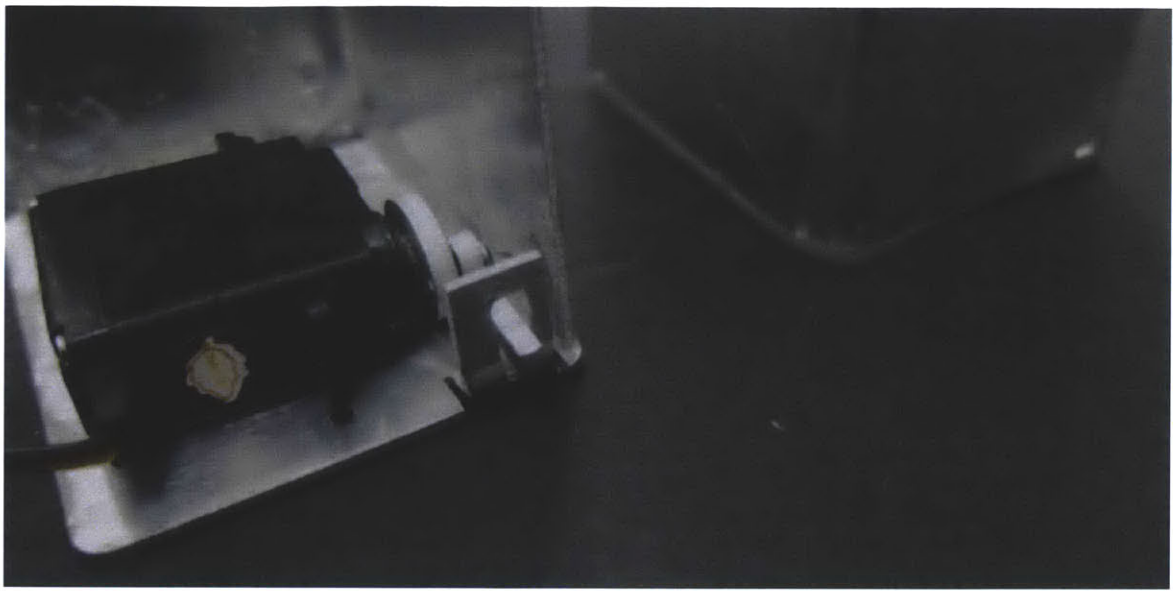

Figure 44: Close-up of servo and opening mechanism with notches in tab and in opposite wall of second angle also shown.

The mechanism converts rotation of the servo into the translation of a little armature in and out of the notches. This is responsible for locking and opening the device.

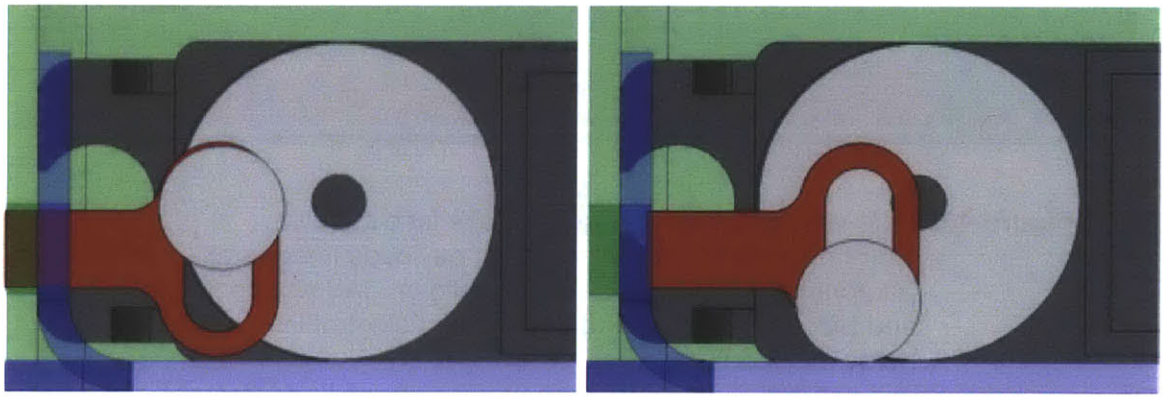

Figure 45: Diagram of mechanism showing pin in locked position (left) and open position (right). Sidewall shown as green, bottom plate as blue, and pin highlighted in red.

A microcontroller was used to control the servo. In practice, the microcontroller will signal the servo to move the pin five seconds after the ejection. To accomplish this, a magnetic switch can be used. A magnet would be placed in

the barrel firing the flare that would mate with a magnetic switch in the sabot. Once the sabot is ejected, the switch activates the circuit and the timer will begin.

5.3.3 Optimizing Space Usage

Once the sabot was designed and fabricated, concerns over space became apparent. The initial rectangular payload would take up the remainder of free space in the sabot, leaving no room for any deployment hardware such as the servo. However, there was a large amount of unused space below the central strut that a payload could potentially go in. With the aid of CAD, all the components of the system were laid out with a new payload geometry.

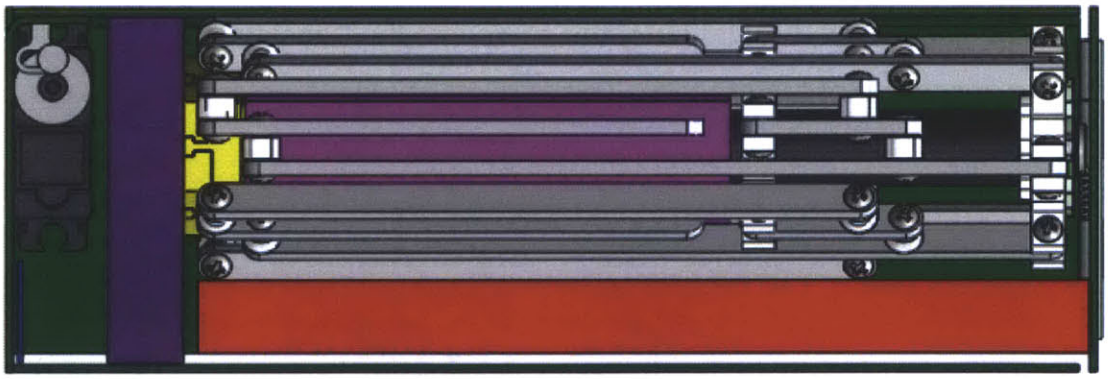

Figure 46: Side view of UAV package with one face cut away. Components: sabot walls (green), payloads (magenta), parachute space (red), springer (yellow), UAV device (white and black in top left), and deployment electronics (bottom below payload).

The payload was changed to a hexagonal tube that would attach to the end of the central rod. The mechanism used to open the device would sit at the bottom of the payload. Once the sabot opens, only the antenna and payload would remain; everything else would fall off and therefore will not add weight and increase the rate of descent. Additionally, another rectangular payload of dimensions 1.7" x 2.32" x 0.50 would also fit in the sabot. This could house PCB

boards or any parts of the payload that needs to be farther from the antenna and then suspended away from the UAV itself. The new payload geometry can accommodate up to a volume of 5.01 in^3, which is even greater than the initial requirement of 3.375 in^3.

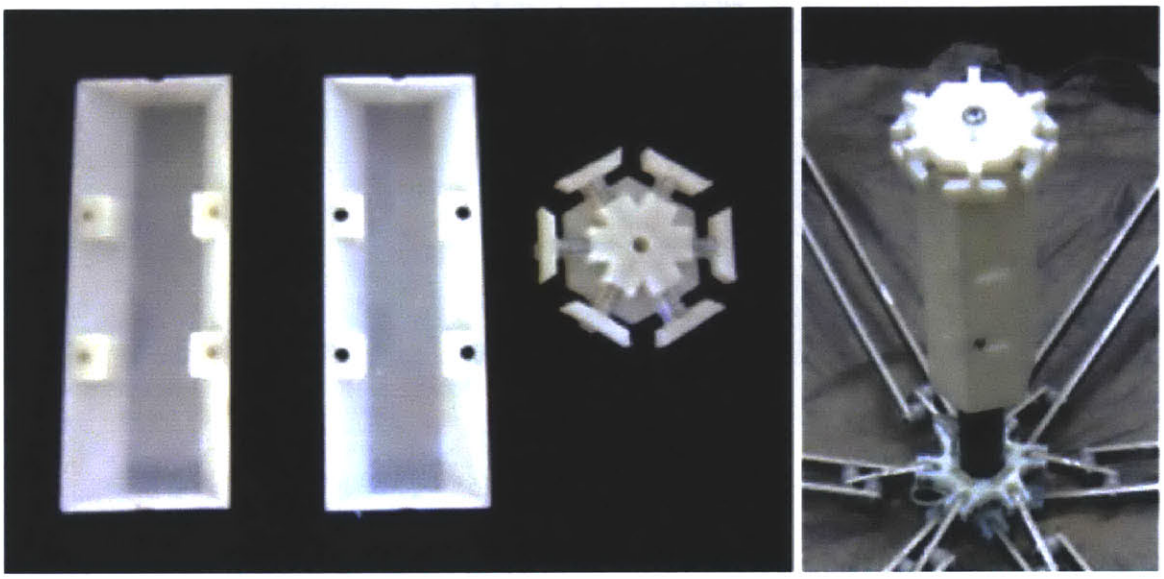

Figure 47: 3D printed payload and springer mechanism.

For the prototype, a 3D printed hexagonal tube was used for the payload. The springer was also kept attached to the payload for testing. The inside of the hexagonal payload was kept hollow so that weight could be added to bring it up to 70 g. The UAV device weighed 0.254 g overall.

Once everything for the prototype was fabricated, the deployment package was assembled.

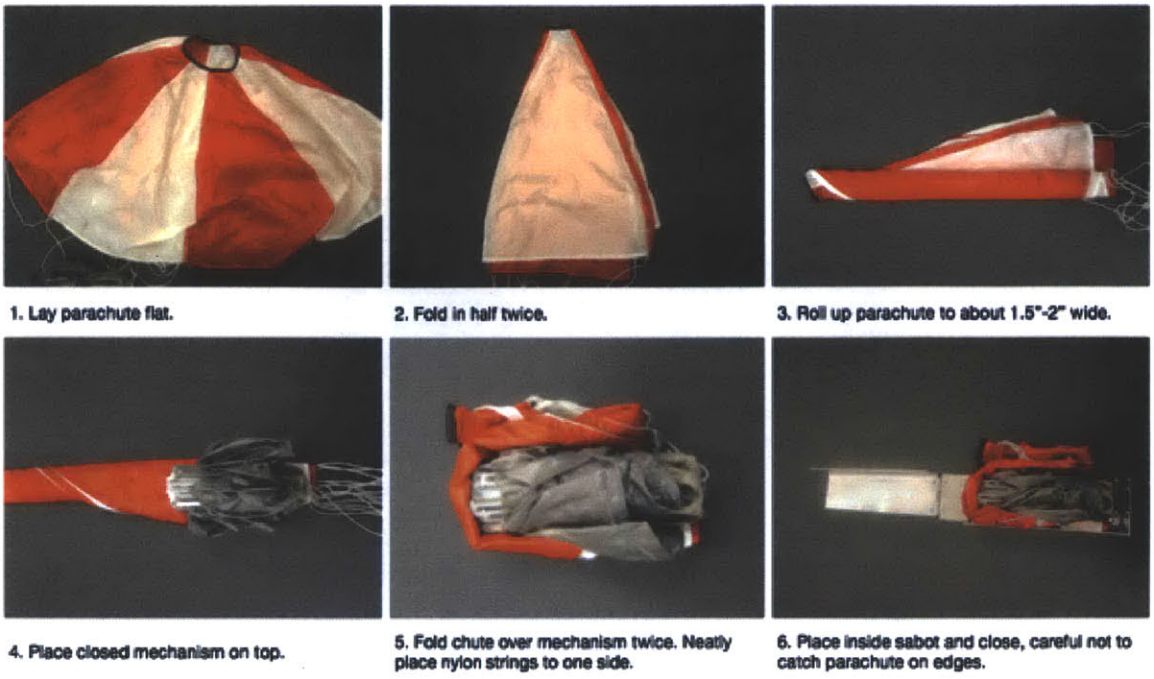

Figure 48: Steps to properly packing the parachute inside the sabot.

The parachute was rolled up tightly and folded around the ground plane so as to not take up any vertical space. Deployment electronics were stuffed inside on the bottom, and enough room was left for what could be a second payload. The sabot was carefully closed to avoid tearing any of the nylon. An RC controller was used to activate the servo and test the deployment mechanism.

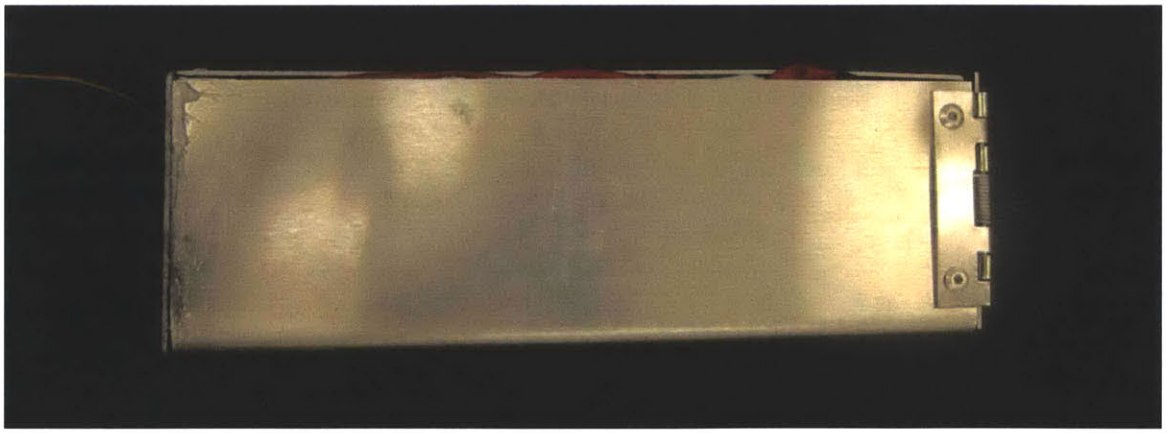

Figure 49: Fully assembled deployment package.

6 Testing the Device

6.1 Impulse Survivability

The UAV package has to undergo a large impulse force when exiting the flare. In order to simulate this, an air cannon was used to shoot out the sabot. The goal of this experiment was to test survivability of the both the sabot and the UAV mechanism.

In the experiment, the air cannon was pressurized to 35 PSI. Such a pressure would impart an impulsive force, accelerating the device up to 146 G. The cannon was angled at 55° from the ground. Two cameras were used to record the shots. One was used to capture the initial shot out of the sabot to determine the speed and another was placed farther away to capture the trajectory. The cannon was stuff with a plastic bag and the sabot was lightly wrapped in another to form an air seal. A small drag ribbon was attached to the projectile to ensure proper orientation during its trajectory.

Figure 50: Testing setup with air cannon and two cameras.

The first test involved shooting a dummy block of the correct weight and dimensions to test the speed and trajectory of the device. After analyzing the video, the ejection velocity is estimated to be about 11.5 m/s.

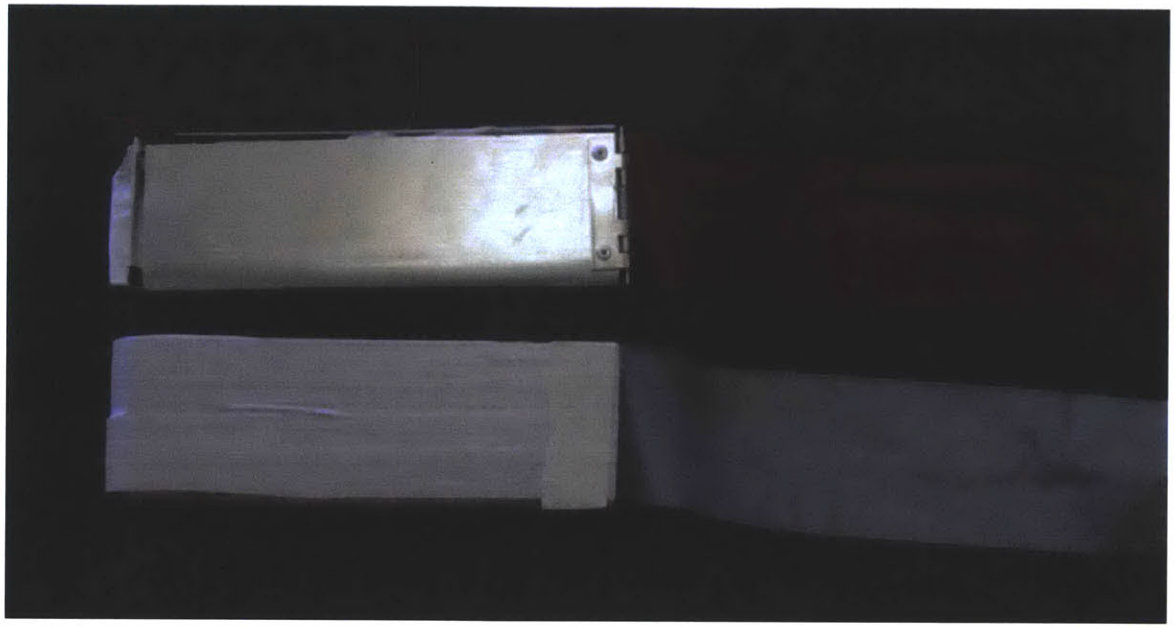

Figure 51: Test block and actual sabot with drag ribbon.

Initially the goal was to fire the sabot from the air cannon and open it at its peak trajectory using RC control. Unfortunately, the sabot became entangled in one of the plastic bags and the RC receiver broke on impact with the ground.

To mitigate this, the sabot was simply cushioned by the bag rather than wrapped. Additionally, the sabot was allowed to open as soon as it came out of the cannon and the bag fell away.

Figure 52: Trajectory of UAV (red) and sabot (blue) after being shot from air cannon at 35 PSI.

The results show that the sabot falls away cleanly and the UAV parachute deploys shortly after. After some sway, the ground plane successfully deploys at well. After analyzing the video, the ejection speed of the sabot was determined to be about 11-12 m/s. Upon impact with the ground, however, the ground plane mechanism's central rod, which is attached to the payload, breaks.

The fact that the central rod of the ground plane broke off also presents a potential concern. In practice, however, the central rod is protected in its folded state inside the sabot and cushioned by the parachute during ejection. The rod broke off during testing only during the crash into the ground so it should not experience any comparable forces during its actual descent from the jet. To gear towards safety, however, a few design changes can be employed to prevent the rod from breaking. For example, in the prototype, the ABS tube is simply epoxied to the top disc and there was little surface area available to

ensure a strong bond. The top disc and rod can be made as one piece to avoid the disconnection or a mechanical mate such as a tap connection can be used instead.

In terms of deployment, the sabot deploys properly each time when the servo is activated. Unfortunately, this deployment strategy could not be tested out of the cannon because the RC electronics failed—a few wires of the RC receiver broke off. The RC receiver chip also took up a lot of space that made it difficult to properly secure down the electronics so they were allowed to shake around quite a bit. In practice, however, the deployment will be timed using a switch and microcontroller rather than RC control, so this is less of a concern. As a safety practice, however, the electronics should be better secured to ensure that wires do not break off during the impulsive shock of the ejection.

The tests show that both the sabot and UAV were able to survive the impulse from the cannon. The damage that occurred was caused in either cases was due to the crash into the ground so it should not have a big impact in the device's performance during its actual use. To be conservative, however, both of these issues are easily remedied by a few design changes.

6.2 Deployment Validation

Another important function of the UAV is that the ground plane properly opens during deployment. It is important to know that the opening of the parachute will open the ground plane and that initial concerns of jamming are not an issue.

During the previous air canon tests, deployment of the ground plane could be observed. However, there was a lot of horizontal velocity imparted on the device so the height it was able to reach was limited. The limited height made it difficult to observe full ground plane deployment since there isn't enough time to reach stability. As a result, a drop test was conducted on the device.

The device would be dropped from three stories to observe its deployment and descent down. Initially, the UAV was dropped without the sabot in its closed state and its descent was observed. Both the parachute and the ground plane fully deployed and the device slowly drifted down. Next, the device was put inside the sabot and it was tossed upward. The sabot opening and device deployment was observed.

Figure 53: Trajectories of sabot (blue) and UAV (red) during drop test.

The sabot would open and separate cleanly from the parachute. Once reaching its peak trajectory, the chute deploys and the UAV begins its descent down. The ground plane opens shortly after. The device sways for a bit before stabilizing and hitting the ground. The test was repeated and similar results were observed.

In all cases, the UAV sustained no damage and successful opened each time almost immediately after opening. No jamming was observed and the ground plane maintained its structure during its descent without closing up. Though in practice, the device does not need to survive the crash into the ground, the tests show that it does and can be repeatedly drop. This only further reinforces its survivability.

7 Conclusion

7.1 Summary of Work

The goal of the project was to design an unpowered micro UAV for device calibration. The UAV could be any type of device as long as it could also function as an omnidirectional antenna. It also had to meet a set of parameters that included antenna operating frequencies, a hang time of 30 minutes, and size constraints. The UAV also needed to be sturdy in order to survive high deployment forces.

The parameters helped to narrow down the scope of the project, but a lot of questions were still left as to which antenna to use and what kind of UAV to pursue. Initially, a good deal of ideation and concept generation was used to come up with several solutions. This process was extremely useful as it allowed quick exploration and discussion of many possible solutions without too much time commitment.

The most promising solutions were selected and analyzed for feasibility through calculations and sketch modeling. These concepts included a lighter than air device, a hang glider, and a parachute with antenna ground plane. The lighter than air device was quickly ruled out as it would require too much space for the compressed air canisters and would also be too difficult to control due to its high sensitivity to changing atmospheric conditions. The hang glider had a lot of potential but was not pursued due to difficulties in maintaining stability and had a lot of structural complexity that would require a lot of time to optimize and fold up. This left the parachute device as the concept with the most potential. It was not only an interesting and novel solution but it also had the least amount of concerns, all of which were easily addressed.

In prototyping the parachute, several sketch models were first created. One sketch model allowed the testing of ground plane effects and geometry. This testing proved that initial concerns over the ground plane were not an issue; rather, the ground plane proved beneficial by adding more drag. The second set of sketch models testing different folding patterns of the ground plane. Both prototypes proved to be effective, but the more structurally stable umbrella design was chosen over the more pack efficient spring-loaded one. The umbrella design also simplified deployment methods by coupling it with the aerodynamic forces from the opening of the parachute. This sketch model also highlighted some concerns over bi-stability and interferences that would need to be addressed in the next iteration.

With a final design chosen for the ground plane and initial concerns tested, a final design was developed. CAD was used to develop an optimal design that would meet all space requirements and FEA was used to analyze its survivability under initial deployment conditions. This gave a lot of insight into material choices and performance of the device. The final design was a conductive nylon 17.5"-diameter fabric ground plane attached to an aluminum folding structure. The UAV, including the 70 g payload, weighed in at 0.254 g. The final payload volume that the device could accommodate was 5.01 in^3. Superflex wires that feed up along the strings of the parachute would form the cone of the antenna. Hardware needed for the antenna was integrated into the design of the final prototype as well. Everything was then fabricated and put together. Once completed, jamming became a potential issue. This was remedied with lubrication for the joints and a spring-loaded mechanism designed to push out the linkages of the ground plane mechanism so as to avoid any singularity points. Finally, a sabot was designed out of aluminum sheet metal and a simple unlock mechanism was developed.

With everything built, it was time for testing. Two tests were conducted to address the main concerns that remained—an impulse survivability test and a

drop test. The survivability test used an air cannon to fire the sabot and UAV. The drop test involved throwing the UAV package off three stories to test the deployment of both the parachute and the ground plane. Overall, both tests were quite successful. The prototypes served as good demonstration device and proved that a viable device could be developed. There were a few concerns over the impulse survivability due to some damage sustained in the crash, but these concerns can be easily addressed with a few design changes and should not have a significant impact in the actual usage of the device since it did not occur until the device crashed into the ground.

The primary challenges of the project came from the initial design constraints given. The antenna integration and performance requirements dictated a minimum size for the device that was quite large. For a simple dipole antenna, the device would have to be over a meter long. The volume constraint for the flare cartridge, however, was very small. This greatly restricted what kinds of devices could be pursued due to difficulties in folding it down. Even when a viable design was chosen, the optimization process was quite difficult since so many constraints needed to be kept in mind. The design was constantly tested in CAD to ensure everything fit within the working volume. Additionally, wall thickness for the sabot, payload requirements, antenna integration, parachute packing, and deployment electronics also required more space than was initially anticipated. This led to a lot of iteration and testing just to ensure everything fit.

Another difficult constraint was the requirement to be unpowered. Because the device was unpowered, it could not generate its own lift and could not have any active control. This made it very difficult to develop something that could meet the endurance time requirements of half an hour. In the end, the final device has an expected performance of a little less than half an hour at 29.4 minutes, but with further development and optimization, and perhaps some relaxing of this constraint, the endurance can be increased.

Overall, the project was a success and achieved its primary goal of developing a viable design. A lot was learned that could be used to improve and further develop a higher fidelity beta prototype.

7.2 Future Work

Though the project has concluded, there is a lot of room for future work on it. There are several design improvements that could be made to increase viability and endurance of the device. This could lead to the fabrication of a fully functional device that could be optimized for different operating frequencies and endurance times. Additionally, if further work was done, alternative designs could even be explored.

7.2.1 Design Improvements

In the next iteration of the device, more exploration of linkage dimensions could be done. During this study, the dimensions were iterated until one working set was found. This resulted in a prototype that would fit the volume constraints and was still functional. The design was evaluated using FEA and once it was found to work, it was pursued. However, this might not be the strongest device since several different sets of linkage dimensions would also work. In order to improve the design, the dimensions should also be optimized for strength and integrity. This can be done by modeling the deformation and stresses mathematical and optimizing these equations along with the dimensional constraint equations.

Additionally, the size and weight of the device could also be improved. Testing different cross sectional designs can not only reduce size and weight but also potential increase strength. Material choice could also be improved. Currently, the analysis shows that the linkages have a safety factor of 27, which is about nine times more than what is needed. This suggests that the device is over designed. Further exploration into material choice could potentially reduce a lot of weight, and as a result, increase endurance time. In selection of a better

material, however, temperature effects should also be taken into account since the device will be performing at low temperatures that change with altitude.

In regards to concerns that arose during prototyping and testing, several design changes can be made to address this. For example, during prototype, jamming became a potential issue due to a singularity point. A fix was created for this by adding an additional springer mechanism. In the next prototype iteration, however, this can simply be designed for within the mechanism itself. Stops can be put in to prevent the mechanism from folding past a certain point or the hinges themselves could be spring-loaded. Attention should be paid, however, to whether the trade-offs in the improved design are worth the increase in weight. Perhaps, an external springer mechanism was in fact the best solution. As for the damage sustained in the impulse testing, they can be remedied by the changes recommended at the end of section 6.1—better securing the electronics and redesigning the connection between the central rod and top center disc.

7.2.2 Progression to a Fully Functional Device

Once further parameter optimization is explored and a beta prototype is developed, the progression to a fully functional device can begin. This would include additional testing to the device that is more realistic to its functional scenario. For example, a drop test from a higher drop platform would be helpful as it would allow the device enough time to deploy and reach stability. Wind tunnel tests could be performed on the device to simulate the high speeds device will experience when it first opens. This would be a dynamic structural study rather than static like the FEA. Direct impact testing on the folding mechanism could also be done to test the initial impulsive drag force created when the parachute opens at high speeds. This could also allow a more quantitative analysis on failure points. Lastly, more realistic deployment

situations such as drops from the plane or deployment tests out of the actual flare can be tested.

Finally, the device is meant to be an antenna. In this project, however, the goal was to prove its mechanical feasibility. This meant that during antenna integration, only the required hardware needed for a discone antenna was be included. The dimensions of these parts, however, were not optimized for performance. For example, adjustment of the insulator disc's thickness or the angle of the cone can greatly affect the antenna's impedance and performance. All these features were designed so that they could be modified. In proceeding to a fully functional device, these parameters would then have to be optimized.

Bibliography

[1] Balanis, C. A. (1982). *AntennaTheory Analysis and Design.* John Wiley & Sons, Inc.

[2] Cook, M., & Spottiswoode, M. (2006, January). Modelling the flight dynamics of the hang glider. *The Auronautical Journal* , 1-19.

[3] Hoskin Scientific Company. (2003-2013). *Weather Balloons and Accessories*. Retrieved January 2012, from Hoskin Scientific Company: http://www.hoskin.ca/catalog/index.php?main_page=index&cPath=1_61_152

[4] Lincoln Laboratories MIT. (2011). Air-Launched Devices for Antenna Calibration.

[5] Saedrey, M. (2009). *Aircraft Performance and Analysis.* Saarbrücken VDM Verlag Dr. Müller .

[6] Shevell, R. S. (1989). *Fundamentals of Flight.* Upper Saddle River, NJ, US: Prentice Hall.

[7] Tao, T. (2012). *Design and Development of a High-Altitude, In-Flight-Deployable Micro-UAV.* Massachusetts Institute of Technology, Department of Aeronautics and Astronautics. Cambridge: MIT.

[8] The Engineering Toolbox. (n.d.). *US Standard Atmosphere*. Retrieved from The Engineering Toolbox: http://www.engineeringtoolbox.com/standard-atmosphere-d_604.html

[9] U.S. Air Force. System Command. (1963). *Performance of and Design Criteria for Deployable Aerodynamic Decelerators.* Wright-Patterson

Airforce Base, OH: Air Force Systems Command, Research and Technology Division, AF Flight Dynamics Laboratory.

Appendix A: Parachute Feasibility MATLAB

I. Parachute Integrator Function

```
% Lauren Hernley

function dX = parachuteIntegrator(t, x, m, CDA0, g)
    % x = [pos, vel]

    pos = x(1);
    vel = x(2);

    dx = vel;
    dv = (1/2 * rho(pos) * vel^2 * CDA0 - m*g)/m;
    dX = [dx; dv];
end

% Computes density as a function of altitude (in metric units)
%Reference: Wikipedia
function rho = rho(h)
    p0 = 101325;     % Standard pressure [Pascals]
    T0 = 288.15;     % Standard temperature [Kelvin]
    L = 0.0065;      % Temperature Lapse Rate [Kelvin/m]
    R = 8.31447;     % Gas Constant [J/(mol K)]
    M = 0.0289644;   % Molar Mass of Dry Air [kg/mol]
    g = 9.80665;     % Gravitational constant [m/s^2]

    p = p0 * (1 - L*h/T0)^((g*M)/(R*L)); % Local pressure calculation
    T = T0 - L*h; % Local temperature calcuation

    rho = (p*M)/(R*T);
end
```

II. Parachute Simulator Function

```
% Lauren Hernley
%
% Parachute fall time calculation
% Assumptions:
%     varying density with altitude
%     no wind conditons
%     no canopy porosity effects
% Constraints:
%     30 min flight time in 10,000 to 30,000ft range
% References:
%     USAF text: (pg 66) Table 3-1 Typical Performance Characteristics
of Parachute Canopies
%     Hoskin Scientific Company parachute properties:
http://www.myhoskin.com/newsletters/PDF/BALLOONS.pdf
% Drag coefficients:
%     Fruity Chutes Elliptical Chutes 1.55
%%
close all
clear all
clc

m = [0.248,0.219,0.254];       % Total mass [kg] 0.311 kg
CD = 1.55;        % Drag coefficient
d = [0.762,0.528,0.803];       % chute diameter [m]
A0= pi*d.^2*0.25;      % Cross-Sectional Area [m^2]
g = 9.80665;    % Gravitational constant [m/s^2]

initialAltitude = 9144; % 30,000 ft
cutoffAltitude = 3048; % 10,000 ft
simLength = 2000;

y = []; % Initialize vectors.
v = [];

for i=1:3
    [t,x] = ode45(@(t,x)parachuteIntegrator(t,x,m(i),CD*A0(i),g),
[0:.5:simLength], [initialAltitude; 0]);
    x(:,1)= x(:,1)/.0254/12000;
    y = [y, x(:,1)];
    v = [v, x(:,2)];
end


figure(2);
% position
subplot(2,1,1); hold on;
plot(t, y(:,1),'r')
plot(t, y(:,2),'g')
plot(t, y(:,3),'g')
plot([0,simLength], [10, 10], 'k-'); % 10,000ft cutoff altitude line
title('Parachute Altitude v. Time');
xlabel('Time [s]');
ylabel('Altitude [1000 ft]');
```

```
legend('30-inch Chute', 'Limits');

% velocity
subplot(2,1,2);
plot(t,v(:,1),'r')
plot(t,v(:,2),'g')
plot(t,v(:,3),'g')
title('Parachute Velocity v. Time');
xlabel('Time [s]');
ylabel('Velocity [m/s]');
```

Appendix B: Balloon Feasibility MATLAB

III. Balloon Integrator Function

```
% Lauren Hernley

function dX = balloonIntegrator(t, x, m_gas, m_ball, g)
    % x = [pos, vel]


    pos = x(1);
    vel = x(2);
    [rhoA rhoG] = getRho(pos);

   % Vball = m_gas/rhoG;
    dx = vel;
    dv = ((rhoA * m_gas / rhoG)*g - m_ball*g - m_gas*g)/(m_gas+m_ball);
    dX = [dx; dv];
end

% Computes density of air and filler gas as a function of altitude (in
metric units)
%Reference: Wikipedia & http://wahiduddin.net/calc/density_altitude.htm
% Only valid in troposphere (<36,000 ft)
%http://www.digitaldutch.com/atmoscalc/
function [rhoA rhoG] = getRho(h)
    p0 = 101325;     % Standard pressure [Pascals]
    T0 = 288.15;     % Standard temperature [Kelvin]
    L = 0.0065;      % Temperature Lapse Rate [Kelvin/m]
    R = 8.31447;     % Gas Constant [J/(mol K)]
    Ma = 0.0289644;  % Molar Mass of Dry Air [kg/mol]
    Mg = 0.0040026;  % Molar Mass of Gas (helium) [kg/mol]
    g = 9.80665;     % Gravitational constant [m/s^2]


    p = p0 * (1 - L*h/T0)^((g*Ma)/(R*L)); % Local pressure calculation
    T = T0 - L*h; % Local temperature calcuation

    rhoA = (p*Ma)/(R*T);
    rhoG = (p*Mg)/(R*T);

end
```

IV. Balloon Volume Function

```
% Lauren Hernley

% Balloon Volume Calculation
% Assumptions: varying air/gas density with altitude
%%

initialAltitude = 9144; % 30,000 ft
cutoffAltitude = 3048; % 10,000 ft
m_gas = .204;
h=cutoffAltitude:1:initialAltitude;

p0 = 101325;     % Standard pressure [Pascals]
T0 = 288.15;     % Standard temperature [Kelvin]
L = 0.0065;      % Temperature Lapse Rate [Kelvin/m]
R = 8.31447;     % Gas Constant [J/(mol K)]
Ma = 0.0289644;  % Molar Mass of Dry Air [kg/mol]
Mg = 0.0040026;  % Molar Mass of Gas (helium) [kg/mol]
g = 9.80665;     % Gravitational constant [m/s^2]


p = p0 * (1 - L*h/T0).^((g*Ma)/(R*L)); % Local pressure calculation
T = T0 - L.*h; % Local temperature calcuation

rhoA = (p*Ma)./(R.*T);
rhoG = (p*Mg)./(R.*T);

%Calculates balloon volume as a function of varying air/gas density.
Vball=m_gas./rhoG;

h=h/.0254/12000

figure(3)
% balloon volume
plot(Vball, h)
title('Balloon Volume v. Altitude');
xlabel('Volume [m^3]');
ylabel('Altitude [1000 ft]');
grid on
```

V. Balloon Range Function

```
% Lauren Hernley

% Successful balloon flight conditions calculation
% For an estimated feasible range of values for filler gas mass
% and balloon payload mass, the solution space for successful
% balloon flight is determined.
% Assumptions:
%     no gas diffusion
%     varying density with altitude
%     no wind conditons
%     no balloon backpressure with respect to inflation
% Constraints:
%     1/2 hour flight time in 10,000 to 30,000ft range
%     maximum payload mass 1.014 kg (wires, batteries, latex)
%     minimum payload mass 0.814 kg
% References:
%     balloon inflation specs, gas capacity, flight time, etc.:
%     http://www.ibaonline.net/Portals/0/Helium%20Latex%20Chart.pdf
%     weather balloon vendor offerings with specs:
%     http://www.myhoskin.com/newsletters/PDF/BALLOONS.pdf

%%
g = 9.80665;    % Gravitational constant [m/s^2]

initialAltitude = 9144; % 30,000 ft
cutoffAltitude = 3048; % 10,000 ft
simLength = 3600; % 1 hr time aloft

% Set range of mass values.
m_gas = 0.001:0.001:0.3; %kg
m_ball = 1.014:0.01:1.814; %kg

sol = [0,0]; % initialize solution matrix
d=0;
for i = 1:length(m_gas)
    for j = 1:length(m_ball)
        [t,x] = ode45(@(t,x)balloonIntegrator(t, x, m_gas(i),
m_ball(j), g), [0, simLength], [initialAltitude; 0]);
        if x(length(x),1) >= cutoffAltitude
            d = d+1;
            sol(d,1) = m_gas(i);
            sol(d,2) = m_ball(j);
        end
    end
end

figure(4)
plot(sol(:,1), sol(:,2),'x')
title('Balloon solution space for payload and helium masses');
xlabel('Mass of Helium Gas [kg]');
ylabel('Balloon/Payload Mass [kg]');

% %%
```

```
% m_gas = sol(:,1);
% initialAltitude = 9144; % 30,000 ft
% cutoffAltitude = 3048; % 10,000 ft
%
% h=cutoffAltitude:1:initialAltitude;
%
% p0 = 101325;     % Standard pressure [Pascals]
% T0 = 288.15;     % Standard temperature [Kelvin]
% L = 0.0065;      % Temperature Lapse Rate [Kelvin/m]
% R = 8.31447;     % Gas Constant [J/(mol K)]
% Ma = 0.0289644;  % Molar Mass of Dry Air [kg/mol]
% Mg = 0.0040026;  % Molar Mass of Gas (helium) [kg/mol]
% g = 9.80665;     % Gravitational constant [m/s^2]
%
%
% p = p0 * (1 - L*h/T0).^((g*Ma)/(R*L)); % Local pressure calculation
% T = T0 - L.*h; % Local temperature calcuation
% %
% rhoA = (p*Ma)./(R.*T);
% rhoG = (p*Mg)./(R.*T);
% % Vball(h)=rhoG(h)/m_gas;
%
% Vball=rhoG./m_gas;
%
% figure(3)
% % balloon volume
% plot(Vball, h)
% title('Balloon Volume v. Altitude');
% xlabel('Volume [m^3]');
% ylabel('Altitude [m]');
```

Appendix C: Glider Feasibility Calculations & MATLAB

I. Glider MathCAD Worksheet

The following worksheet takes inputs (highlighted in yellow) from the corresponding columns of the table below and outputs the endurance time of the glider (highlighted in green).

Glider parameters.

$\Lambda := 30\text{deg}$ $\quad b := 64\text{in} = 1.626\text{m}$ $\quad \text{height} := 23\text{in} = 0.584\text{m}$ $\quad \text{length} := \frac{\text{height}}{\sin(\Lambda)} = 1.168\text{m}$

$S := \frac{b \cdot \text{height}}{2} = 0.475\text{m}^2$ $\quad AR := \frac{b^2}{S} = 5.565$

$$\varepsilon := \left[\varepsilon \leftarrow \begin{cases} 4.61 \cdot \left[1 - .045 \cdot (AR)^{.68}\right] \cdot \cos(\Lambda)^{.15} - 3.1 & \text{if } \Lambda \geq 30\text{deg} \\ 1.78 \cdot \left[1 - .045 \cdot (AR)^{.68}\right] - 0.64 & \text{otherwise} \end{cases} \right] = 0.759$$

$K_1 := \frac{1}{\pi \cdot AR \cdot \varepsilon} = 0.075$

$\text{payload} := .070\text{kg}$

$W_{glider} := 1600\frac{\text{kg}}{\text{m}^3} \cdot (b + 2 \cdot \text{length}) \cdot \pi \cdot (.125\text{in})^2 + .061\frac{\text{kg}}{\text{m}^2} \cdot 0.5 \cdot b \cdot \text{height} = 0.23\text{kg}$

$W := (W_{glider} + \text{payload})g = 2.939\text{N}$

Values at sea level & constants.

$T_{SL} := 288.15\text{K}$ $\quad p_{SL} := 101.325\text{kPa}$ $\quad K_{ELR} := -.0065\frac{\text{K}}{\text{m}}$ $\quad R := 8.31447\frac{\text{J}}{\text{mol} \cdot \text{K}}$

$M_{air} := .0289644\frac{\text{kg}}{\text{mol}}$ $\quad \rho_{SL} := \frac{p_{SL} \cdot M_{air}}{R \cdot T_{SL}} = 1.225\frac{\text{kg}}{\text{m}^3}$

Determine lift and drag coefficients at minimum power from average zero-lift drag coefficient for gliders (Sadraey M.)

$$C_{D0} := \begin{pmatrix} .012 \\ .015 \end{pmatrix} \qquad C_L := \sqrt{\frac{3 \cdot C_{D0}}{K_1}} = \begin{pmatrix} 0.691 \\ 0.773 \end{pmatrix}$$

$$C_{Dwing} := C_{D0} + K_1 \cdot C_L^{\,2} = \begin{pmatrix} 0.048 \\ 0.06 \end{pmatrix} \qquad C_{Drod} := \frac{1.25\text{m} \cdot 1\text{in}}{S} \cdot 1.18 = 0.079$$

$$C_D := C_{Dwing} + C_{Drod} = \begin{pmatrix} 0.127 \\ 0.139 \end{pmatrix}$$

Calculate max time of flight (TOF) for glide from h_i to h_f.

$$h_i := 30000\text{ft} \qquad h_{f1} := 20000\text{ft} \qquad h_{f2} := 10000\text{ft}$$

$$t(h_f) := \left(-\sqrt{\frac{S \cdot C_L}{2 \cdot W}} \cdot \frac{C_L}{C_D} \right) \cdot \int_{h_i}^{h_f} \sqrt{\frac{p_{SL} \cdot \left[1 + \frac{\left(K_{ELR} \cdot h \right)}{T_{SL}} \right]^{\frac{-g \cdot M_{air}}{R \cdot K_{ELR}}} \cdot M_{air}}{R \cdot \left(T_{SL} + h \cdot K_{ELR} \right)}} \, dh$$

$$t_{30K\_to\_20K} := t(h_{f1}) = \begin{pmatrix} 48.482 \\ 52.363 \end{pmatrix} \cdot \text{mi}$$

$$t_{total} := t(h_{f2}) = \begin{pmatrix} 6.356 \times 10^3 \\ 6.864 \times 10^3 \end{pmatrix} \cdot \text{s}$$

II. Glider Integrator Function

```
function dx = gliderIntegrator(t, x, m, Cd, Cl, A, g)

    dx = -Cd/Cl*sqrt(2*m*g/(rho(x)*A*Cl));

end

% Computes density as a function of altitude (in metric units)
%Reference: Wikipedia
function rho = rho(h)
    p0 = 101325;     % Standard pressure [Pascals]
    T0 = 288.15;     % Standard temperature [Kelvin]
    L = 0.0065;      % Temperature Lapse Rate [Kelvin/m]
    R = 8.31447;     % Gas Constant [J/(mol K)]
    M = 0.0289644;   % Molar Mass of Dry Air [kg/mol]
    g = 9.80665;     % Gravitational constant [m/s^2]

    p = p0 * (1 - L*h/T0)^((g*M)/(R*L)); % Local pressure calculation
    T = T0 - L*h; % Local temperature calcuation

    rho = (p*M)/(R*T);
end
```

III. Glider Simulator Function

```
% Glider fall time calculation
% Assumptions:
%     varying density with altitude
%     no wind conditons
% Constraints:
%     30 min flight time in 10,000 to 30,000ft range
% References:
%     Shevell, R. S. (1989). Fundamentals of Flight.

%%
close all
clear all
clc

% Glider Geometry
theta = 30; % Sweep Angle
l = 1.168; % Length of Sides
b = 1.626; % Base
h = 0.584; % Height


m = .070+1600*(pi*(.125*.0254)^2)*(2*l+b)+.061*b*h*.5; % Calculate
total mass
A0= 1/2*b*h;       % Cross-Sectional Area [m^2]
AR= b^2/A0;
```

```
% Calculate epsilon
if theta>=30
    epsilon = 4.61*(1-.045*AR.^0.68)*(cos(theta*pi/180))^.15-3.1;
else
    epsilon = 1.78*(1-.045*AR.^0.68)-0.64;
end

K = 1/(pi*epsilon*AR);   % Calculate K constant.

CD0=[0.012, 0.015]      % Zero drag coefficient (from Saedrey);
CL = sqrt(3*CD0/K) ;    % Calculate CL
CD = CD0+K*CL.^2+.079;
g = 9.80665;     % Gravitational constant [m/s^2]

initialAltitude = 9144; % 30,000 ft
cutoffAltitude = 3048; % 10,000 ft
simLength = 7000;


[t,x] = ode45(@(t,x)gliderIntegrator(t,x,m,CD(1),CL(1),A0,g),
[0:1:simLength], [initialAltitude]);
y1 = x(:,1)/.0254/12000;
[t,x] = ode45(@(t,x)gliderIntegrator(t,x,m,CD(2),CL(2),A0,g),
[0:1:simLength], [initialAltitude]);
y2 = x(:,1)/.0254/12000;

figure(2)
hold on;
plot(t, y1, 'r')
plot(t, y2, 'g')
plot([0,simLength], [10, 10], 'k-'); % 10,000ft cutoff altitude line
plot([1800,1800], [30, 0], 'k-'); % 1/2 hr cutoff time line
title('Glider Altitude v. Time');
legend('CD0 = 0.012','CD0 = 0.015');
xlabel('Time [s]');
ylabel('Altitude [1000 ft]');
```

Appendix D: Carbon Fiber FEA Report

Assumptions

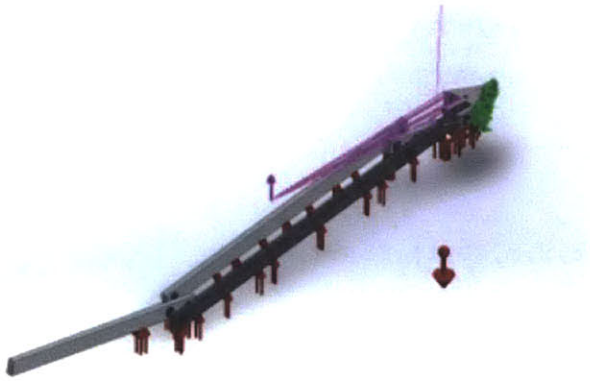

Original Model

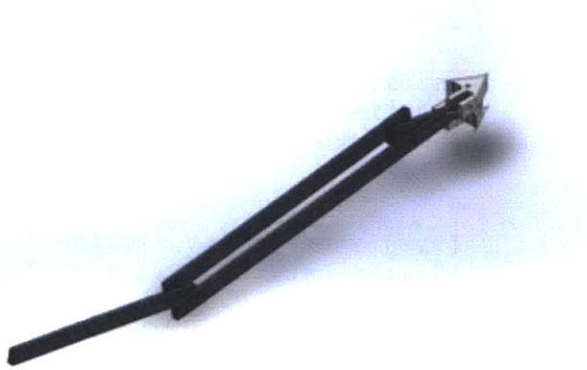

Model Analyzed

Model Information

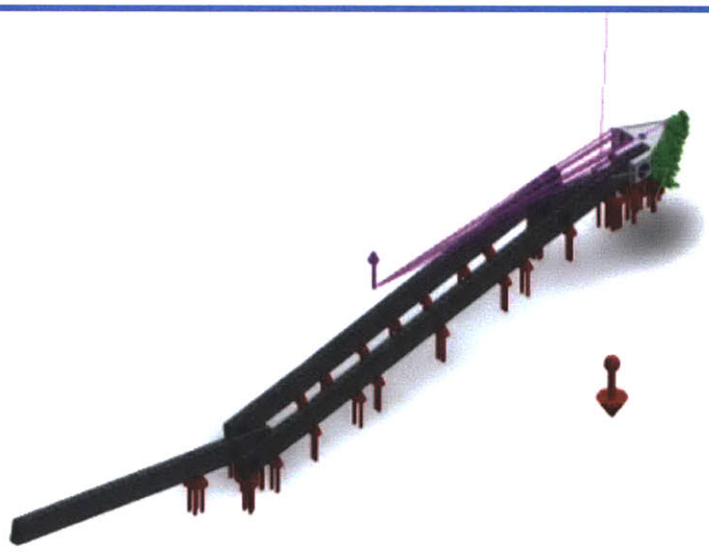

Model name: Proto2_Study2
Current Configuration: Default

Solid Bodies			
Document Name and Reference	**Treated As**	**Volumetric Properties**	**Document Path/Date Modified**
Stock-Proto2-1 	Solid Body	Mass:0.00281574 kg Volume:1.75983e-006 m^3 Density:1600 kg/m^3 Weight:0.0275942 N	G:\Thesis\Proto2\L2.sldprt Jul 02 01:53:32 2013
Stock-Proto2-1 	Solid Body	Mass:0.000539267 kg Volume:3.37042e-007 m^3 Density:1600 kg/m^3 Weight:0.00528481 N	G:\Thesis\Proto2\L3.sldprt Jul 02 01:53:32 2013
Stock-Proto2-1 	Solid Body	Mass:0.0023429 kg Volume:1.46431e-006 m^3 Density:1600 kg/m^3 Weight:0.0229604 N	G:\Thesis\Proto2\L4.sldprt Jul 02 01:53:32 2013
Stock-Proto2-1 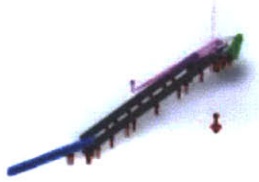	Solid Body	Mass:0.00175759 kg Volume:1.09849e-006 m^3 Density:1600 kg/m^3 Weight:0.0172244 N	G:\Thesis\Proto2\L5.sldprt Jul 02 01:53:32 2013
Split1[1] 	Solid Body	Mass:0.000425521 kg Volume:4.17177e-007 m^3 Density:1020 kg/m^3 Weight:0.0041701 N	G:\Thesis\Proto2\Plate Bottom.sldprt Jul 02 01:53:24 2013

Split1[1] 	Solid Body	Mass:0.000596552 kg Volume:5.84855e-007 m^3 Density:1020 kg/m^3 Weight:0.00584621 N	G:\Thesis\Proto2\Plate.sldprt Jul 02 01:53:24 2013

Study Properties

Study name	Initial Carbon Fiber
Analysis type	Static
Mesh type	Solid Mesh
Thermal Effect:	On
Thermal option	Include temperature loads
Zero strain temperature	298 Kelvin
Include fluid pressure effects from SolidWorks Flow Simulation	Off
Solver type	FFEPlus
Inplane Effect:	Off
Soft Spring:	Off
Inertial Relief:	Off
Incompatible bonding options	Automatic
Large displacement	Off
Compute free body forces	On
Friction	Off
Use Adaptive Method:	Off
Result folder	SolidWorks document (G:\Thesis\Proto2)

Units

Unit system:	SI (MKS)
Length/Displacement	mm
Temperature	Kelvin
Angular velocity	Rad/sec
Pressure/Stress	N/m^2

Material Properties

Model Reference	Properties	Components
	Name: AISI 304 Model type: Linear Elastic Isotropic Default failure criterion: Unknown Yield strength: 2.06807e+008 N/m^2 Tensile strength: 5.17017e+008 N/m^2 Elastic modulus: 1.9e+011 N/m^2 Poisson's ratio: 0.29 Mass density: 8000 kg/m^3 Shear modulus: 7.5e+010 N/m^2 Thermal expansion coefficient: 1.8e-005 /Kelvin	SolidBody 1(Stock-Proto2-1)(L2-1), SolidBody 1(Stock-Proto2-1)(L3-1), SolidBody 1(Stock-Proto2-1)(L4-1), SolidBody 1(Stock-Proto2-1)(L5-1)
Curve Data:N/A		
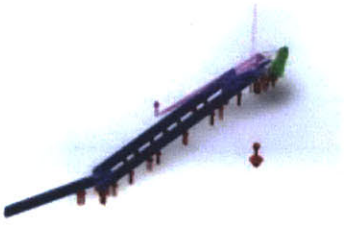	Name: Default Model type: Linear Elastic Isotropic Default failure criterion: Max von Mises Stress Yield strength: 3.5e+009 N/m^2 Tensile strength: 3.5e+009 N/m^2 Compressive strength: 1.2e+009 N/m^2 Elastic modulus: 1.35e+011 N/m^2 Poisson's ratio: 0.3 Mass density: 1600 kg/m^3 Shear modulus: 5e+009 N/m^2 Thermal expansion coefficient: 0.3 /Kelvin	SolidBody 1(Split1[1])(Plate Bottom-2), SolidBody 1(Split1[1])(Plate-1)
Curve Data:N/A		
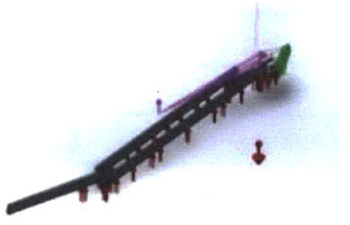	Name: Nylon 6/10 Model type: Linear Elastic Isotropic Default failure criterion: Unknown Yield strength: 1.39043e+008 N/m^2 Tensile strength: 1.42559e+008 N/m^2 Elastic modulus: 8.3e+009 N/m^2 Poisson's ratio: 0.28 Mass density: 1400 kg/m^3 Shear modulus: 3.2e+009 N/m^2 Thermal expansion coefficient: 3e-005 /Kelvin	<Material_ComponentList1/>

Curve Data:N/A			
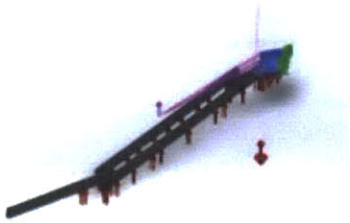	Name: Model type: Default failure criterion: Tensile strength: Elastic modulus: Poisson's ratio: Mass density: Shear modulus:	ABS Linear Elastic Isotropic Unknown 3e+007 N/m^2 2e+009 N/m^2 0.394 1020 kg/m^3 3.189e+008 N/m^2	<Material_ComponentList1/ >
Curve Data:N/A			

Loads and Fixtures

Fixture name	Fixture Image	Fixture Details
Circular Symmetry-1		Entities: **2 face(s)** Type: **Circular Symmetry**

Resultant Forces

Components	X	Y	Z	Resultant
Reaction force(N)	0.790443	-0.256061	-10.245	10.2787
Reaction Moment(N-m)	0	0	0	0

Circular Symmetry-2		Entities: **2 face(s)** Type: **Circular Symmetry**

Resultant Forces

Components	X	Y	Z	Resultant
Reaction force(N)	0.794077	7.48188e-007	2.64203	2.75879
Reaction Moment(N-m)	0	0	0	0

Fixed-1	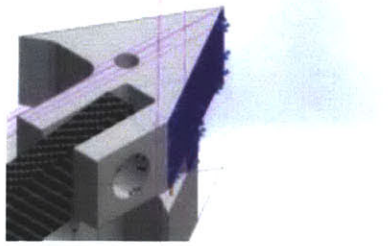	Entities: **3 face(s)** Type: **Fixed Geometry**

Resultant Forces

Components	X	Y	Z	Resultant
Reaction force(N)	-0.0826515	-85.7433	-128.932	154.84
Reaction Moment(N-m)	0	0	0	0

On Cylindrical Faces-1	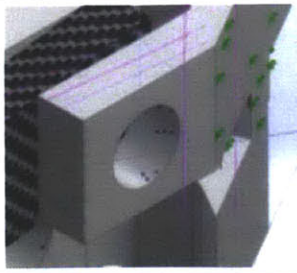	Entities: **1 face(s)** Type: **On Cylindrical Faces** Translation: **0, 0 rad., ---** Units: **mm**

Resultant Forces

Components	X	Y	Z	Resultant
Reaction force(N)	-0.927781	-2.41543e-006	-33.2611	33.2741
Reaction Moment(N-m)	0	0	0	0

Load name	Load Image	Load Details
Gravity-1	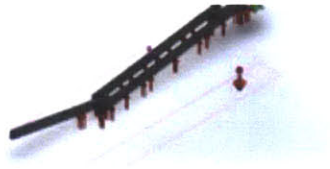	Reference: **Top Plane** Values: **0 0 -9.81** Units: **SI**
Pressure-1		Entities: **7 face(s)** Type: **Normal To Plane** Value: **623.68** Units: **N/m^2**
Remote Load/Mass (Rigid connection) -1	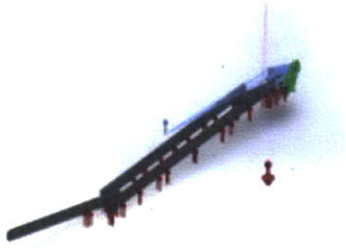	Entities: **1 edge(s), 1 face(s)** Type: **Load/Mass (Rigid connection)** Coordinate System: **Global cartesian coordinates** Force Values: **---, 11.7, --- N** Moment Values: **---, ---, --- N-m** Reference coordinates: **0 3 4 in** Components transferred: **Force**

Remote Load/Mass (Rigid connection) -2	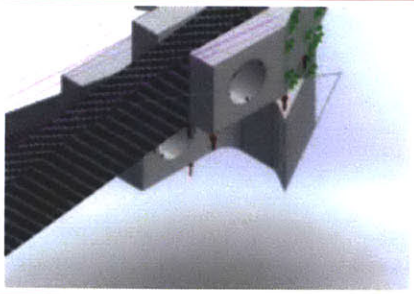	Entities: **1 face(s)** Type: **Load (Direct transfer)** Coordinate System: **Global cartesian coordinates** Force Values: **---, 73.475, --- N** Moment Values: **---, ---, --- N-m** Reference coordinates: **0 18.84 0 in** Components transferred: **Force**

Connector Definitions

Pin/Bolt/Bearing Connector

Model Reference	Connector Details	Strength Details
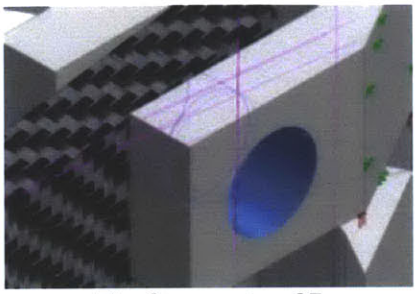 Pin Connector-25	Entities: 2 face(s) Type: Pin Connection type: With retaining ring (No translation) Rotational stiffness value: 0 Units: SI	Bolt Check: OK Calculated FOS: 97.4952 Desired FOS: 2 

Connector Forces

Type	X-Component	Y-Component	Z-Component	Resultant
Axial Force (N)	0.25507	0	0	0.25507
Shear Force (N)	0	6.5931	1.3544	6.7308
Torque (N-m)	-3.4829e-011	-0	-0	-3.4829e-011
Bending moment (N-m)	0	0.0052053	-0.0023203	0.005699

Model Reference	Connector Details	Strength Details
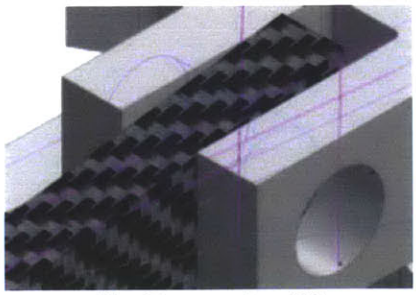 Pin Connector-26	Entities: 2 face(s) Type: Pin Connection type: With retaining ring (No translation) Rotational stiffness value: 0 Units: SI	Bolt Check: OK Calculated FOS: 37.8477 Desired FOS: 2 

Connector Forces

Type	X-Component	Y-Component	Z-Component	Resultant
Axial Force (N)	0.37617	0	0	0.37617
Shear Force (N)	0	6.2237	-3.7268	7.2542
Torque (N-m)	-2.4414e-012	-0	-0	-2.4414e-012
Bending moment (N-m)	0	-0.016462	-0.01308	0.021026

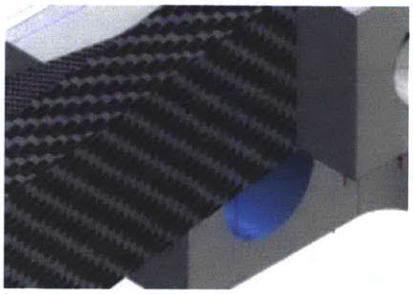

Pin Connector-27

Entities: 2 face(s)
Type: Pin
Connection type: With retaining ring (No translation)
Rotational stiffness value: 0
Units: SI

Bolt Check:	OK
Calculated FOS:	81.9659
Desired FOS:	2

Connector Forces

Type	X-Component	Y-Component	Z-Component	Resultant
Axial Force (N)	1.5971	0	0	1.5971
Shear Force (N)	0	-6.9526	-5.2236	8.6962
Torque (N-m)	1.8855e-010	0	0	1.8855e-010
Bending moment (N-m)	0	-0.0035563	0.0034942	0.0049856

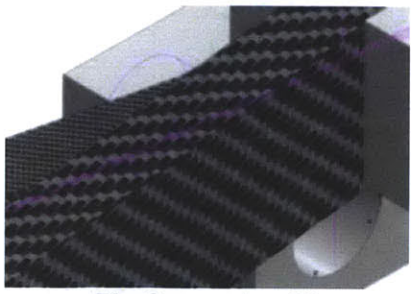

Pin Connector-28

Entities: 2 face(s)
Type: Pin
Connection type: With retaining ring (No translation)
Rotational stiffness value: 0
Units: SI

Bolt Check:	OK
Calculated FOS:	43.7989
Desired FOS:	2

Connector Forces

Type	X-Component	Y-Component	Z-Component	Resultant

Axial Force (N)	1.4758	0	0	1.4758
Shear Force (N)	0	-6.1096	-0.14369	6.1113
Torque (N-m)	1.1161e-012	0	0	1.1161e-012
Bending moment (N-m)	0	-0.0050642	0.016875	0.017619

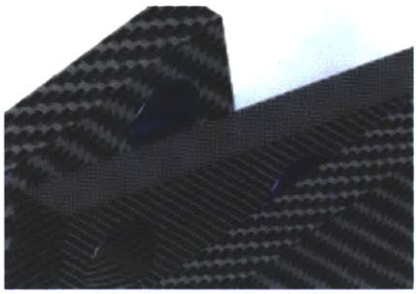

Pin Connector-29

Entities: 2 face(s)
Type: Pin
Connection type: With retaining ring (No translation)
Rotational stiffness value: 0
Units: SI

Bolt Check:	OK
Calculated FOS:	125.69
Desired FOS:	2

Connector Forces

Type	X-Component	Y-Component	Z-Component	Resultant
Axial Force (N)	0.0097047	-0	-0	-0.0097047
Shear Force (N)	0	-0.072265	1.0107	1.0133
Torque (N-m)	-2.0812e-012	0	0	2.0812e-012
Bending moment (N-m)	0	-0.006443	-0.00086185	0.0065004

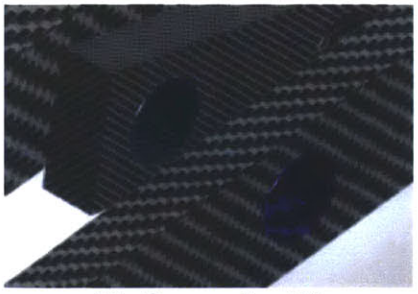

Pin Connector-30

Entities: 2 face(s)
Type: Pin
Connection type: With retaining ring (No translation)
Rotational stiffness value: 0
Units: SI

Bolt Check:	OK
Calculated FOS:	24.3804
Desired FOS:	2

Connector Forces

Type	X-Component	Y-Component	Z-Component	Resultant
Axial Force (N)	0.1309	-0	-0	-0.1309
Shear Force (N)	0	-0.86892	-4.0691	4.1608

Torque (N-m)	1.0854e-012	-0	-0	-1.0854e-012
Bending moment (N-m)	0	0.012198	-0.031247	0.033544

Pin Connector-31

Entities:	2 face(s)
Type:	Pin
Connection type:	With retaining ring (No translation)
Rotational stiffness value:	0
Units:	SI

Bolt Check:	OK
Calculated FOS:	108.029
Desired FOS:	2

Connector Forces

Type	X-Component	Y-Component	Z-Component	Resultant
Axial Force (N)	-0.0095653	0	0	0.0095653
Shear Force (N)	0	0.21804	-1.0109	1.0342
Torque (N-m)	-1.7902e-012	0	0	1.7902e-012
Bending moment (N-m)	0	0.0074947	0.0010141	0.007563

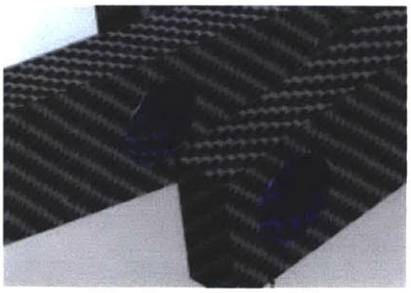

Pin Connector-32

Entities:	2 face(s)
Type:	Pin
Connection type:	With retaining ring (No translation)
Rotational stiffness value:	0
Units:	SI

Bolt Check:	OK
Calculated FOS:	5797.81
Desired FOS:	2

Connector Forces

Type	X-Component	Y-Component	Z-Component	Resultant
Axial Force (N)	-0.009243	0	0	0.009243
Shear Force (N)	0	0.32318	-1.0118	1.0621
Torque (N-m)	-4.1293e-011	0	0	4.1293e-011
Bending moment (N-m)	0	0.00098325	-0.00042142	0.0010698

Contact Information

Contact	Contact Image	Contact Properties
Global Contact	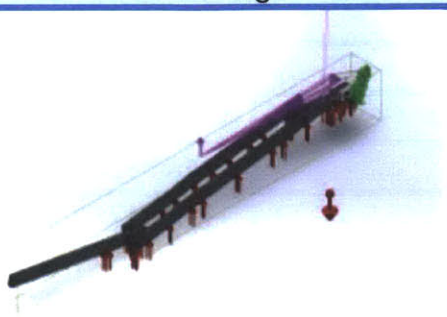	Type: **Node to node** Components: **1 component(s)**

Mesh Information

Mesh type	Solid Mesh
Mesher Used:	Standard mesh
Automatic Transition:	Off
Include Mesh Auto Loops:	Off
Jacobian points	4 Points
Element Size	0.0663525 in
Tolerance	0.00331763 in
Mesh Quality	High
Remesh failed parts with incompatible mesh	Off

7.3 Mesh Information - Details

Total Nodes	20303
Total Elements	10768
Maximum Aspect Ratio	10.474
% of elements with Aspect Ratio < 3	97.3
% of elements with Aspect Ratio > 10	0.00929
% of distorted elements(Jacobian)	0
Time to complete mesh(hh;mm;ss):	00:00:03
Computer name:	TROYN-PC

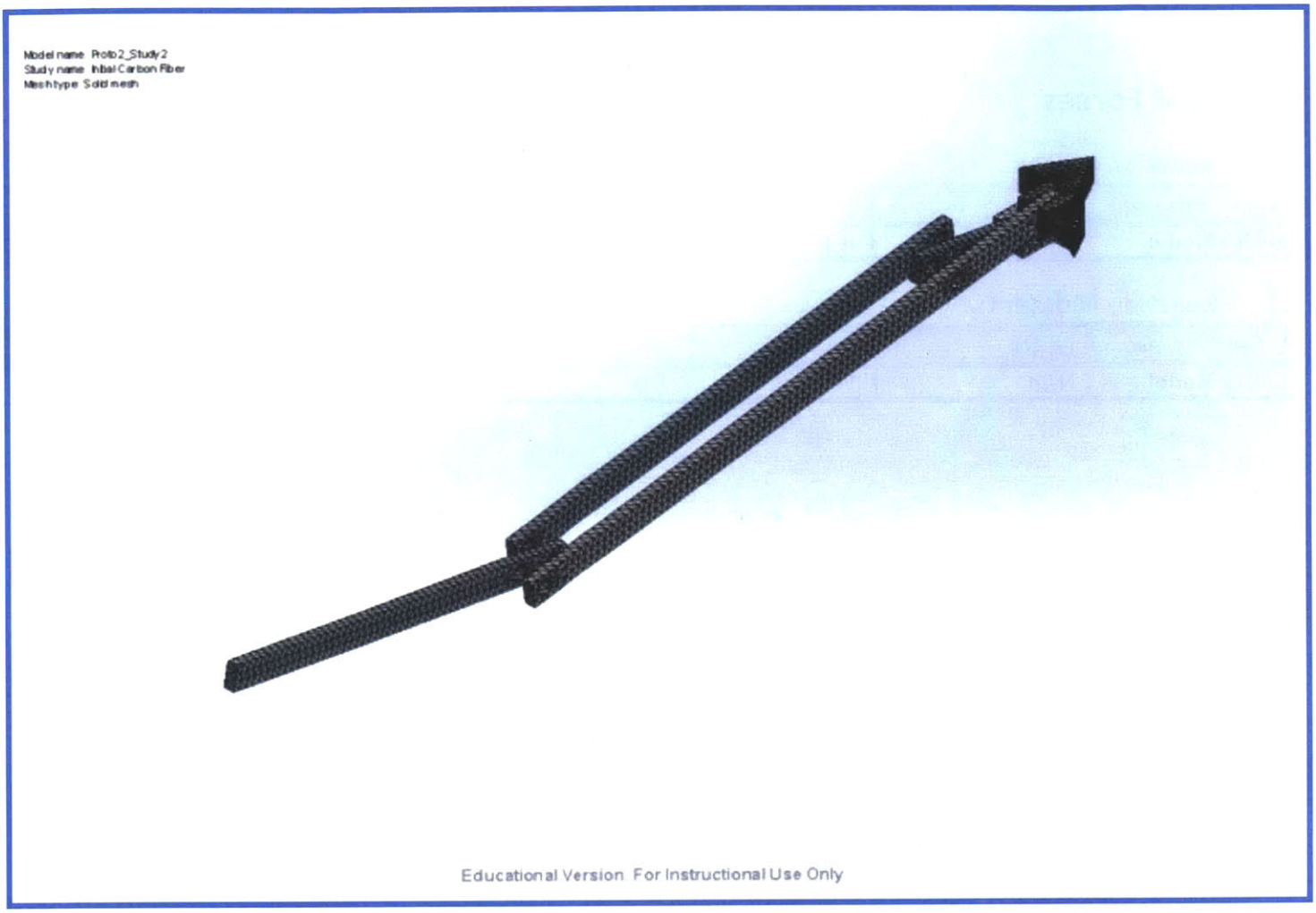

Sensor Details

Sensor name	Location	Sensor Details
Stress1	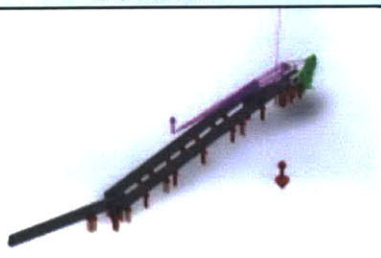	Value : 382.74 Entities : Result :Stress Component :VON: von Mises Stress Criterion :Model Max Step Criterion : Across all Steps Step No.:1 Alert Value: NA

Resultant Forces

7.4 Reaction Forces

Selection set	Units	Sum X	Sum Y	Sum Z	Resultant
Entire Model	N	-1.01043	-85.7433	-162.193	183.466

7.5 Reaction Moments

Selection set	Units	Sum X	Sum Y	Sum Z	Resultant
Entire Model	N-m	0	0	0	0

Beams

No Data

Study Results

Name	Type	Min	Max
Stress1	VON: von Mises Stress	18.9418 N/m^2 Node: 14563	3.9501e+007 N/m^2 Node: 15316

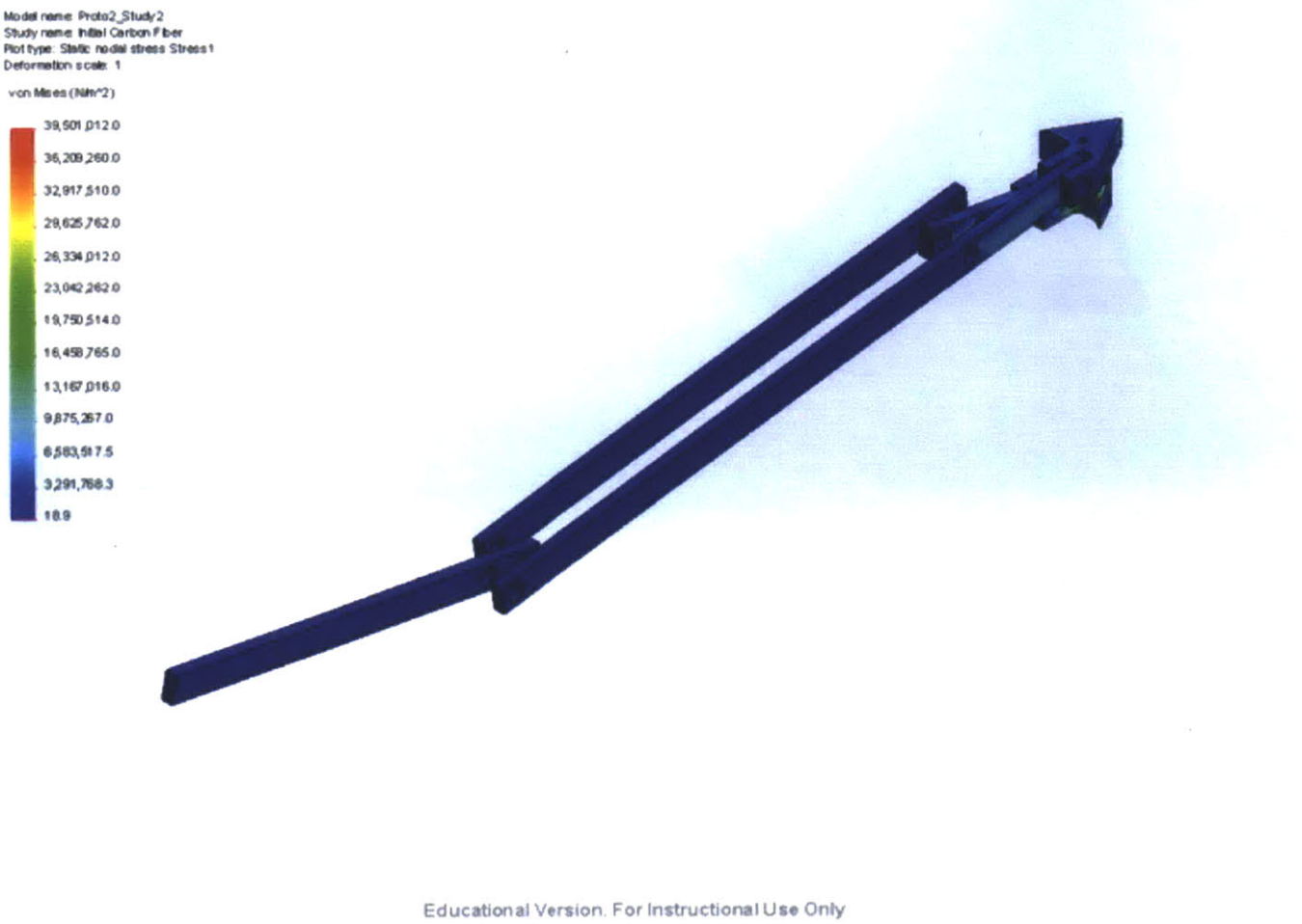

Proto2_Study2-Initial Carbon Fiber-Stress-Stress1

Name	Type	Min	Max
Displacement1	URES: Resultant Displacement	0 mm Node: 17435	0.474577 mm Node: 11716

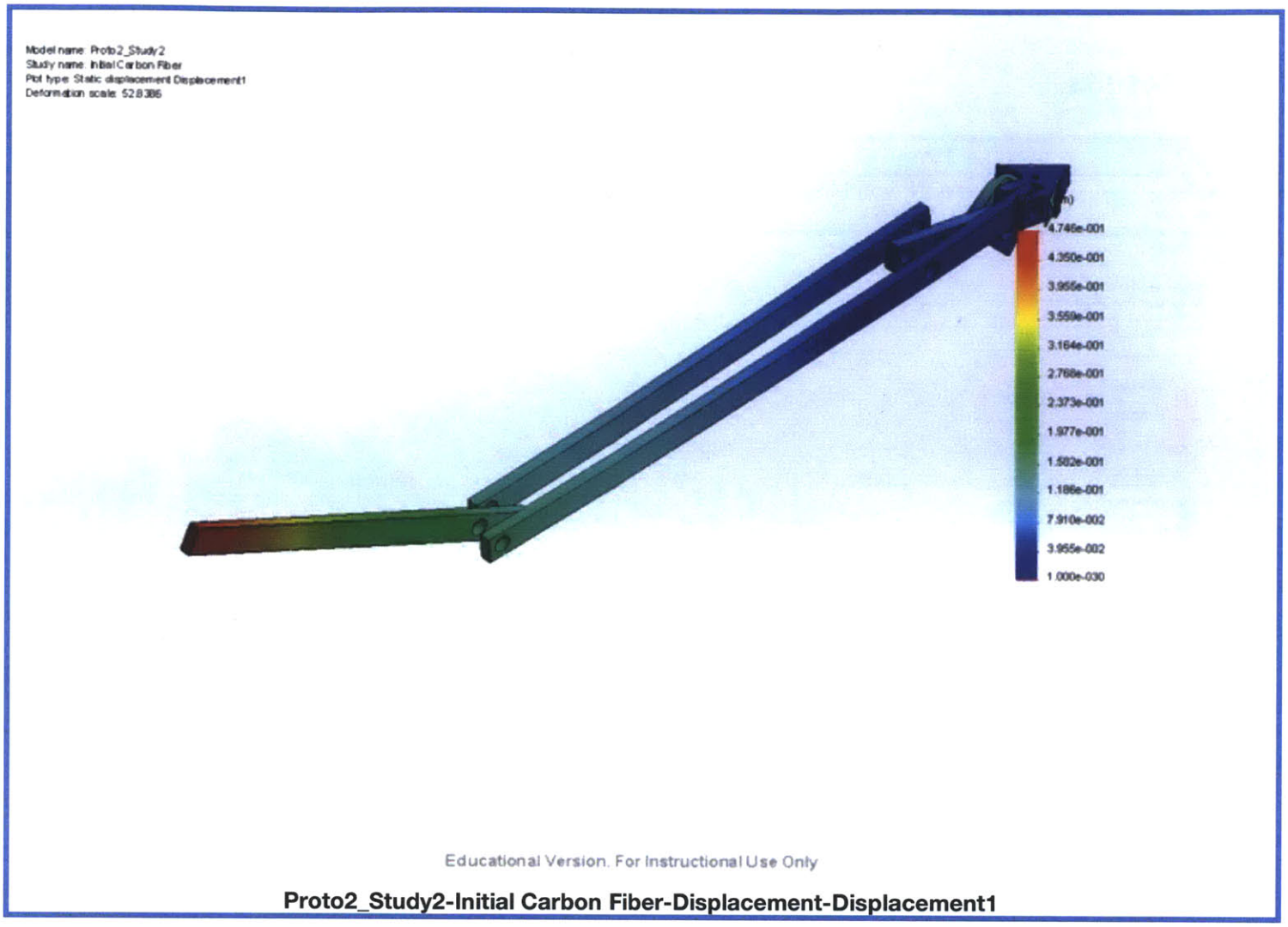

Proto2_Study2-Initial Carbon Fiber-Displacement-Displacement1

Name	Type	Min	Max
Strain1	ESTRN: Equivalent Strain	1.87023e-010 Element: 6207	0.0119015 Element: 8455

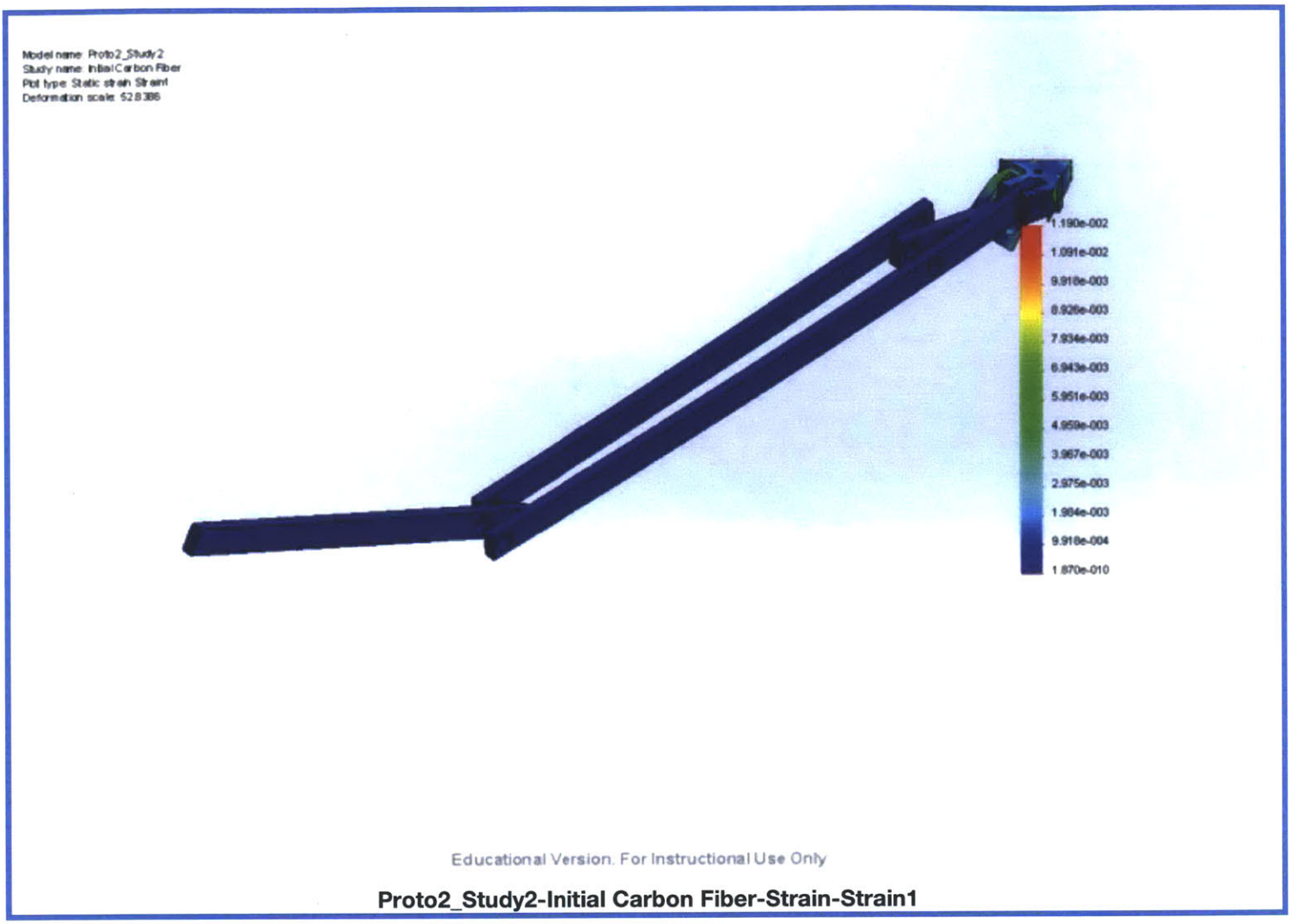

Proto2_Study2-Initial Carbon Fiber-Strain-Strain1

Name	Type
Displacement1{1}	Deformed Shape

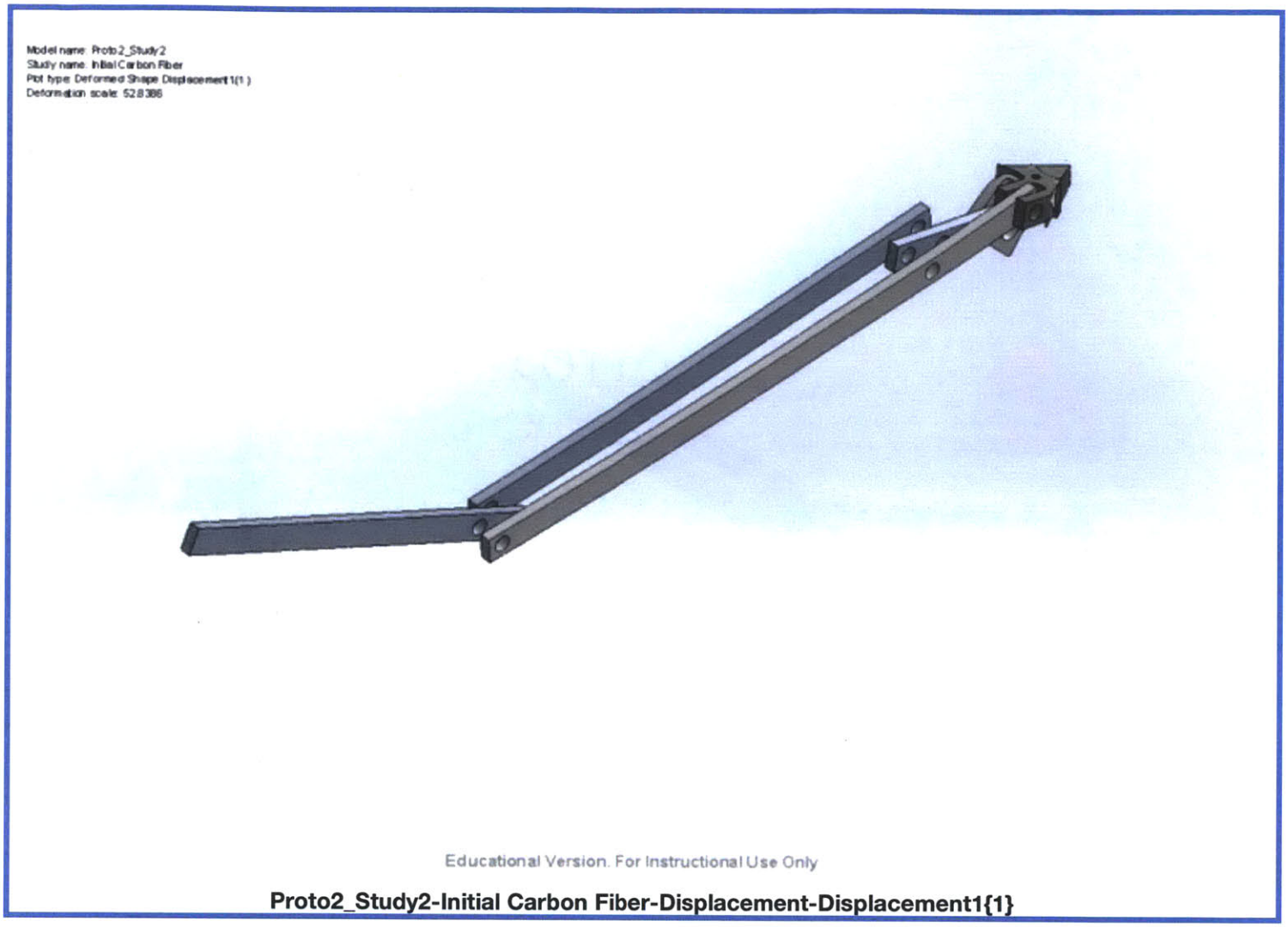

Proto2_Study2-Initial Carbon Fiber-Displacement-Displacement1{1}

Name	Type
Design Insight1	Design Insight

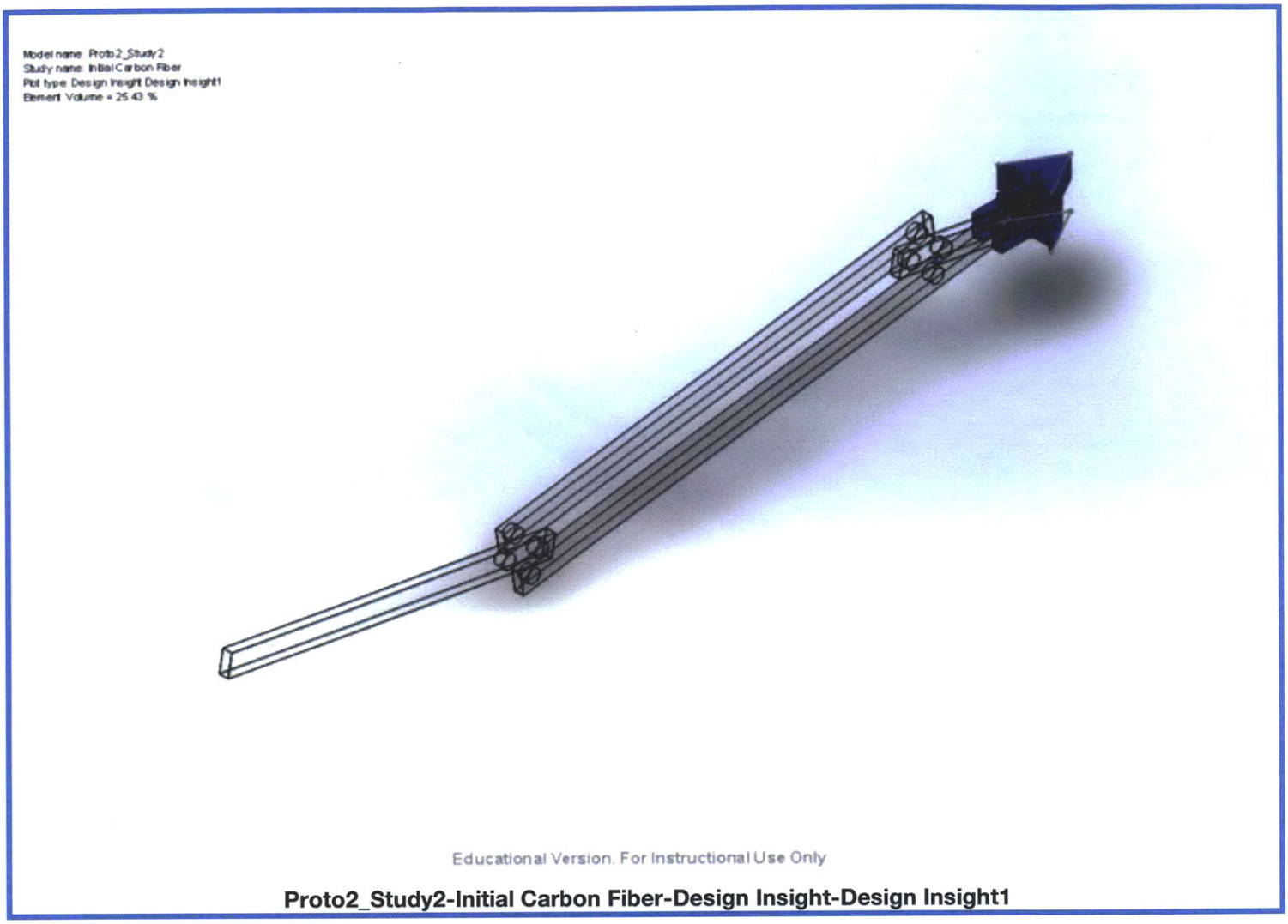

Proto2_Study2-Initial Carbon Fiber-Design Insight-Design Insight1

Name	Type	Min	Max
Factor of Safety1	Automatic	382.74 Node: 5493	1.84776e+008 Node: 14563

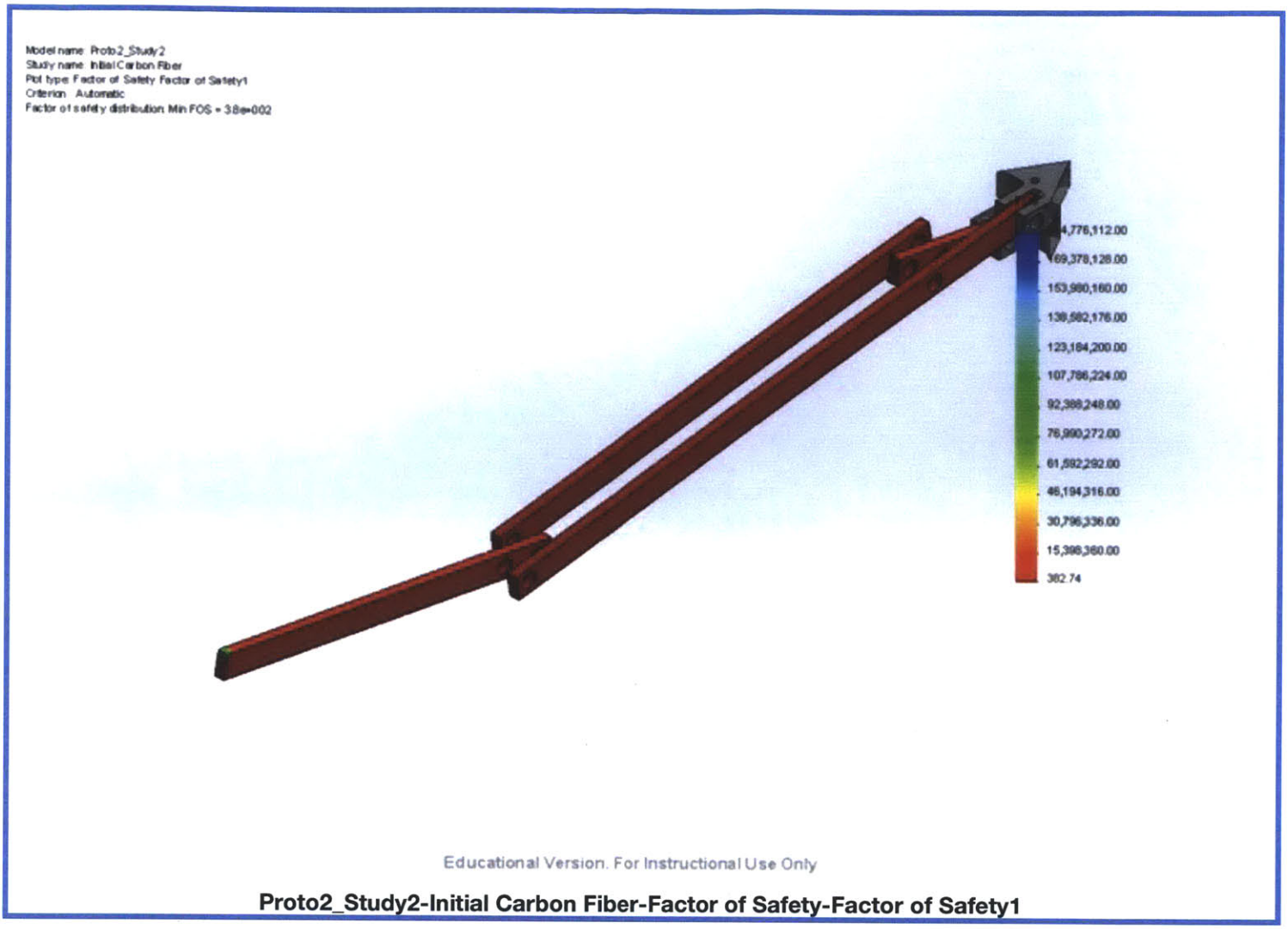

Proto2_Study2-Initial Carbon Fiber-Factor of Safety-Factor of Safety1

Name	Type
Pin/Bolt Check1	Static Bolt & Pin Results

Proto2_Study2-Initial Carbon Fiber-Pin/Bolt Check-Pin/Bolt Check1

Image-1

Appendix E: Aluminum FEA Report

Assumptions

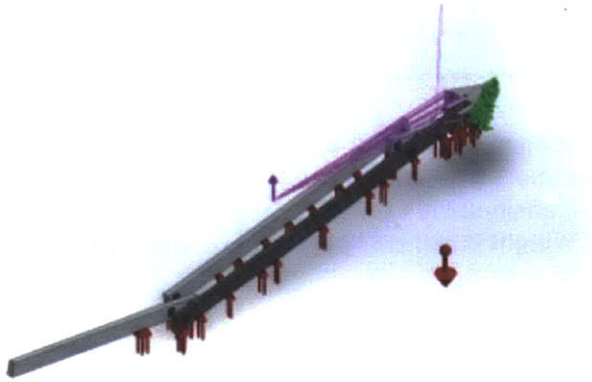

Original Model

Model Analyzed

Model Information

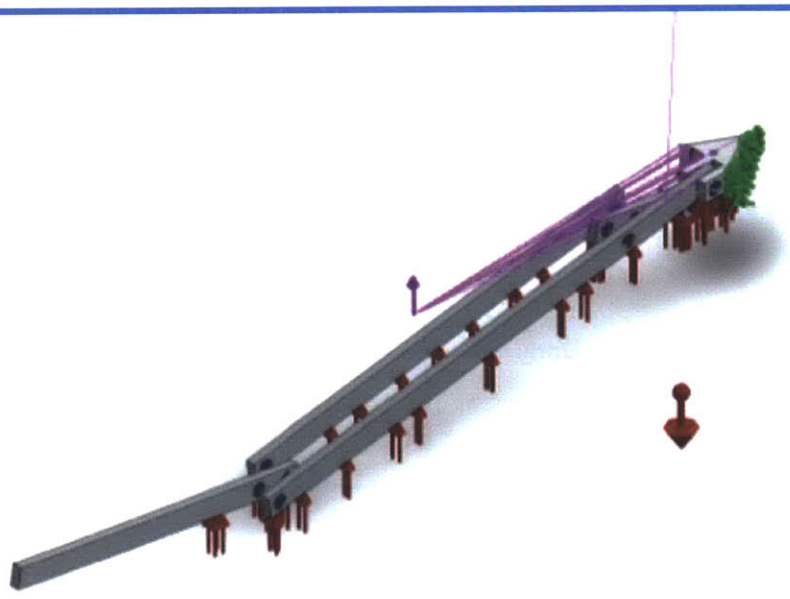

Model name: Proto2_Study2
Current Configuration: Default

Solid Bodies			
Document Name and Reference	Treated As	Volumetric Properties	Document Path/Date Modified
Stock-Proto2-1 	Solid Body	Mass:0.00475155 kg Volume:1.75983e-006 m^3 Density:2700 kg/m^3 Weight:0.0465652 N	G:\Thesis\Proto2\L2.sldprt Jul 02 01:53:32 2013
Stock-Proto2-1 	Solid Body	Mass:0.000910013 kg Volume:3.37042e-007 m^3 Density:2700 kg/m^3 Weight:0.00891812 N	G:\Thesis\Proto2\L3.sldprt Jul 02 01:53:32 2013
Stock-Proto2-1 	Solid Body	Mass:0.00395364 kg Volume:1.46431e-006 m^3 Density:2700 kg/m^3 Weight:0.0387456 N	G:\Thesis\Proto2\L4.sldprt Jul 02 01:53:32 2013
Stock-Proto2-1 	Solid Body	Mass:0.00296593 kg Volume:1.09849e-006 m^3 Density:2700 kg/m^3 Weight:0.0290661 N	G:\Thesis\Proto2\L5.sldprt Jul 02 01:53:32 2013
Split1[1] 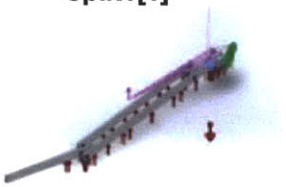	Solid Body	Mass:0.000425521 kg Volume:4.17177e-007 m^3 Density:1020 kg/m^3 Weight:0.0041701 N	G:\Thesis\Proto2\Plate Bottom.sldprt Jul 02 01:53:24 2013

Split1[1] 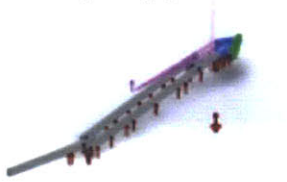	Solid Body	Mass:0.000596552 kg Volume:5.84855e-007 m^3 Density:1020 kg/m^3 Weight:0.00584621 N	G:\Thesis\Proto2\Plate.sldprt Jul 02 01:53:24 2013

Study Properties

Study name	Initial Aluminum
Analysis type	Static
Mesh type	Solid Mesh
Thermal Effect:	On
Thermal option	Include temperature loads
Zero strain temperature	298 Kelvin
Include fluid pressure effects from SolidWorks Flow Simulation	Off
Solver type	FFEPlus
Inplane Effect:	Off
Soft Spring:	Off
Inertial Relief:	Off
Incompatible bonding options	Automatic
Large displacement	Off
Compute free body forces	On
Friction	Off
Use Adaptive Method:	Off
Result folder	SolidWorks document (G:\Thesis\Proto2)

Units

Unit system:	SI (MKS)
Length/Displacement	mm
Temperature	Kelvin
Angular velocity	Rad/sec
Pressure/Stress	N/m^2

Material Properties

Model Reference	Properties	Components
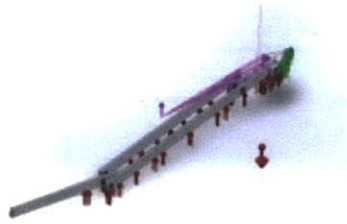	Name: AISI 304 Model type: Linear Elastic Isotropic Default failure criterion: Unknown Yield strength: 2.06807e+008 N/m^2 Tensile strength: 5.17017e+008 N/m^2 Elastic modulus: 1.9e+011 N/m^2 Poisson's ratio: 0.29 Mass density: 8000 kg/m^3 Shear modulus: 7.5e+010 N/m^2 Thermal expansion coefficient: 1.8e-005 /Kelvin	SolidBody 1(Stock-Proto2-1)(L2-1), SolidBody 1(Stock-Proto2-1)(L3-1), SolidBody 1(Stock-Proto2-1)(L4-1), SolidBody 1(Stock-Proto2-1)(L5-1)
Curve Data:N/A		
	Name: 6063-T6 Model type: Linear Elastic Isotropic Default failure criterion: Max von Mises Stress Yield strength: 2.15e+008 N/m^2 Tensile strength: 2.4e+008 N/m^2 Elastic modulus: 6.9e+010 N/m^2 Poisson's ratio: 0.33 Mass density: 2700 kg/m^3 Shear modulus: 2.58e+010 N/m^2 Thermal expansion coefficient: 2.34e-005 /Kelvin	SolidBody 1(Split1[1])(Plate Bottom-2), SolidBody 1(Split1[1])(Plate-1)
Curve Data:N/A		

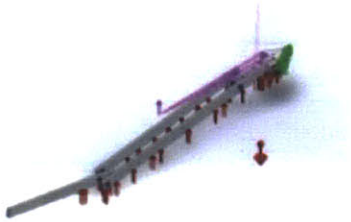	Name: Nylon 6/10 Model type: Linear Elastic Isotropic Default failure criterion: Unknown Yield strength: 1.39043e+008 N/m^2 Tensile strength: 1.42559e+008 N/m^2 Elastic modulus: 8.3e+009 N/m^2 Poisson's ratio: 0.28 Mass density: 1400 kg/m^3 Shear modulus: 3.2e+009 N/m^2 Thermal expansion coefficient: 3e-005 /Kelvin	<Material_ComponentList1/>
Curve Data:N/A		
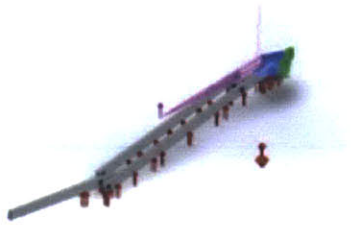	Name: ABS Model type: Linear Elastic Isotropic Default failure criterion: Unknown Tensile strength: 3e+007 N/m^2 Elastic modulus: 2e+009 N/m^2 Poisson's ratio: 0.394 Mass density: 1020 kg/m^3 Shear modulus: 3.189e+008 N/m^2	<Material_ComponentList1/>
Curve Data:N/A		

Loads and Fixtures

Fixture name	Fixture Image	Fixture Details
Circular Symmetry-1	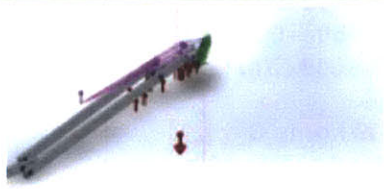	Entities: **2 face(s)** Type: **Circular Symmetry**

Resultant Forces

Components	X	Y	Z	Resultant
Reaction force(N)	0.776924	-0.258227	-10.705	10.7363
Reaction Moment(N-m)	0	0	0	0

Circular Symmetry-2		Entities: **2 face(s)** Type: **Circular Symmetry**

Resultant Forces

Components	X	Y	Z	Resultant
Reaction force(N)	0.851411	2.20863e-007	2.80338	2.92982
Reaction Moment(N-m)	0	0	0	0

Fixed-1	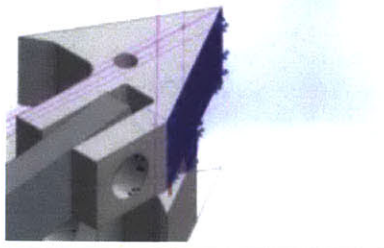	Entities: **3 face(s)** Type: **Fixed Geometry**

Resultant Forces

Components	X	Y	Z	Resultant
Reaction force(N)	-0.724691	-89.4151	-134.801	161.762
Reaction Moment(N-m)	0	0	0	0

On Cylindrical Faces-1	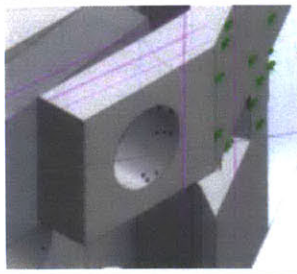	Entities: **1 face(s)** Type: **On Cylindrical Faces** Translation: **0, 0 rad., ---** Units: **mm**

Resultant Forces

Components	X	Y	Z	Resultant
Reaction force(N)	-0.451721	4.03943e-006	-34.4645	34.4674
Reaction Moment(N-m)	0	0	0	0

Load name	Load Image	Load Details
Gravity-1	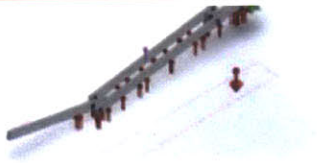	Reference: **Top Plane** Values: **0 0 -9.81** Units: **SI**
Pressure-1		Entities: **7 face(s)** Type: **Normal To Plane** Value: **651.97** Units: **N/m^2**
Remote Load/Mass (Rigid connection)-1	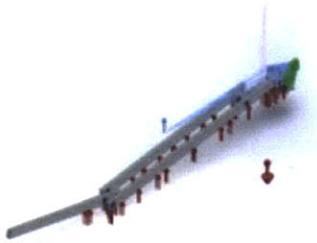	Entities: **1 edge(s), 1 face(s)** Type: **Load/Mass (Rigid connection)** Coordinate System: **Global cartesian coordinates** Force Values: **---, 12.22, --- N** Moment Values: **---, ---, --- N-m** Reference coordinates: **0 3 4 in** Components transferred: **Force**

Remote Load/Mass (Rigid connection)-2	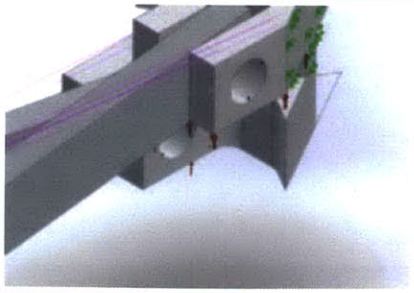	Entities: **1 face(s)** Type: **Load (Direct transfer)** Coordinate System: **Global cartesian coordinates** Force Values: **---, 76.6667, --- N** Moment Values: **---, ---, --- N-m** Reference coordinates: **0 18.84 0 in** Components transferred: **Force**

Connector Definitions

Pin/Bolt/Bearing Connector

Model Reference	Connector Details	Strength Details
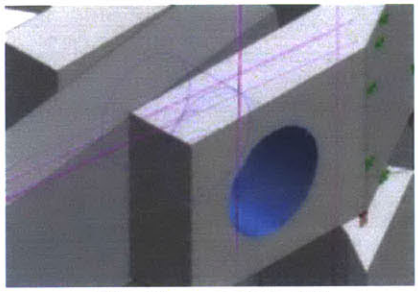 Pin Connector-25	**Entities:** 2 face(s) **Type:** Pin **Connection type:** With retaining ring (No translation) **Rotational stiffness value:** 0 **Units:** SI	Bolt Check: OK Calculated FOS: 106.922 Desired FOS: 2 

Connector Forces

Type	X-Component	Y-Component	Z-Component	Resultant
Axial Force (N)	0.23554	0	0	0.23554
Shear Force (N)	0	5.3624	1.8232	5.6639
Torque (N-m)	-3.6393e-011	-0	-0	-3.6393e-011
Bending moment (N-m)	0	0.0050817	-0.0027444	0.0057755

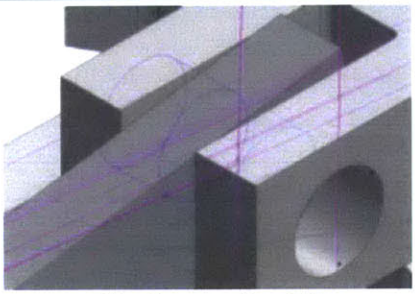 Pin Connector-26	**Entities:** 2 face(s) **Type:** Pin **Connection type:** With retaining ring (No translation) **Rotational stiffness value:** 0 **Units:** SI	Bolt Check: OK Calculated FOS: 45.3841 Desired FOS: 2

Connector Forces

Type	X-Component	Y-Component	Z-Component	Resultant
Axial Force (N)	0.45874	0	0	0.45874
Shear Force (N)	0	5.004	-3.0479	5.8592
Torque (N-m)	-3.5042e-012	-0	-0	-3.5042e-012
Bending moment (N-m)	0	-0.014727	-0.0094414	0.017493

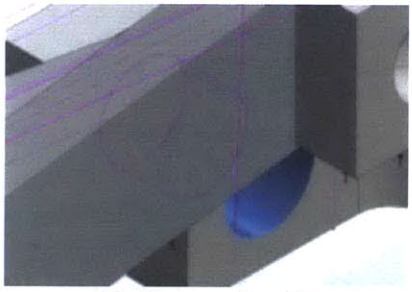

Pin Connector-27

Entities:	2 face(s)
Type:	Pin
Connection type:	With retaining ring (No translation)
Rotational stiffness value:	0
Units:	SI

Bolt Check:	OK
Calculated FOS:	72.7836
Desired FOS:	2

Connector Forces

Type	X-Component	Y-Component	Z-Component	Resultant
Axial Force (N)	1.7486	0	0	1.7486
Shear Force (N)	0	-6.6308	-5.4664	8.5936
Torque (N-m)	1.9899e-010	0	0	1.9899e-010
Bending moment (N-m)	0	-0.0038798	0.0063873	0.0074733

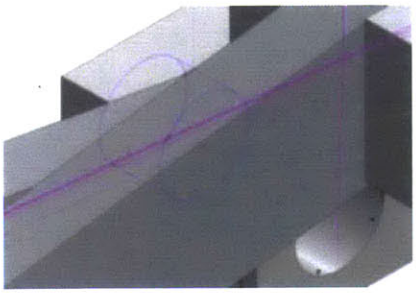

Pin Connector-28

Entities:	**2 face(s)**
Type:	**Pin**
Connection type:	**With retaining ring (No translation)**
Rotational stiffness value:	**0**
Units:	**SI**

Bolt Check:	OK
Calculated FOS:	49.3381
Desired FOS:	2

Connector Forces

Type	X-Component	Y-Component	Z-Component	Resultant
Axial Force (N)	1.5255	0	0	1.5255
Shear Force (N)	0	-5.8435	-0.59542	5.8737
Torque (N-m)	-3.2472e-012	-0	-0	-3.2472e-012
Bending moment (N-m)	0	-0.0064082	0.014061	0.015453

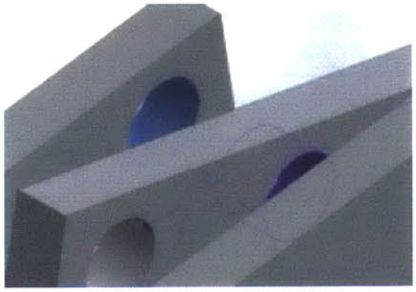

Pin Connector-29

Entities:	**2 face(s)**
Type:	**Pin**
Connection type:	**With retaining ring (No translation)**
Rotational stiffness value:	**0**
Units:	**SI**

Bolt Check:	OK
Calculated FOS:	132.963
Desired FOS:	2

Connector Forces

Type	X-Component	Y-Component	Z-Component	Resultant
Axial Force (N)	0.0087376	-0	-0	-0.0087376
Shear Force (N)	0	-0.067794	0.95155	0.95396
Torque (N-m)	-2.9663e-012	0	0	2.9663e-012
Bending moment (N-m)	0	-0.0060667	-0.00097774	0.006145

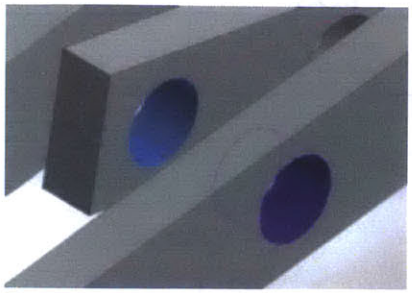

Pin Connector-30

Entities:	2 face(s)
Type:	Pin
Connection type:	With retaining ring (No translation)
Rotational stiffness value:	0
Units:	SI

Bolt Check:	OK
Calculated FOS:	30.3304
Desired FOS:	2

Connector Forces

Type	X-Component	Y-Component	Z-Component	Resultant
Axial Force (N)	0.23179	-0	-0	-0.23179
Shear Force (N)	0	-0.83352	-3.9193	4.007
Torque (N-m)	-3.303e-012	0	0	3.303e-012
Bending moment (N-m)	0	0.011398	-0.024415	0.026945

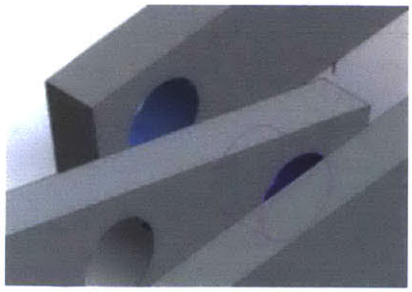

Pin Connector-31

Entities:	2 face(s)
Type:	Pin
Connection type:	With retaining ring (No translation)
Rotational stiffness value:	0
Units:	SI

Bolt Check:	OK
Calculated FOS:	115.06
Desired FOS:	2

Connector Forces

Type	X-Component	Y-Component	Z-Component	Resultant
Axial Force (N)	-0.0087617	0	0	0.0087617
Shear Force (N)	0	0.20421	-0.95172	0.97339
Torque (N-m)	-2.4322e-012	0	0	2.4322e-012
Bending moment (N-m)	0	0.0070133	0.0011122	0.0071009

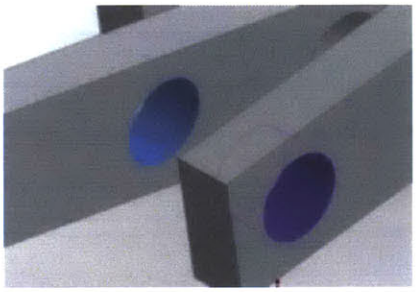

Pin Connector-32

Entities:	**2 face(s)**
Type:	**Pin**
Connection type:	**With retaining ring (No translation)**
Rotational stiffness value:	**0**
Units:	**SI**

Bolt Check:	OK
Calculated FOS:	641.717
Desired FOS:	2

Connector Forces

Type	X-Component	Y-Component	Z-Component	Resultant
Axial Force (N)	**-0.0087009**	**0**	**0**	**0.0087009**
Shear Force (N)	**0**	**0.30788**	**-0.95182**	**1.0004**
Torque (N-m)	**-8.1103e-011**	**0**	**0**	**8.1103e-011**
Bending moment (N-m)	**0**	**0.00087848**	**-0.00024045**	**0.00091079**

Contact Information

Contact	Contact Image	Contact Properties
Global Contact	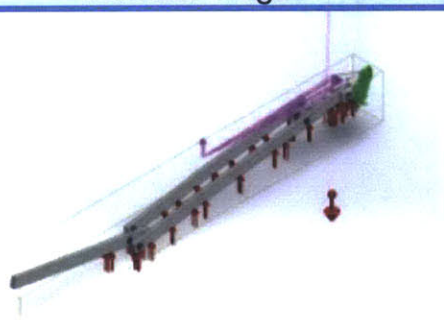	Type: **Node to node** Components: **1 component(s)**

Mesh Information

Mesh type	Solid Mesh
Mesher Used:	Standard mesh
Automatic Transition:	Off
Include Mesh Auto Loops:	Off
Jacobian points	4 Points
Element Size	0.0663525 in
Tolerance	0.00331763 in
Mesh Quality	High
Remesh failed parts with incompatible mesh	Off

7.6 Mesh Information - Details

Total Nodes	20303
Total Elements	10768
Maximum Aspect Ratio	10.474
% of elements with Aspect Ratio < 3	97.3
% of elements with Aspect Ratio > 10	0.00929
% of distorted elements(Jacobian)	0
Time to complete mesh(hh;mm;ss):	00:00:03
Computer name:	TROYN-PC

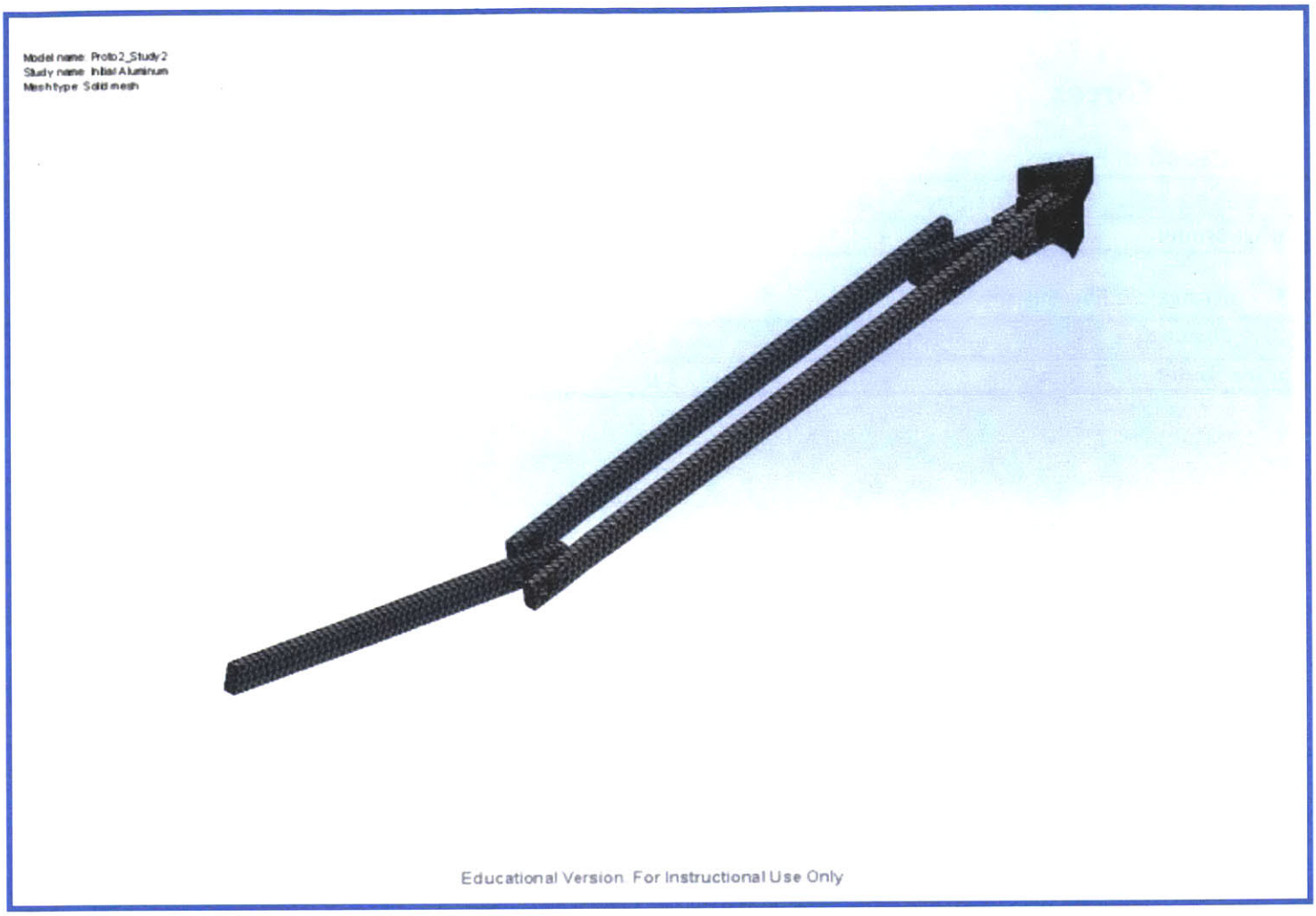

Sensor Details

Sensor name	Location	Sensor Details
Stress1	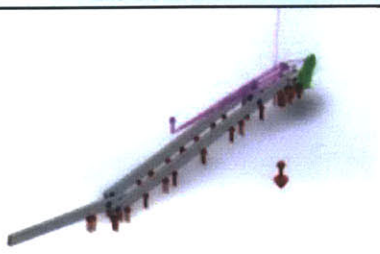	Value : 27.4629 Entities : Result :Stress Component :VON: von Mises Stress Criterion :Model Max Step Criterion : Across all Steps Step No.:1 Alert Value: NA

Resultant Forces

7.7 Reaction Forces

Selection set	Units	Sum X	Sum Y	Sum Z	Resultant
Entire Model	N	-1.17641	-89.4151	-169.266	191.435

7.8 Reaction Moments

Selection set	Units	Sum X	Sum Y	Sum Z	Resultant
Entire Model	N-m	0	0	0	0

Study Results

Name	Type	Min	Max
Stress1	VON: von Mises Stress	25.9289 N/m^2 Node: 13291	4.21041e+007 N/m^2 Node: 15316

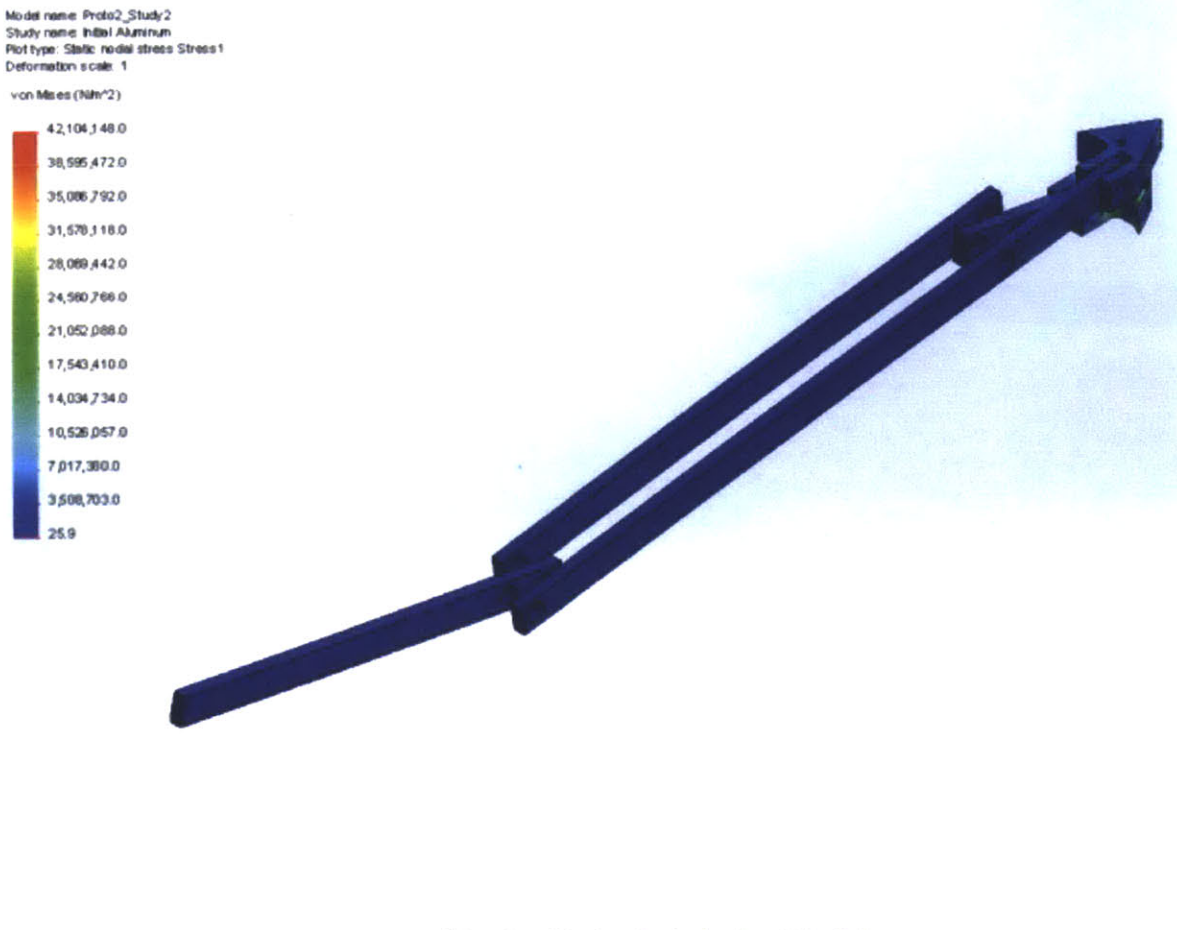

Proto2_Study2-Initial Aluminum-Stress-Stress1

Name	Type	Min	Max
Displacement1	URES: Resultant Displacement	0 mm Node: 17435	0.856992 mm Node: 11716

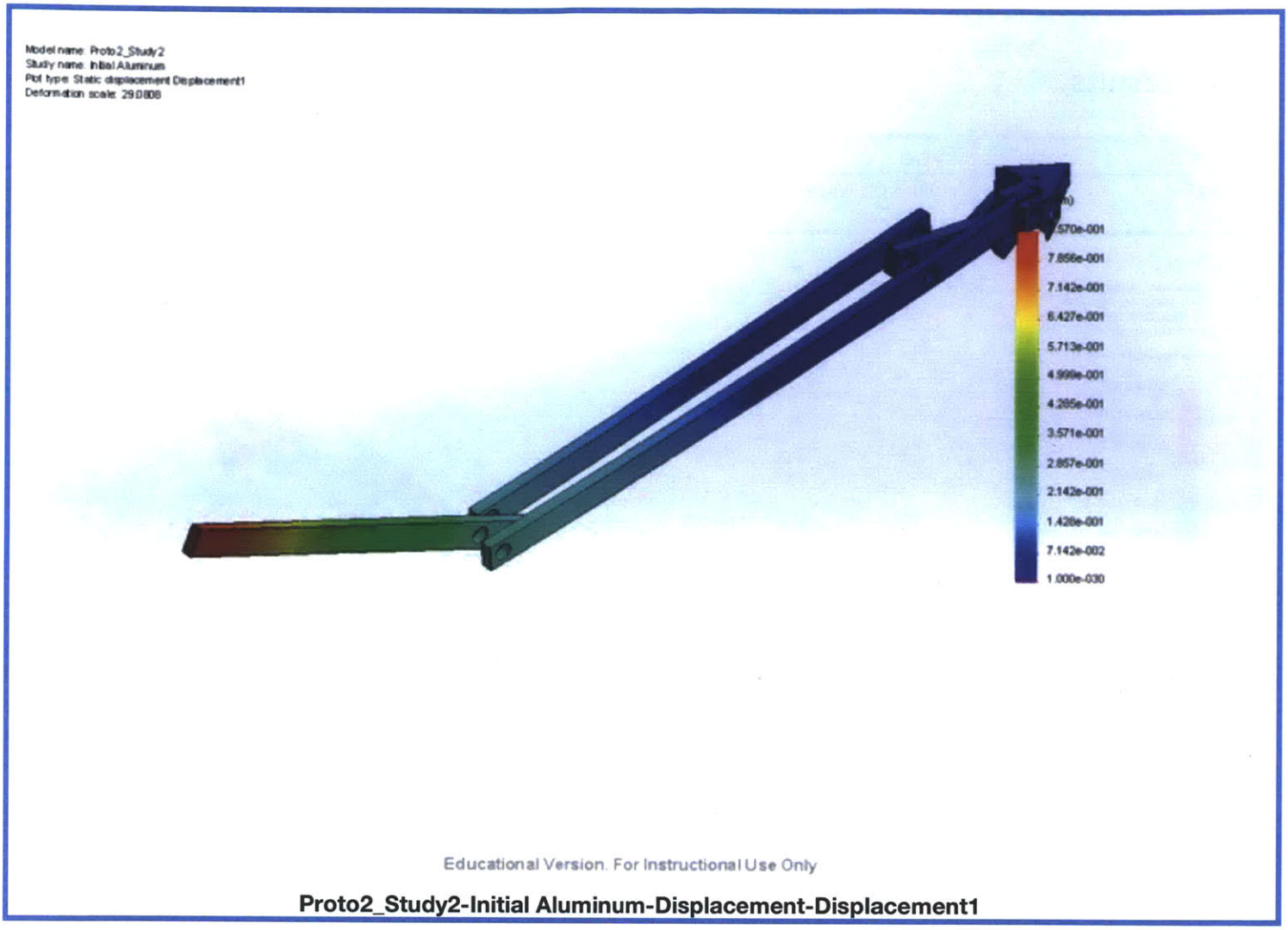

Proto2_Study2-Initial Aluminum-Displacement-Displacement1

Name	Type	Min	Max
Strain1	ESTRN: Equivalent Strain	3.99786e-010 Element: 7922	0.0126929 Element: 8455

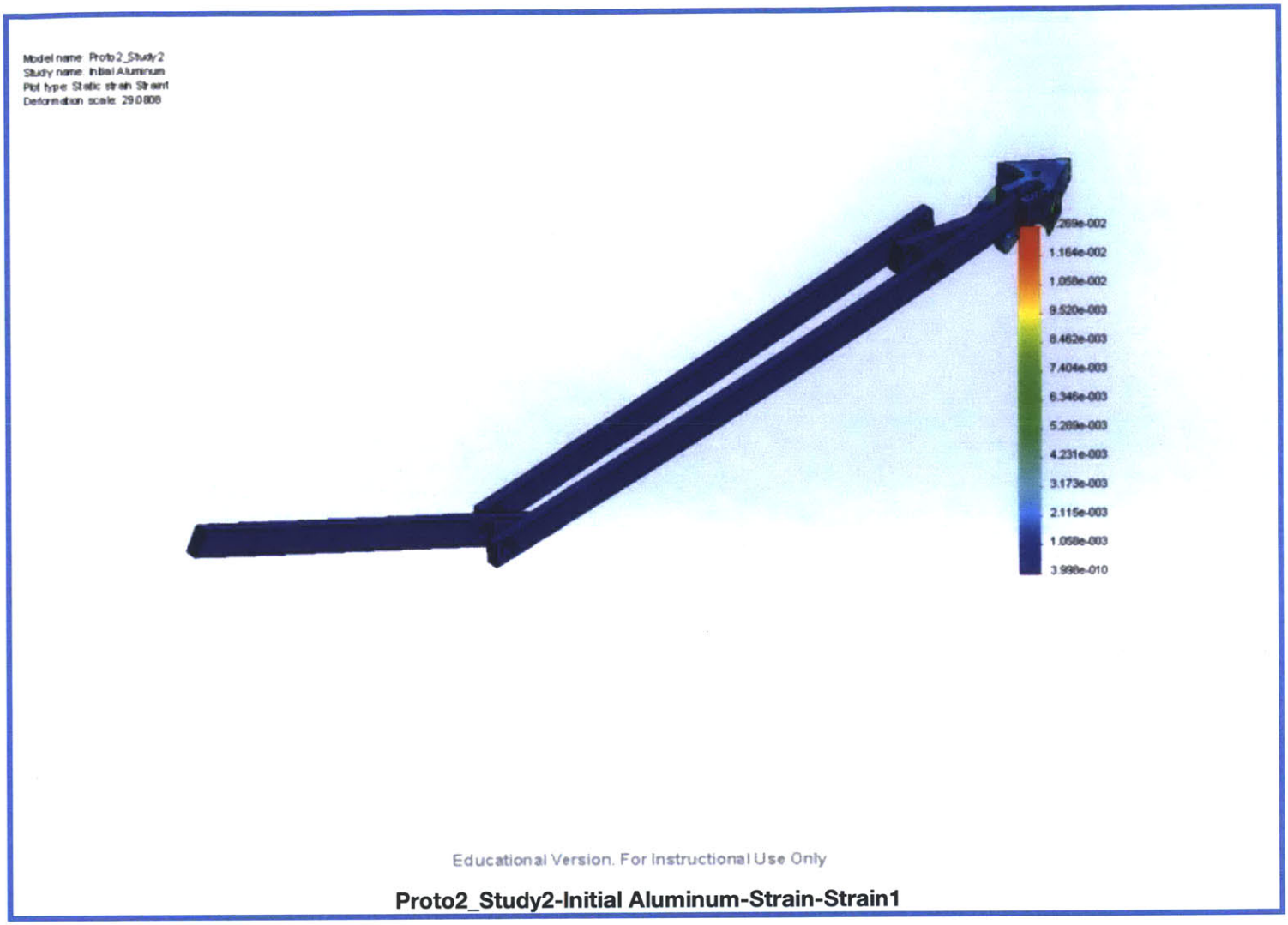

Proto2_Study2-Initial Aluminum-Strain-Strain1

Name	Type
Displacement1{1}	Deformed Shape

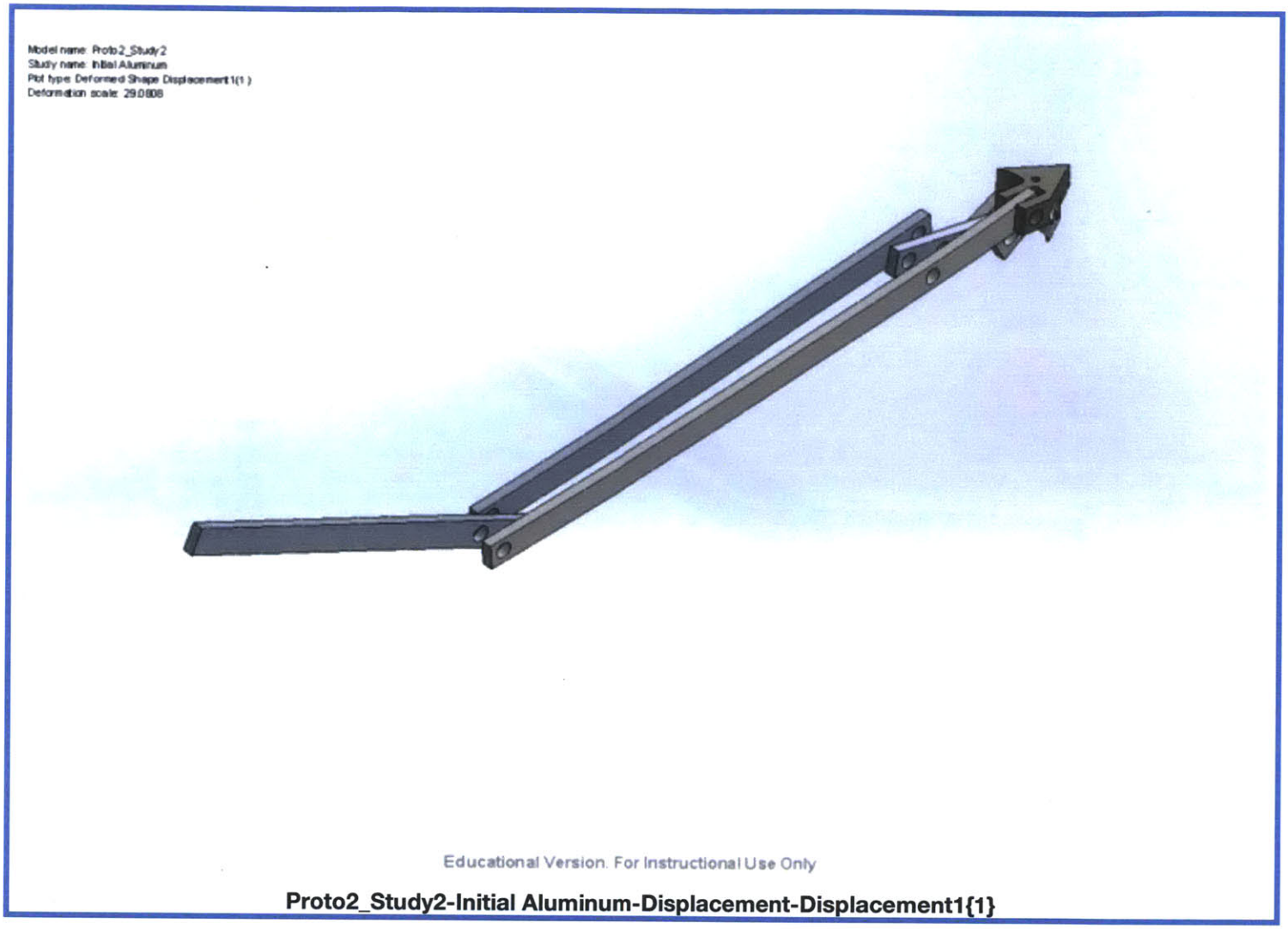

Proto2_Study2-Initial Aluminum-Displacement-Displacement1{1}

Name	Type
Design Insight1	Design Insight

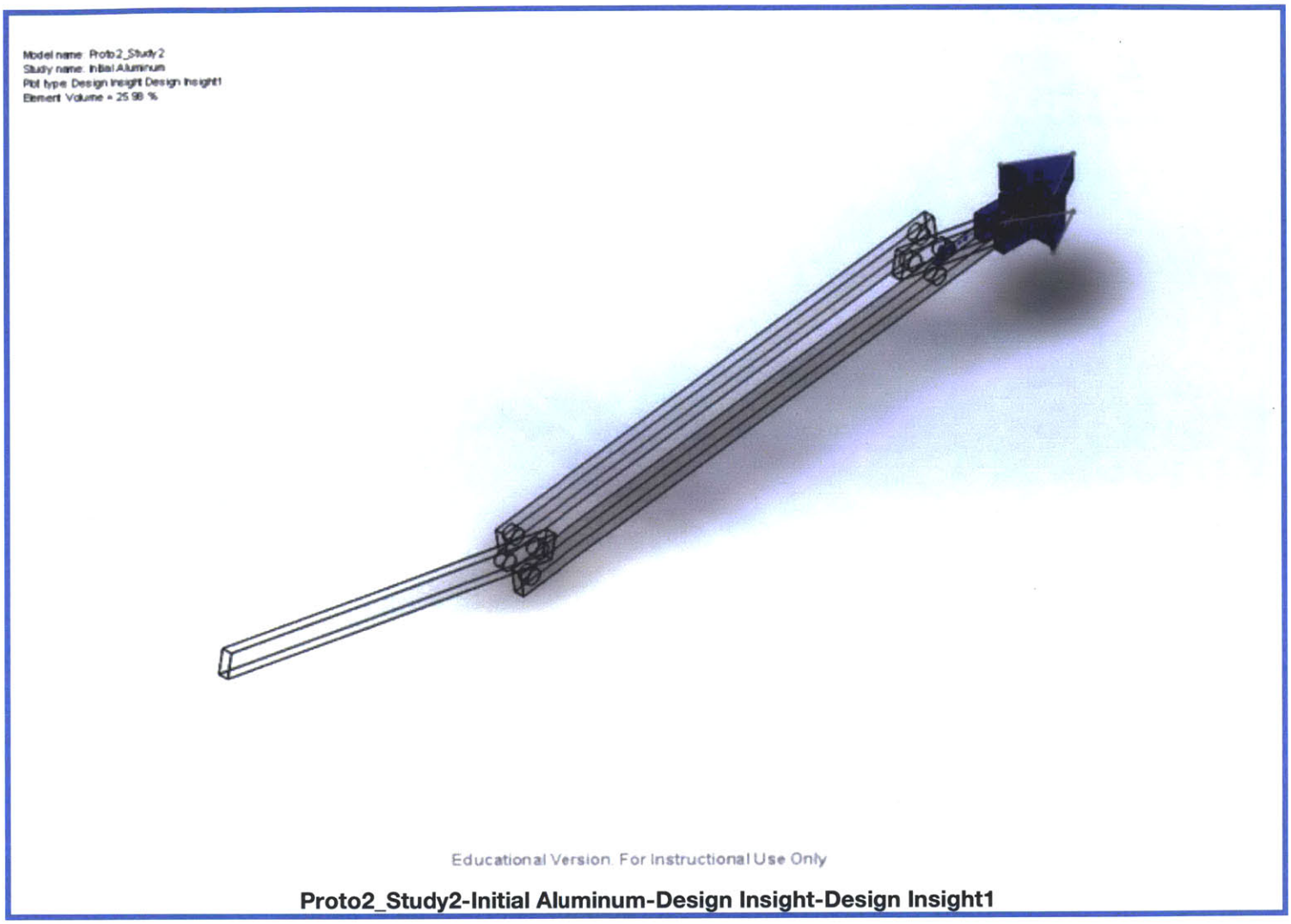

Proto2_Study2-Initial Aluminum-Design Insight-Design Insight1

Name	Type	Min	Max
Factor of Safety1	Automatic	27.4629 Node: 5493	8.29192e+006 Node: 13291

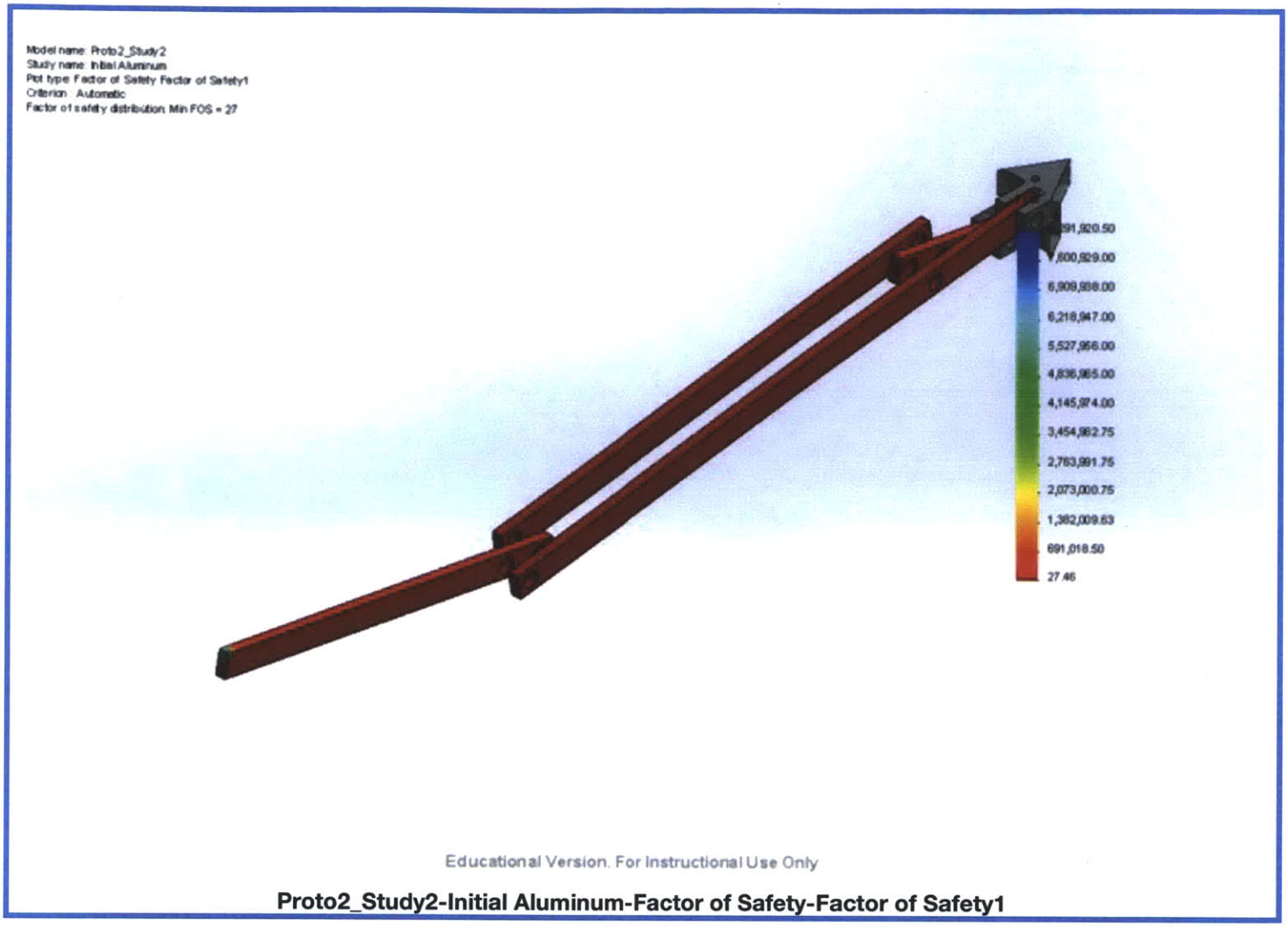

Proto2_Study2-Initial Aluminum-Factor of Safety-Factor of Safety1

Name	Type
Pin/Bolt Check1	Static Bolt & Pin Results

Proto2_Study2-Initial Aluminum-Pin/Bolt Check-Pin/Bolt Check1

Image-1